

Modelling of Marine Dispersion and Transfer of Radionuclides Accidentally Released from Land Based Facilities

*Report of Working Group 10
Modelling of Marine Dispersion and Transfer
of Radionuclides Accidentally Released
from Land Based Facilities
of MODARIA Topical Heading
Marine Modelling*

*Modelling and Data for Radiological Impact
Assessments (MODARIA) Programme*



IAEA

International Atomic Energy Agency

IAEA SAFETY STANDARDS AND RELATED PUBLICATIONS

IAEA SAFETY STANDARDS

Under the terms of Article III of its Statute, the IAEA is authorized to establish or adopt standards of safety for protection of health and minimization of danger to life and property, and to provide for the application of these standards.

The publications by means of which the IAEA establishes standards are issued in the **IAEA Safety Standards Series**. This series covers nuclear safety, radiation safety, transport safety and waste safety. The publication categories in the series are **Safety Fundamentals**, **Safety Requirements** and **Safety Guides**.

Information on the IAEA's safety standards programme is available on the IAEA Internet site

<http://www-ns.iaea.org/standards/>

The site provides the texts in English of published and draft safety standards. The texts of safety standards issued in Arabic, Chinese, French, Russian and Spanish, the IAEA Safety Glossary and a status report for safety standards under development are also available. For further information, please contact the IAEA at: Vienna International Centre, PO Box 100, 1400 Vienna, Austria.

All users of IAEA safety standards are invited to inform the IAEA of experience in their use (e.g. as a basis for national regulations, for safety reviews and for training courses) for the purpose of ensuring that they continue to meet users' needs. Information may be provided via the IAEA Internet site or by post, as above, or by email to Official.Mail@iaea.org.

RELATED PUBLICATIONS

The IAEA provides for the application of the standards and, under the terms of Articles III and VIII.C of its Statute, makes available and fosters the exchange of information relating to peaceful nuclear activities and serves as an intermediary among its Member States for this purpose.

Reports on safety in nuclear activities are issued as **Safety Reports**, which provide practical examples and detailed methods that can be used in support of the safety standards.

Other safety related IAEA publications are issued as **Emergency Preparedness and Response** publications, **Radiological Assessment Reports**, the International Nuclear Safety Group's **INSAG Reports**, **Technical Reports** and **TECDOCs**. The IAEA also issues reports on radiological accidents, training manuals and practical manuals, and other special safety related publications.

Security related publications are issued in the **IAEA Nuclear Security Series**.

The **IAEA Nuclear Energy Series** comprises informational publications to encourage and assist research on, and the development and practical application of, nuclear energy for peaceful purposes. It includes reports and guides on the status of and advances in technology, and on experience, good practices and practical examples in the areas of nuclear power, the nuclear fuel cycle, radioactive waste management and decommissioning.

MODELLING OF MARINE DISPERSION
AND TRANSFER OF RADIONUCLIDES
ACCIDENTALLY RELEASED FROM
LAND BASED FACILITIES

The following States are Members of the International Atomic Energy Agency:

AFGHANISTAN	GERMANY	PAKISTAN
ALBANIA	GHANA	PALAU
ALGERIA	GREECE	PANAMA
ANGOLA	GRENADA	PAPUA NEW GUINEA
ANTIGUA AND BARBUDA	GUATEMALA	PARAGUAY
ARGENTINA	GUYANA	PERU
ARMENIA	HAITI	PHILIPPINES
AUSTRALIA	HOLY SEE	POLAND
AUSTRIA	HONDURAS	PORTUGAL
AZERBAIJAN	HUNGARY	QATAR
BAHAMAS	ICELAND	REPUBLIC OF MOLDOVA
BAHRAIN	INDIA	ROMANIA
BANGLADESH	INDONESIA	RUSSIAN FEDERATION
BARBADOS	IRAN, ISLAMIC REPUBLIC OF	RWANDA
BELARUS	IRAQ	SAINT LUCIA
BELGIUM	IRELAND	SAINT VINCENT AND
BELIZE	ISRAEL	THE GRENADINES
BENIN	ITALY	SAN MARINO
BOLIVIA, PLURINATIONAL STATE OF	JAMAICA	SAUDI ARABIA
BOSNIA AND HERZEGOVINA	JAPAN	SENEGAL
BOTSWANA	JORDAN	SERBIA
BRAZIL	KAZAKHSTAN	SEYCHELLES
BRUNEI DARUSSALAM	KENYA	SIERRA LEONE
BULGARIA	KOREA, REPUBLIC OF	SINGAPORE
BURKINA FASO	KUWAIT	SLOVAKIA
BURUNDI	KYRGYZSTAN	SLOVENIA
CAMBODIA	LAO PEOPLE'S DEMOCRATIC REPUBLIC	SOUTH AFRICA
CAMEROON	LATVIA	SPAIN
CANADA	LEBANON	SRI LANKA
CENTRAL AFRICAN REPUBLIC	LESOTHO	SUDAN
CHAD	LIBERIA	SWEDEN
CHILE	LIBYA	SWITZERLAND
CHINA	LIECHTENSTEIN	SYRIAN ARAB REPUBLIC
COLOMBIA	LITHUANIA	TAJIKISTAN
CONGO	LUXEMBOURG	THAILAND
COSTA RICA	MADAGASCAR	TOGO
CÔTE D'IVOIRE	MALAWI	TRINIDAD AND TOBAGO
CROATIA	MALAYSIA	TUNISIA
CUBA	MALI	TURKEY
CYPRUS	MALTA	TURKMENISTAN
CZECH REPUBLIC	MARSHALL ISLANDS	UGANDA
DEMOCRATIC REPUBLIC OF THE CONGO	MAURITANIA	UKRAINE
DENMARK	MAURITIUS	UNITED ARAB EMIRATES
DJIBOUTI	MEXICO	UNITED KINGDOM OF GREAT BRITAIN AND NORTHERN IRELAND
DOMINICA	MONACO	UNITED REPUBLIC OF TANZANIA
DOMINICAN REPUBLIC	MONGOLIA	UNITED STATES OF AMERICA
ECUADOR	MONTENEGRO	URUGUAY
EGYPT	MOROCCO	UZBEKISTAN
EL SALVADOR	MOZAMBIQUE	VANUATU
ERITREA	MYANMAR	VENEZUELA, BOLIVARIAN REPUBLIC OF
ESTONIA	NAMIBIA	VIET NAM
ESWATINI	NEPAL	YEMEN
ETHIOPIA	NETHERLANDS	ZAMBIA
FIJI	NEW ZEALAND	ZIMBABWE
FINLAND	NICARAGUA	
FRANCE	NIGER	
GABON	NIGERIA	
GEORGIA	NORTH MACEDONIA	
	NORWAY	
	OMAN	

The Agency's Statute was approved on 23 October 1956 by the Conference on the Statute of the IAEA held at United Nations Headquarters, New York; it entered into force on 29 July 1957. The Headquarters of the Agency are situated in Vienna. Its principal objective is "to accelerate and enlarge the contribution of atomic energy to peace, health and prosperity throughout the world".

MODELLING OF MARINE DISPERSION
AND TRANSFER OF RADIONUCLIDES
ACCIDENTALLY RELEASED FROM
LAND BASED FACILITIES

REPORT OF WORKING GROUP 10
MODELLING OF MARINE DISPERSION AND TRANSFER
OF RADIONUCLIDES ACCIDENTALLY RELEASED
FROM LAND BASED FACILITIES
OF MODARIA TOPICAL HEADING MARINE MODELLING
MODELLING AND DATA FOR RADIOLOGICAL IMPACT
ASSESSMENTS (MODARIA) PROGRAMME

COPYRIGHT NOTICE

All IAEA scientific and technical publications are protected by the terms of the Universal Copyright Convention as adopted in 1952 (Berne) and as revised in 1972 (Paris). The copyright has since been extended by the World Intellectual Property Organization (Geneva) to include electronic and virtual intellectual property. Permission to use whole or parts of texts contained in IAEA publications in printed or electronic form must be obtained and is usually subject to royalty agreements. Proposals for non-commercial reproductions and translations are welcomed and considered on a case-by-case basis. Enquiries should be addressed to the IAEA Publishing Section at:

Marketing and Sales Unit, Publishing Section
International Atomic Energy Agency
Vienna International Centre
PO Box 100
1400 Vienna, Austria
fax: +43 1 26007 22529
tel.: +43 1 2600 22417
email: sales.publications@iaea.org
www.iaea.org/publications

For further information on this publication, please contact:

Waste and Environmental Safety Section
International Atomic Energy Agency
Vienna International Centre
PO Box 100
1400 Vienna, Austria
Email: Official.Mail@iaea.org

© IAEA, 2019
Printed by the IAEA in Austria
August 2019

IAEA Library Cataloguing in Publication Data

Names: International Atomic Energy Agency.
Title: Modelling of marine dispersion and transfer of radionuclides accidentally released from land based facilities / International Atomic Energy Agency.
Description: Vienna : International Atomic Energy Agency, 2019. | Series: IAEA TECDOC series, ISSN 1011-4289 ; no. 1876 | Includes bibliographical references.
Identifiers: IAEAL 19-01252 | ISBN 978-92-0-103619-3 (paperback : alk. paper)
Subjects: LCSH: Radioisotopes — Migration. | Simulation methods. | Radioactive substances in rivers, lakes, etc.

FOREWORD

Models are essential tools for evaluating radiological impacts within the safety assessment process and for regulatory control of nuclear facilities and activities in planned, existing and emergency exposure situations. Modelling the fate of radionuclides in the environment and assessing the resulting radiation doses to people and the environment is needed, for example, for evaluating the radiological relevance of routine and accidental releases of radionuclides, for decision making during remediation activities, in the framework of long term safety assessments of nuclear waste disposal facilities, and for clearance and exemption of material with low levels of radioactivity from the need for regulatory control.

The IAEA has been organizing programmes of international model testing since the 1980s. These programmes have contributed to a general improvement in models, in the transfer of data and in the capabilities of modellers in Member States. IAEA publications on this subject over the past three decades demonstrate the comprehensive nature of the programmes and record the associated advances that have been made.

From 2012 to 2015, the IAEA implemented the Modelling and Data for Radiological Impact Assessments (MODARIA) programme, which concentrated on testing the performance of models; developing and improving models for particular environments; reaching consensus on datasets that are generally applicable in environmental transfer models; and providing an international forum for the exchange of experience, ideas and research information.

Different aspects were addressed by ten working groups within MODARIA, covering four thematic areas: remediation of contaminated areas; uncertainties and variability; exposures and effects on biota; and marine modelling. This publication describes the work of Working Group 10, Modelling of Marine Dispersion and Transfer of Radionuclides Accidentally Released from Land-based Facilities.

The IAEA is grateful to all those who participated in Working Group 10, in particular its leader, R. Periañez (Spain). The IAEA officers responsible for this publication were P. McGinnity of the IAEA Environment Laboratories, and A. Kennedy and D. Telleria of the Division of Radiation, Transport and Waste Safety.

EDITORIAL NOTE

This publication has been prepared from the original material as submitted by the contributors and has not been edited by the editorial staff of the IAEA. The views expressed remain the responsibility of the contributors and do not necessarily represent the views of the IAEA or its Member States.

Neither the IAEA nor its Member States assume any responsibility for consequences which may arise from the use of this publication. This publication does not address questions of responsibility, legal or otherwise, for acts or omissions on the part of any person.

The use of particular designations of countries or territories does not imply any judgement by the publisher, the IAEA, as to the legal status of such countries or territories, of their authorities and institutions or of the delimitation of their boundaries.

The mention of names of specific companies or products (whether or not indicated as registered) does not imply any intention to infringe proprietary rights, nor should it be construed as an endorsement or recommendation on the part of the IAEA.

The authors are responsible for having obtained the necessary permission for the IAEA to reproduce, translate or use material from sources already protected by copyrights.

The IAEA has no responsibility for the persistence or accuracy of URLs for external or third party Internet web sites referred to in this publication and does not guarantee that any content on such web sites is, or will remain, accurate or appropriate.

CONTENTS

SUMMARY	1
1. INTRODUCTION	3
1.1. BACKGROUND OF THE MODARIA PROGRAMME	3
1.2. THE REQUIREMENT FOR ADVANCED MODELS TO PREDICT MARINE DISTRIBUTION OF RADIONUCLIDES AFTER LAND- BASED ACCIDENTAL RELEASES.....	4
2. THE BALTIC SEA RADIOLOGICAL SCENARIO	6
2.1. INTRODUCTION	6
2.2. DESCRIPTION OF THE BALTIC SEA	6
2.2.1. Physical description	6
2.2.2. Radionuclide inputs	11
2.3. MODELLING EXERCISE	12
2.3.1. Previous modelling studies	12
2.3.2. Model descriptions.....	13
2.3.3. Modelling endpoints	13
2.4. RESULTS AND DISCUSSION.....	15
2.5. CONCLUSIONS	21
3. THE PACIFIC OCEAN RADIOLOGICAL SCENARIO	22
3.1. INTRODUCTION	22
3.1.1. Previous modelling studies	22
3.1.2. Present modelling exercises and applied models.....	24
3.2. EXERCISE 1: INITIAL MODEL COMPARISON	25
3.2.1. Modelling exercise.....	25
3.2.2. Results.....	25
3.3. EXERCISE 2: HOMOGENIZATION OF WATER CIRCULATION ...	29
3.3.1. Introduction.....	29
3.3.2. Comparison of hydrodynamic fields.....	30
3.3.3. Quantitative comparison	32
3.3.4. Tracer dispersion.....	37
3.3.5. ¹³⁷ Cs dispersion.....	37
3.4. EXERCISE 3: HOMOGENIZATION OF WATER–SEDIMENT INTERACTIONS	43
3.4.1. Introduction.....	43
3.4.2. Tracer dispersion.....	44
3.4.3. ¹³⁷ Cs dispersion and no SPM in the water column	44
3.4.4. ¹³⁷ Cs dispersion and constant and uniform SPM distribution in the water column.....	45
3.5. EXERCISE 4: COMPARISONS WITH FIELD DATA.....	52
3.5.1. Source term	52
3.5.2. Results.....	56
3.6. CONCLUSIONS	66
4. OVERALL SUMMARY AND CONCLUSIONS	69
REFERENCES.....	71

ANNEX I. DESCRIPTION OF THE NRPA BOX MODEL	77
ANNEX II. POSEIDON BOX MODEL DESCRIPTION.....	83
ANNEX III. DESCRIPTION OF THE THREETOX MODEL	87
ANNEX IV. DESCRIPTION OF THE SELFE/IMMSP/KIOST MODEL.....	94
ANNEX V. DESCRIPTION OF THE UNIVERSITY OF SEVILLE (USEV) 2-D DEPTH AVERAGED MODEL (BAL TIC SEA APPLICATION)	101
ANNEX VI. DESCRIPTION OF THE KAERI: LORAS MODEL.....	107
ANNEX VII. DESCRIPTION OF THE NATIONAL TECHNICAL UNIVERSITY OF ATHENS (NTUA), DISPERSION MODEL.....	111
ANNEX VIII. DESCRIPTION OF THE SISBAHIA HYDRODYNAMIC AND TRANSPORT MODELLING APPROACH.....	112
ANNEX IX. DESCRIPTION OF THE JAEA: SEA-GEARN MODEL.....	117
ANNEX X. DESCRIPTION OF THE UNIVERSITY OF SEVILLE (USEV) 3-D MODEL (PACIFIC OCEAN APPLICATION)	121
ANNEX XI. HYDRODYNAMIC MODELS APPLIED TO THE PACIFIC OCEAN RADIOLOGICAL SCENARIO	125
CONTRIBUTORS TO DRAFTING AND REVIEW	131
LIST OF PARTICIPANTS	133

SUMMARY

This report describes the work undertaken by the Modelling of Marine Dispersion and Transfer of Radionuclides Accidentally Released from Land-based Facilities Working Group 10 (WG10) of the IAEA MODARIA Programme. Two marine scenarios have been studied: (i) the dispersion of Chernobyl accident fallout in the Baltic Sea [1]; and (ii) the dispersion of radionuclides released from the Fukushima Daiichi nuclear power plant (NPP) accident into the Pacific Ocean [2].

For the modelling of radionuclides within the Baltic Sea, four models were used to compare the distribution of ^{137}Cs through time and space after five years of simulation. Significant conceptual, numerical and parameterization differences between models in addition to the complexity of the Baltic Sea hydrodynamics contribute to differences in model outputs. However, generally there is good agreement between the models and measured data.

For the modelling of radionuclides within the Pacific Ocean, a sequential chain of dispersion exercises was carried out using selected models in which a progressive harmonization of models (understood as using the same forcing and parameterizations) was performed. This allowed the causes of variability between model results to be analysed. Model harmonization was required to achieve a relatively close agreement between model outputs for the Pacific Ocean radiological scenario. The coastal waters of Fukushima represent a more dynamic system, therefore, the output of models is found to be very dependent on the ocean model used.

Some general conclusions close this report with a comparison of model performances when applied to the Baltic Sea and Pacific Ocean radiological scenarios. The difficulties of developing operative modelling systems for supporting decision making in cases of emergencies in highly dynamic environments is highlighted. It is concluded that a multi-model approach may be valuable when environmental processes are complex. Through this approach, the predictions that obtain the greatest degree of consensus among modellers are made evident and the aspects that are subject to disagreement, and which ought therefore to be handled carefully, also become clear.

Thus, the report is divided into four parts, beginning with an introductory section. Section 2¹ describes the Baltic Sea radiological scenario. Section 3 summarizes the Pacific Ocean radiological scenario and Section 4 provides the general conclusions. Models which have been applied are summarized in the corresponding Annexes I–XI, where full details on each model may be consulted in the references given.

¹ The core of the work presented in Sections 2 and 3 of this report is based on research papers published during the course of the project but has been expanded to include new material and more detailed information. Where applicable, the content from the research papers has been reproduced with permission from Elsevier Ltd. The two relevant papers are *A comparison of marine radionuclide dispersion models for the Baltic Sea in the frame of IAEA MODARIA program*, Journal of Environmental Radioactivity **139** (2015) 66–77 and *A new comparison of marine dispersion model performances for Fukushima Daiichi releases in the frame of IAEA MODARIA program*, Journal of Environmental Radioactivity **150** (2015) 247–269.

1. INTRODUCTION

1.1. BACKGROUND OF THE MODARIA PROGRAMME

The International Atomic Energy Agency (IAEA) organized a programme from 2012 to 2015 entitled MODelling and Data for Radiological Impact Assessments (MODARIA), which had the general aim of improving capabilities in the field of environmental radiation dose assessment by means of acquisition of improved data for model testing, model testing and comparison, reaching consensus on modelling philosophies, approaches and parameter values, development of improved methods and exchange of information.

The following topics were addressed in ten working groups:

Remediation of Contaminated Areas

- Working Group 1: Remediation strategies and decision-aiding techniques
- Working Group 2: Exposures in contaminated urban environments and effect of remedial measures
- Working Group 3: Application of models for assessing radiological impacts arising from Naturally Occurring Radioactive Material (NORM) and radioactively contaminated legacy sites to support the management of remediation

Uncertainties and Variability

- Working Group 4: Analysis of radioecological data in IAEA Technical Reports Series publications to identify key radionuclides and associated parameter values for human and wildlife exposure assessment
- Working Group 5: Uncertainty and variability analysis for assessments of radiological impacts arising from routine discharges of radionuclides
- Working Group 6: Common framework for addressing environmental change in long term safety assessments of radioactive waste disposal facilities
- Working Group 7: Harmonization and intercomparison of models for accidental tritium releases

Exposures and Effects on Biota

- Working Group 8: Biota modelling: Further development of transfer and exposure models and application to scenarios
- Working Group 9: Models for assessing radiation effects on populations of wildlife species

Marine Modelling

- Working Group 10: Modelling of marine dispersion and transfer of radionuclides accidentally released from land-based facilities

The activities and results achieved by the Working Groups will be described in individual IAEA Technical Documents (IAEA-TECDOCs) where appropriate. This report describes the work of the Modelling of marine dispersion and transfer of radionuclides accidentally released from land-based facilities Working Group (Working Group 10).

1.2. THE REQUIREMENT FOR ADVANCED MODELS TO PREDICT MARINE DISTRIBUTION OF RADIONUCLIDES AFTER LAND-BASED ACCIDENTAL RELEASES

Models play a major role in the cases of accidental releases of pollutants in order to obtain rapid assessments and decisions for countermeasures to minimize the potential impact on humans and the environment. The IAEA has been organizing programmes of international model testing since the 1980s.

The possible benefits of carrying out model validation and testing at an international level were recognized by the Swedish Radiation Protection Institute, which sponsored the Biospheric Model Validation Study (BIOMOVS and BIOMOVS II) programmes starting in 1985 [3]. The Chernobyl accident in 1986 created a renewed need for reliable assessment tools in many countries and provided an increased impetus for work in this area. It also created new data sets that could be put to use for model testing. As a consequence, the IAEA was prompted to start a programme on the Validation of Model Predictions (VAMP) in 1988, which concluded in 1996 [4].

More recently, the Environmental Modelling for Radiation Safety (EMRAS) Programme, which ran 2003–2007, included a working group on Testing of Models for Predicting the Behaviour of Radionuclides in Fresh Water Systems and Coastal Areas [5]. Five scenarios were studied as part of this programme, including two estuaries (Dnieper-Bug in Ukraine and Huelva in Spain). However, a solely marine environment was not considered and the aquatic environment was also not included in the EMRAS II Programme² (2009–2011) which followed on from EMRAS.

In this context, a number of marine models have been used to evaluate the transport and dispersion of oil, radionuclides and other pollutants both for short term predictions and also for long term assessments of the impact to humans by the consumption of marine food, as well as for the impact to the environment and biota. In relation to radionuclide dispersion modelling, major international exercises on modelling of transport and transfer of radionuclides in the marine environment were related to deep-sea dumping [6], disposal of intermediate and high-level waste in Arctic coastal seas [7] and nuclear weapons testing in the South Pacific [8].

During the recent decade several significant developments indicate that a new international modelling exercise is warranted. Recent developments include: advances in modelling (complex three dimensional (3-D) hydrodynamic models, optimized coding allowing implementation of complex models, techniques involving various scales and deterministic/statistical approaches, ecological modelling, dynamic transfer models, etc.), improved knowledge of oceanographic and atmospheric drivers, increased database of generic and specific parameters, new knowledge of chemical form specific biogeochemistry and the effect of environmental change (e.g. ocean acidification) on the fate of radionuclides in the marine environment.

The Fukushima Daiichi NPP accident in Japan, March 2011, resulted in significant releases to the marine environment, which prompted a large interest from modellers worldwide. Tracking contaminated seawater of defined origin can be used as a tool to validate oceanographic models

² For more information on EMRAS II programme, see <http://www-ns.iaea.org/projects/emras/emras2/>

and to follow ocean circulation over long periods and distances. Another example was the high deposition of the Chernobyl accident fallout over the Baltic Sea and the significant contamination of this semi-enclosed brackish sea area. Within HELCOM³ (Helsinki Convention on the Protection of the Marine Environment of the Baltic Sea Area) the group MORS (Monitoring of Radioactive Substances) established an internationally agreed monitoring network among the Contracting Parties in 1986 and collected all of the available data in a common database. Therefore, this sea area would be a good example to test hydrodynamic marine models in order to simulate the dispersion and behaviour of radionuclides.

The IAEA's MODARIA⁴ Programme was initiated to make progress in relation to the assessment of radioactive substances in the environment and its impact to humans and biota. MODARIA Working Group 10 was set up to deal with modelling of marine dispersion and transfer of radionuclides accidentally released from land-based facilities. Different models developed in Member States were applied to estimate marine activity concentration distribution in two radiological scenarios: (i) the accidental releases from the Fukushima Daiichi NPP accident in the Pacific and (ii) the accidental fallout deposition on the Baltic Sea from the Chernobyl accidental release in 1986. The latter case caused a significant long lasting contamination in this semi-enclosed sea area, primarily with ¹³⁷Cs and ¹³⁴Cs. The Baltic Sea and Fukushima coastal waters are very different marine environments, with the latter being a highly dynamic system with strong and variable currents, as well as being characterized by the presence of unsteady eddies. On the other hand, the Baltic Sea is a semi-enclosed basin.

Models showing different characteristics and complexity were used in MODARIA, from those based on a box type approach to those making use of the shallow water and advection–diffusion equations [9]. Although different approaches, simplifications and approximations are used by the models, there are some conceptual and structural similarities that are apparent in an overall perspective. An obvious example is the modelling of radionuclide interaction with suspended matter and bottom sediments by means of a compartmental approach. The exercises performed provided an opportunity to learn more about the proper usage of models for the management of complex environmental problems in view of model parameter uncertainty and the compatibility of different kinds of models applied to a specific contamination scenario.

Modellers from nine institutes participated in the exercises: Instituto de Engenharia Nuclear (IEN/CNEN, Brazil), Institut de Radioprotection et de Sûreté Nucléaire (IRSN, France), National Technical University of Athens (NTUA, Greece), Japan Atomic Energy Agency (JAEA, Japan), Korean Institute of Ocean Science and Technology (KIOST, Republic of Korea), Korea Atomic Energy Research Institute (KAERI, Republic of Korea), Norwegian Radiation Protection Authority (NRPA, Norway), University of Seville (USEV, Spain) and Institute of Mathematical Machines and System Problem (IMMSP, Ukraine).

³ For more information see <http://www.helcom.fi/>

⁴ Modelling and Data for Radiological Impact Assessments. Further information can be found here: <http://www-ns.iaea.org/projects/modaria/default.asp?l=116>

2. THE BALTIC SEA RADIOLOGICAL SCENARIO

2.1. INTRODUCTION

This section of the report describes the results of simulations with four models and compares the distribution of ^{137}Cs activity concentration within the Baltic Sea. Simulations are run for a period of five years, starting from October 1986. The objective of this benchmark exercise is to compare predictions and to further develop models for dispersion and transfer of radionuclides in the marine environment, which can be used for radiological and environmental impact assessments in support of decision making regarding accidental releases of radionuclides to the marine environment.

The Baltic Sea is a marine environment that is very well suited for this type of modelling exercise given the large volume of radiological measurements which have been undertaken in the region, mainly after the Chernobyl accident, within the framework of HELCOM⁵.

The Baltic Sea is a complex marine system, characterized by significant salinity gradients, both horizontally and vertically (stratification), with stratification reduced towards the northern Baltic. The Baltic Sea is partially covered with ice during part of the year and water exchanges with the North Sea mainly occurs in pulses.

Thus, the Baltic Sea also presents a challenging marine environment in which to test marine dispersion models. The main features of the Baltic Sea are described in Section 2.2, including physical and oceanographic characteristics and the main sources of radionuclides. The modelling exercise and brief description of the models which have been applied are presented in Section 2.3 with additional information on the models included in the annexes. Finally, results are presented and discussed in Section 2.4.

2.2. DESCRIPTION OF THE BALTIC SEA

2.2.1. Physical description

The Baltic Sea is shallow, with a mean depth of around 50 m (bathymetry given in Figure 1), connected to the North Sea through the Danish Straits. A map of the Baltic Sea, indicating locations of interest for the present study, is presented in Figure 2.

Tides in the Baltic Sea are very small, with amplitudes smaller than 5 cm in most of the sea, due to its limited connectivity with the North Sea [10]. The mass balance indicates that there is an excess of precipitation and river runoff over evaporation in the Baltic. Thus, there is an outflow of fresher low salinity water in the surface layer and a deep inflow of more dense water through the Belt Sea around Denmark. This channel is very shallow (sill depth around 18 m) and significant mixing between both water layers occurs. However, this results in a permanent halocline and thermocline in the Baltic Sea, which extend over the different basins. As a result, the average inflow of saline water from the North Sea via the Skagerrak and Kattegat into the Baltic is small [11]. There is a high frequency exchange of water going on all of the time, but it has almost no effect on the Baltic Sea, as generally the same water going back and forth have similar characteristics. Only during very exceptional conditions do influx and salt water intrusion events last long enough (over two weeks) to reach far enough into the Baltic Sea, not receding again. During such significant pulses, the Baltic Sea receives between 200 and 400

⁵ <http://www.helcom.fi/>

cubic kilometres (km³) of salty ocean water within a few weeks [12–14]. Even infrequent pulses are sufficient to keep the Baltic Sea a saline body of water below the permanent halocline. The path followed by such saline pulses is presented in Figure 2.

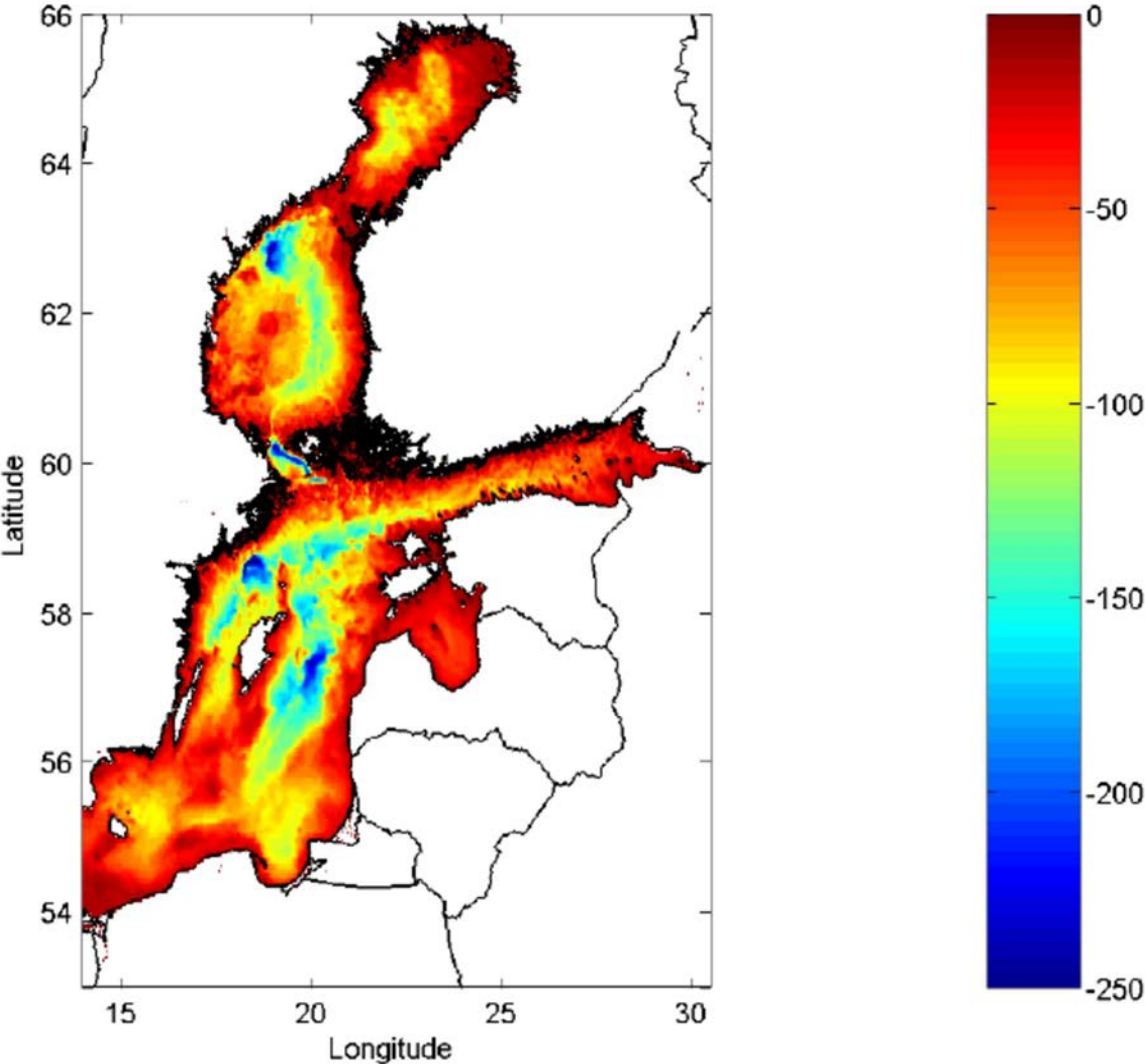


FIG. 1. Bathymetry of the Baltic Sea. Water depths are given in meters (m).

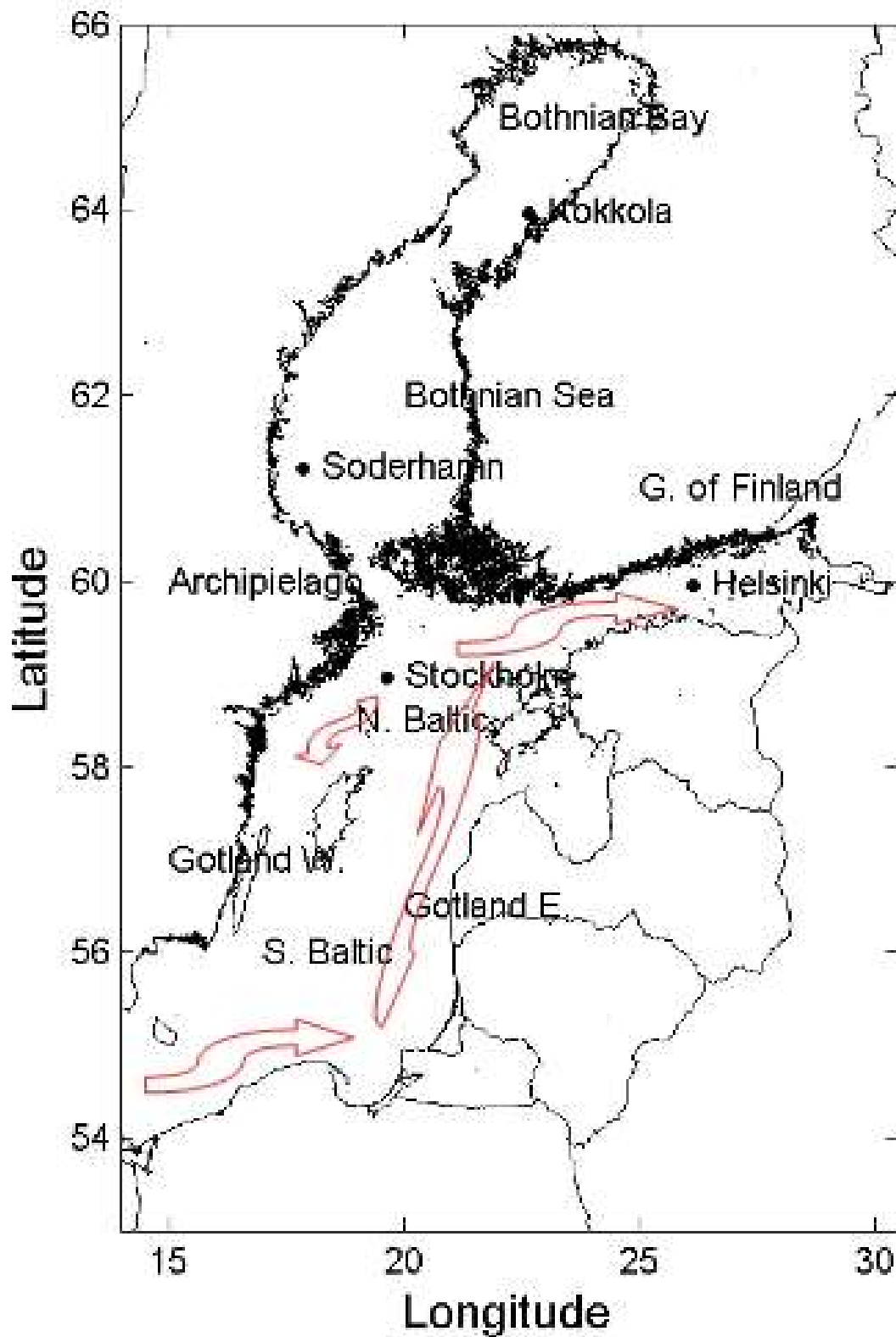


FIG. 2. Map of the Baltic Sea showing the different sub-basins considered in this study. Bullets indicate points where daily time series of radionuclide concentrations are obtained. Red arrows indicate the route of the saline pulse into the Baltic Sea.

Salinity decreases from the Belt Sea to the Gulf of Finland and the Bothnian Bay. Stratification is reduced with distance from the Baltic Sea entrance. Almost no salinity difference between bottom and surface water is apparent in the most northern areas of the Baltic Sea and the Gulf of Finland. Mean salinity in surface and deep water layers for different basins may be seen in Table 1.

Prevailing winds in the area of the Baltic Sea are from the west and southwest. Characteristic values of the wind speed 10 m above the sea surface are 8, 6, 5 and 7 m/s for winter, spring, summer and autumn respectively [15]. The annual mean wind speed is approximately 6 m/s. The global frequency of winds in the Baltic is shown in Table 2. These data correspond to Vilsandi Island located in the Baltic proper, which are very similar to those of the Swedish island Gotland.

The Baltic may be significantly covered by ice during the winter months. However, there is currently no scientific consensus on the influence this has on circulation in the Baltic Sea. The periods during which the ice cover is present in different areas of the Baltic Sea for mild, normal and severe winters are presented in Table 3.

TABLE 1. SALINITY IN SURFACE AND DEEP WATERS FOR DIFFERENT ZONES IN THE BALTIC

Zone	<i>S_{surface}</i>	<i>S_{deep}</i>
Arkona	8.5	17
Bornholm	8	16
Central Baltic	7.5	11.5
Gulf of Finland	6.5	10
Bothnian Sea	6	7
Bothnian Bay	3.5	4

TABLE 2. GLOBAL FREQUENCY OF WINDS IN THE BALTIC SEA

Wind	E	SE	S	SW	W	NW	N	NE
Frequency (%)	8	10	14	20	14	10	16	8

TABLE 3. DURATION (DAYS) OF THE ICE COVER [16]

Zone	Mild winter	Normal winter	Severe winter
Bothnian Bay	90	120	150
Bothnian Sea	0	90	120
Gulf of Finland	90	120	150
Baltic Proper	0	0	90

TABLE 4. MEAN FRESHWATER SUPPLIES TO SEVERAL SUB-BASINS [17] AND SPM CONCENTRATIONS [18]

Basin	Supply (m³/s)	SPM (g/m³)
Bothnian Bay	3104	5.0 ± 1.5
Bothnian + Aland Sea	2860	4.5 ± 1.5
Gulf of Finland	3556	5.5 ± 1.5
Gotland + Northern + Southern Baltic	4630	3.0 ± 1.5

The main sources of suspended particulate matter (SPM) into the Baltic Sea are river supply and primary production, with both sources being of the same order of magnitude. Around 10^{10} kg (10 Tg) of SPM are annually introduced into the sea [19]. It has been estimated that the mean SPM concentration in freshwater entering the Baltic from rivers is 20 g/m^3 [17]. This freshwater is introduced from the main rivers: Neva ($2460 \text{ m}^3/\text{s}$), Vistula ($1065 \text{ m}^3/\text{s}$), Neman ($632 \text{ m}^3/\text{s}$), Oder ($573 \text{ m}^3/\text{s}$), Kemijoki ($562 \text{ m}^3/\text{s}$) and Angermanälven ($489 \text{ m}^3/\text{s}$), where figures correspond to mean flows. However, a large number of small rivers more or less uniformly distributed along the coast need be considered as well and mean freshwater supplies in several basins are summarized in Table 4.

In general, SPM concentrations in the Baltic are low and present low seasonal variability. Mean SPM concentrations in the surface layer are also presented in Table 4 and have been obtained from Secchi disk measurements [18]. Absolute maximum concentrations (up to 10 g/m^3) are found in the east of the Gulf of Finland, due to the large discharge of Neva River. Close to the seabed, SPM concentrations are $1\text{--}2 \text{ g/m}^3$ larger than in the surface.

The fraction of fine (muddy) sediments in the seabed is generally required to calculate adsorption rates of radionuclides from the water column to the sediment (f). This information is summarized in Figure 3, where HARD soil is composed of stones, thus $f=0$. The same value is given to a SAND soil. A SOFT soil consists of muds, thus $f=1$. A HARD-SOFT soil is composed of stones and muds in the same proportion, thus $f=1/2$. Finally, a HARD-soft soil is also composed of stones and muds but with more abundance of the first, thus, $f=1/5$.

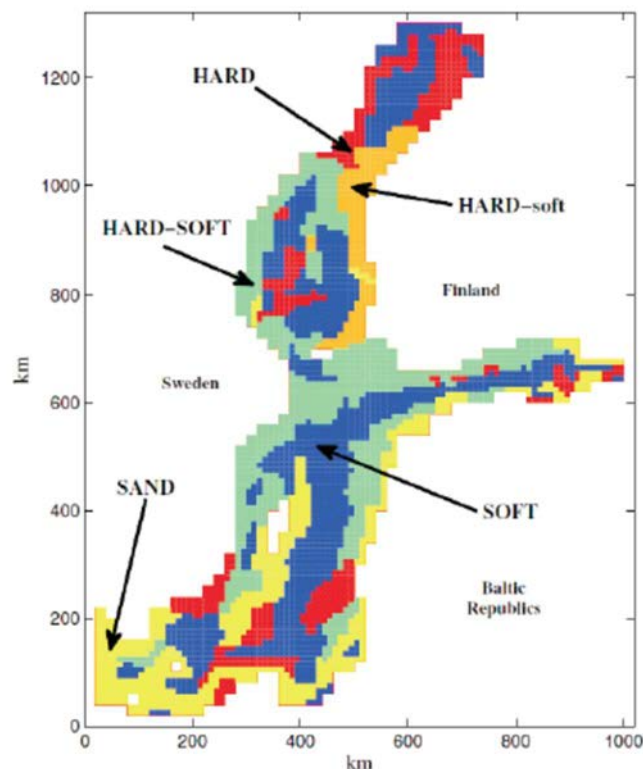


FIG. 3. Types of soils in the Baltic Sea. Reproduced courtesy of the University of Seville [17].

2.2.2. Radionuclide inputs

The occurrence of man-made radionuclides in the Baltic Sea has four main causes:

- Fallout from atmospheric nuclear weapons tests;
- The Chernobyl accident in 1986;
- Discharges from the two European facilities for the reprocessing of spent nuclear fuel, at Sellafield in the UK and La Hague in France;
- Authorized discharges of radioactivity into the Baltic Sea occurring during the routine operation of other nuclear installations.

The impact of non-nuclear facilities (e.g. hospitals, industry, etc.) on the radioactivity in the Baltic Sea is negligible and very local [20]. The relative contributions of each source is given in Table 5 [21]. From this table it is obvious that Chernobyl fallout is the main source, accounting for 83% of the total input. It is noted that ^{134}Cs was also deposited by this fallout with a $^{134}\text{Cs}/^{137}\text{Cs}$ activity ratio of approximately 0.5, but due to its half-life of only approximately 2 years, this radionuclide was only detectable until the beginning of the 1990s [22].

Deposition from the Chernobyl accident was evenly distributed, and the highest contaminated areas were the Gulf of Finland and Bothnian Sea. A map of ^{137}Cs activities in surface water (sampling depth less than 10 m) in October 1986 is presented in Figure 4. The distribution also reflects the deposition on land in the drainage area of the Baltic Sea. This map has been constructed from an interpolation of measurements [23–25]. Reported mean values in different basins (see Figure 2 above) are listed in Table 6.

TABLE 5. TOTAL AND RELATIVE ^{137}Cs INPUTS TO THE BALTIC SEA UP TO 2010. ADAPTED FROM REF. [21]

Source	Total (TBq)	Relative contribution (%)
Nuclear weapon tests	800	13
Chernobyl fallout	4700	83
Sellafield and La Hague	250	4
Authorized discharges	2.4	0.04

TABLE 6. ^{137}Cs MEAN ACTIVITY CONCENTRATIONS IN SURFACE WATER FOR 1986 [21]

Basin	^{137}Cs (Bq/m ³)
Bothnian Bay	100
Bothnian Sea	470
Aland Sea	800
Gulf of Finland	480
Northern Baltic	375
Gotland	150
Southern Baltic	75

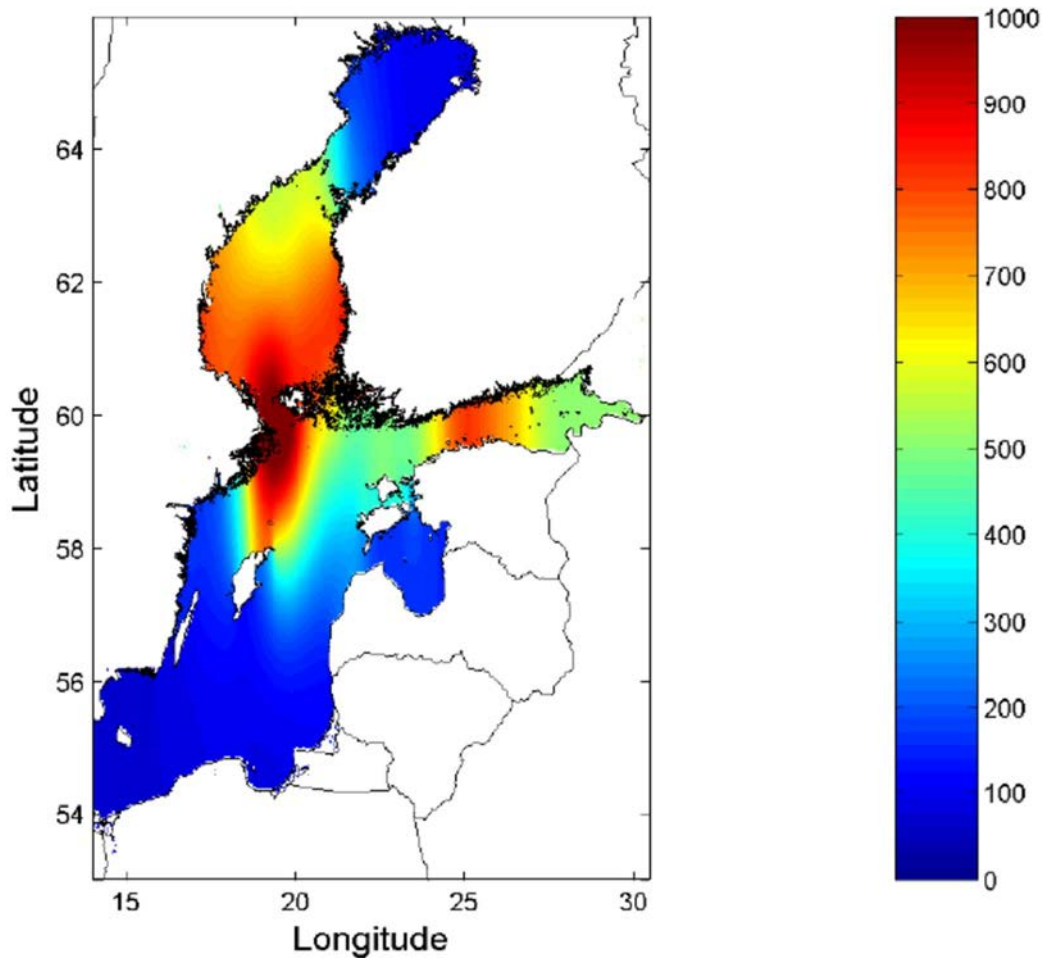


FIG. 4. ^{137}Cs (Bq/m^3) in surface water of the Baltic Sea in October 1986 interpolated from measurements.

2.3. MODELLING EXERCISE

2.3.1. Previous modelling studies

Despite the large amount of radionuclide data generated for the Baltic Sea, mainly in the period since the Chernobyl accident on 26 April 1986, relatively few modelling studies on radionuclide transport have been carried out for this environment.

A one dimensional (1-D) vertical dispersion model was used to explain the distribution of Cs isotopes in the water column of the central Bothnian Sea for the first 6 months after the accident [26] and a box model was later applied to ^{137}Cs and ^{90}Sr [27]. Very local applications within the Baltic Sea have been described for ^{14}C [28] and for isotopes of Ni, Cs and Th [29]. A Lagrangian model has been described and then applied to ^{137}Cs deposition over the whole Baltic but on a very limited time window [30]. More recently, ^{137}Cs transport has been studied with the box model implemented within the MOIRA-PLUS decision system [31]. A blind application was first carried out (using model default parameters) and, later, model output was improved by tuning parameters.

2.3.2. Model descriptions

Four models were configured and run for the Baltic Sea intercomparison exercise. The models used include two box models (POSEIDON and NRPA model) and a three dimensional (3-D) model accounting for density gradients and incorporating ice thermodynamics (THREETOX). Lastly, an intermediate approach, consisting of a two dimensional (2-D) depth averaged model forced with annual mean winds (USEV model), has also been used. These are described in Annex I (NRPA model), II (POSEIDON), III (THREETOX) and V (USEV model). It is clear therefore that the intercomparison included a wide range of modelling approaches.

For THREETOX and the USEV model, hydrodynamic models were used to calculate the current fields and used as inputs in the simulation of the transport of radionuclides. An advection–diffusion equation is solved for this purpose, which incorporates additional terms accounting for radionuclide exchanges between water, suspended matter and bed sediments. In the case of box models, water fluxes between boxes are used in the conventional way. The main characteristics of the applied models are summarized in Table 7.

2.3.3. Modelling endpoints

Simulations were started in October 1986 and ran for a duration of five years. This start time is around 6 months after the Chernobyl accident deposition event took place and when the first measurements of the fallout distribution in the Baltic Sea were carried out (see Figure 4 above; which was prepared using various measurements [23–25]). The same endpoints were calculated with each model in order to facilitate model–model and model–measurement comparisons, the latter with data from the HELCOM database. Also, estimates of annual inventories in the water column and bed sediments have been made from various measurements [32].

The modelling endpoints are:

- Time series of total ^{137}Cs inventories in the Baltic water column and in bed sediments (a single value at the end of each month) (see Figure 5);
- Time series of ^{137}Cs activity concentrations in surface water and bed sediments at locations indicated in Table 8 (daily values) (see Figures 6 and 7);
- Time series of mean activity concentrations of ^{137}Cs in the water column and bed sediment in the regions described in Figure 2 above (a single value at the end of each month) (see Figures 8 and 9);
- Maps of ^{137}Cs activity concentration in surface water (Bq/m^3) and bed sediments (Bq/kg) at the end of the simulation time (31 October 1991) (see Figure 10).

No calibration using the results of measurements was performed for the POSEIDON, THREETOX and NRPA models. Instead, default parameters were used. In the case of the USEV model, data on ^{137}Cs inventories in the water column and seabed were used to calibrate uptake/release processes, as described in Annex V.

TABLE 7. MAIN MODEL CHARACTERISTICS

	USEV	THREETOX	NRPA	POSEIDON
Spatial resolution	2 minutes of arc	2 minutes of arc	10 boxes	98 boxes including 47 marine boxes and 16 river boxes for the Baltic Sea
Vertical levels	1	20 σ -layers	3	2
Time resolution	30 min	16 s	21.9 hours	1 year
Hydrodynamic forcing	Annual mean wind	Open boundary: temperature, salinity, water elevation and velocity from MyOcean ⁶ reanalysis; Atmospheric forcing from ERA ⁷ Interim, seasonal river discharges	NAOSIM ⁸ Arctic model (from RISØ)	Averaged currents from SMHI ⁹ , 10 year re-analysis. River discharges
Ice dynamics	No	Yes	Yes for the Arctic, No for Baltic Sea	No
SPM	4.5 mg/l (constant)	Sediment transport model for one fraction with $d_{\theta} = 30 \mu\text{m}$	1 mg/l (constant)	Averaged values from THREETOX
Interactions with solid phases	Kinetic model	Kinetic model	Distribution coefficient (equilibrium)	Distribution coefficient (equilibrium)
Biota	No	No	Concentration factor	Dynamic food web model
¹³⁷Cs source	Chornobyl (Figure 4)	Chornobyl (Figure 4)	Chornobyl (Figure 4); Global deposition; Sellafeld/La Hague	Chornobyl (Figure 4); Global deposition; Sellafeld/La Hague

⁶ Ocean monitoring and forecasting program (for more information see <http://marine.copernicus.eu/>).

⁷ Performed by the European Centre for Medium-Range Weather Forecasts.

⁸ North Atlantic/Arctic Ocean Sea Ice Model [33].

⁹ Swedish Meteorological and Hydrological Institute.

TABLE 8. GEOGRAPHIC COORDINATES OF LOCATIONS FOR TIME SERIES

Location	Latitude	Longitude
Helsinki	25°00'E	60°00'N
Stockholm	19°30'E	59°00'N
Soderhamn	17°40'E	61°15'N
Kokkola	22°30'E	64°00'N

2.4. RESULTS AND DISCUSSION

A comparison of the temporal evolution of ^{137}Cs inventories in water and bed sediments calculated by the four models is presented in Figure 5. Values estimated from measurements [32] are also presented. The water column inventory estimated from measurements decreases as ^{137}Cs is progressively fixed to bed sediments, which leads to an increase in the seabed inventory. It can be seen that calculated temporal trends by all models reproduce the observed behaviour. Moreover, results are very close for all models, especially for water.

Calculated time series of ^{137}Cs activity concentrations in water and in bed sediments, for 4 points indicated in Figure 2 above, are presented in Figures 6 and 7, respectively. All models predict an exponential decay of activity concentrations in water except in Kokkola. Predicted activity concentrations are also very similar. In Kokkola, there is a difference between the hydrodynamic (THREETOX and USEV) and box (NRPA and POSEIDON) models, which may be attributed to these different model types. While the box model results indicate decreases in ^{137}Cs activity concentrations, essentially constant (or slightly increasing) ^{137}Cs activity concentrations were predicted by the hydrodynamic models. In the case of bed sediments, the differences between the model results are larger than for the dissolved phase (water). Nevertheless, all models predict essentially the same temporal trends. It is also interesting to note that results from the two hydrodynamic models remain close, i.e. the maximum differences in the predicted ^{137}Cs activity concentrations are less than double in all cases and is much smaller in some locations.

Figure 8 shows the predicted ^{137}Cs activity concentrations in water in several basins of the Baltic Sea. The calculated results correspond to the mean value for the considered basin (i.e. mean values between all boxes or grid cells which cover the basin). Accordingly, for each basin, mean values and uncertainties (1σ standard deviations) were calculated from measurement results (from the HELCOM database). These observed temporal trends of ^{137}Cs activity concentrations are generally reproduced by all models in all basins. An abrupt increase in levels of ^{137}Cs at the moment of the deposition event following the Chernobyl accident was reproduced and, from this time onwards, a gradual decrease in most basins due to horizontal and vertical dilution and, to a lesser extent, to uptake on suspended matter in the water column. In the long term, the decrease in levels of ^{137}Cs can be attributed to both the transport of radionuclides to bed sediments and to the export of radionuclides from the Baltic Sea through the Kattegat and Skagerrak into the North Sea. This leads to slightly enhanced levels of ^{137}Cs in these areas and south of Norway [34, 35].

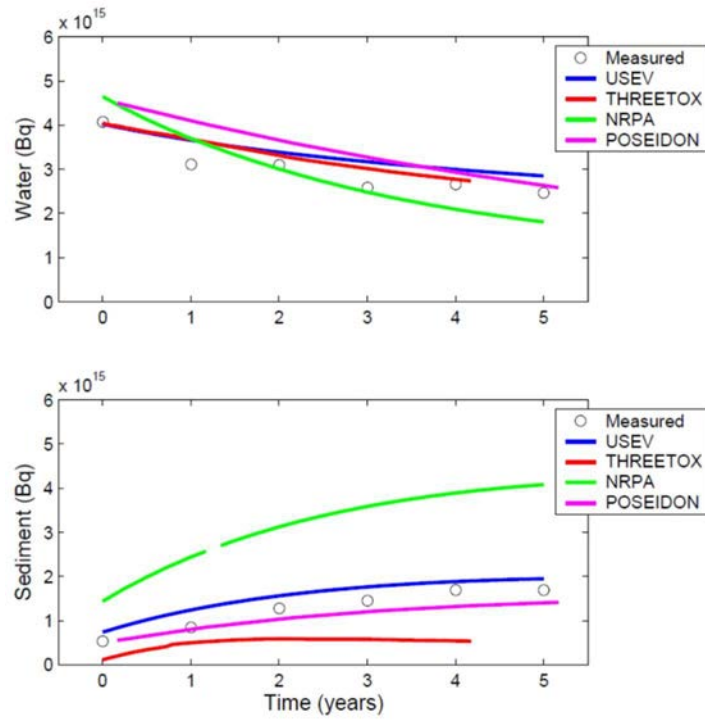


FIG. 5. Calculated ^{137}Cs inventories in water and bed sediment for the whole Baltic Sea, as well as values estimated from measurements. The time origin corresponds to October 1986.

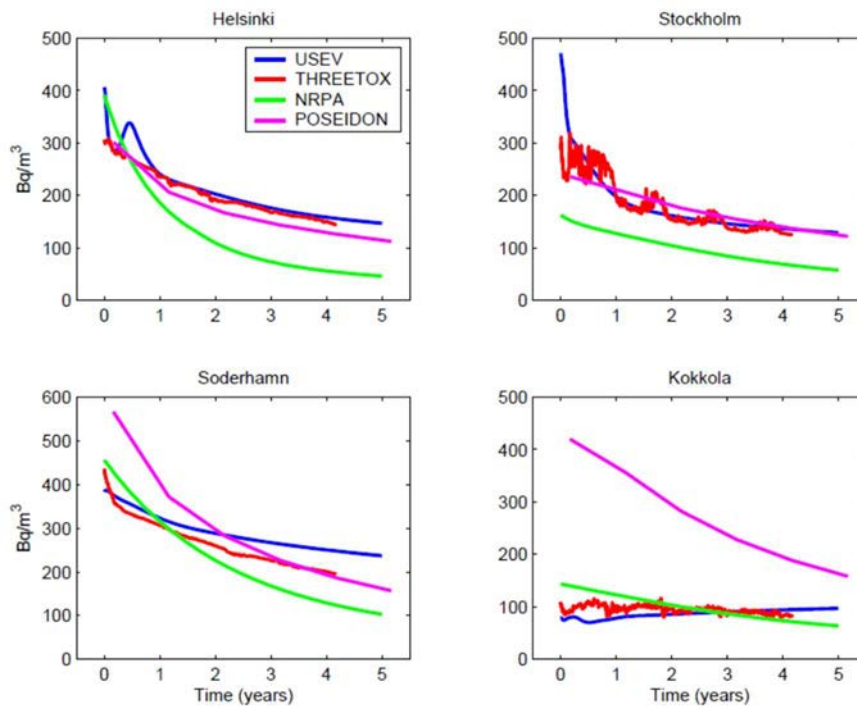


FIG. 6. Calculated ^{137}Cs activity concentrations in surface water at points indicated in Figure 2 (above). The time origin corresponds to October 1986.

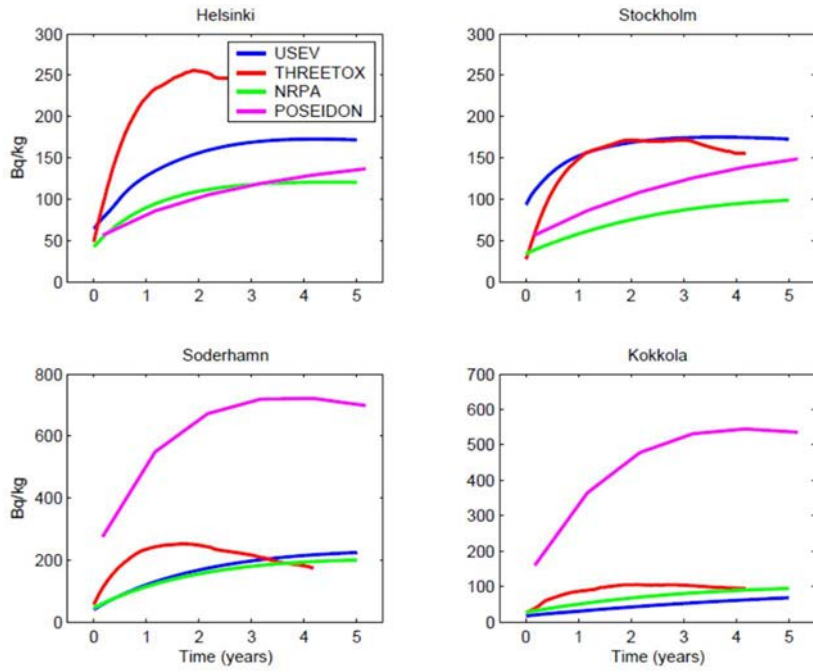
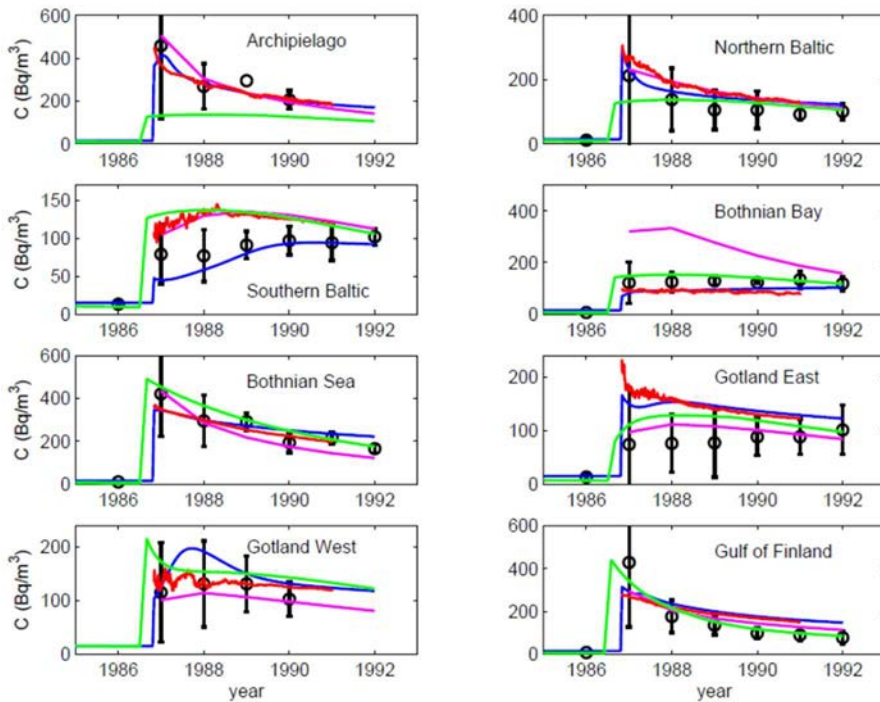


FIG. 7. Calculated ^{137}Cs activity concentrations in bed sediments at points indicated in Figure 2. The time origin corresponds to October 1986.



Key: ■ USEV, ■ POSEIDON, ■ THREETOX, ■ NRPA.

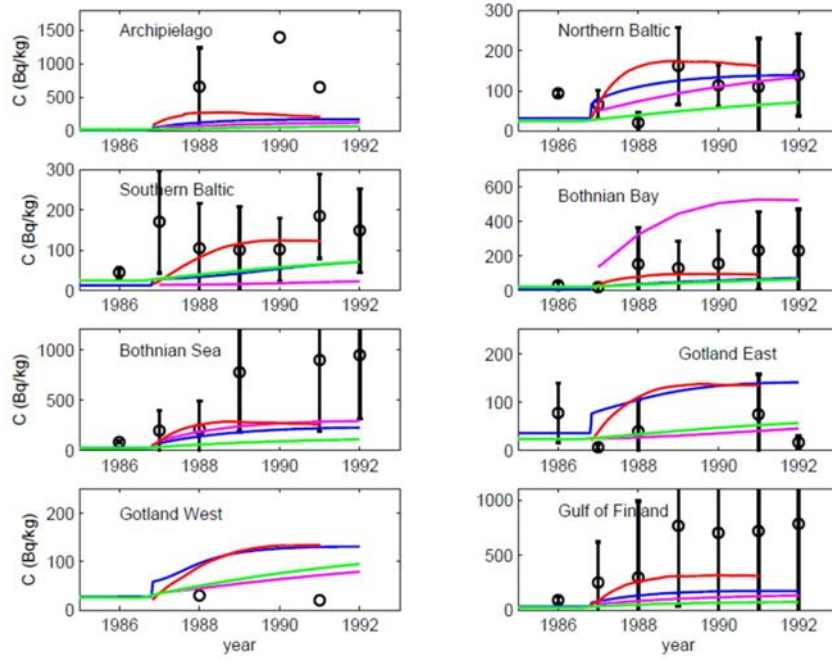
FIG. 8. Calculated and measured mean ^{137}Cs activity concentrations in water in several basins. Error bars are 1σ standard deviations of the measured mean values. In cases where only one sample was measured error bars are not shown.

Results for bed sediments are presented in Figure 9. In this case measurement results have a much larger spread than for water. Thus, model results generally lie within error bars. Nevertheless, the trends produced by all models are very similar. In this case there is an increase in ^{137}Cs activity concentrations due to the input of radionuclides from the water column. Moreover, even differences between predicted values are relatively small. Model results shown in Figures 8 and 9 are mean values over a number of grid cells or boxes, thus differences between models could be reduced because of this averaging process. Nevertheless, differences between models in specific points (time series shown in Figures 6 and 7) also remain relatively small. Consequently, it can be concluded that effectively there is a considerable agreement between all model predictions.

Maps of calculated ^{137}Cs activity concentrations in water and bed sediments for January 1991 using the hydrodynamic models (THREETOX and USEV) are presented in Figure 10. It is evident that the calculated distributions are very similar, both for water and sediments. The USEV model produces slightly higher activity concentrations than THREETOX in the Bothnian Sea. The high activity concentrations produced by THREETOX in the eastern Gulf of Finland may be attributed to the high SPM concentrations in this area (see Section 2.3). The USEV model uses uniform SPM distribution, but THREETOX includes a SPM transport model. Thus, these high concentrations are reproduced by THREETOX but not by the USEV model. A high SPM concentration increases scavenging of radionuclides from the water column to bed sediments.

As described above, models with very different structures (box and hydrodynamic models) have been applied to simulate the dispersion of ^{137}Cs in the Baltic, including interactions of radionuclides with suspended matter particles and bed sediments. These interactions are also described in different ways: using an equilibrium distribution coefficient or using a dynamic approach. In spite of the differences between the applied models, results are consistent. Similar levels of ^{137}Cs in water and sediments are predicted for the selected locations and basins, as well as for inventories in the water column and in the seabed.

A major component of uncertainty associated with model results is due to the difficulties of representing interactions of dissolved contaminants with the solid phases [36–37]. However, in a previous intercomparison exercise for the Dnieper-Bug estuary [37], it is noted that these difficulties did not affect model performances. Such an estuary is a relatively energetic environment, with significant currents. Thus, it was suggested that the relatively fast water dynamics meant that water–sediment interactions did not significantly affect radionuclide transport and dispersion [37]. However, currents in the Baltic Sea are not significantly larger than in the Dnieper-Bug estuary. Moreover, the Baltic Sea is an almost closed and shallow water system with several deeper basins. Consequently, interactions of dissolved radionuclides with the solid phases may be significant. Nevertheless, in this environment, water–sediment interactions also do not appear to be a significant source of discrepancy between model results.



Key: ■ USEV, ■ POSEIDON, ■ THREETOX, ■ NRPA.

FIG. 9. Calculated and measured mean ^{137}Cs activity concentrations for bed sediments in several basins. Error bars are 1σ standard deviations of the measured mean values. Only one sample was measured if error bars do not appear.

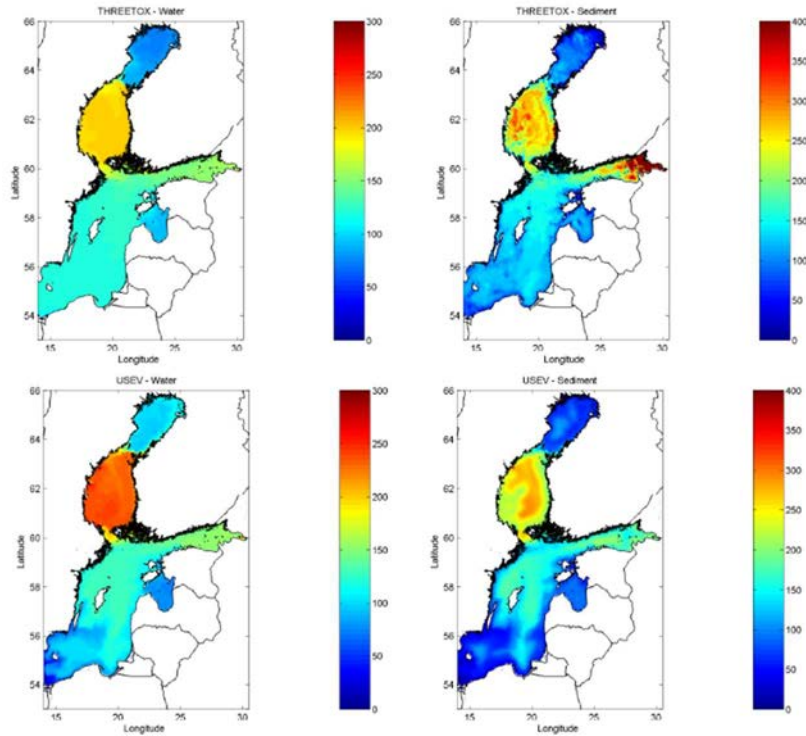


FIG. 10. Calculated ^{137}Cs activity concentrations for January 1991 in water (Bq/m^3) and sediments (Bq/kg) by hydrodynamic models THREETOX and USEV. Although THREETOX domain is slightly larger, maps are drawn over the same area (USEV domain) for a better comparison.

As described above, the Baltic Sea is a very complex marine system, with vertical stratification, significant horizontal density gradients and fresh water supplies. Furthermore, it is partially covered with ice, particularly the Northern parts in the Gulf of Bothnia and the Gulf of Finland, during some months each year (which affects not only deposition events taking place during winter but also has implications on water circulation itself). In spite of this, model results are consistent, even in the case of hydrodynamic models. The USEV model constitutes a very simple approach in which all these processes are neglected. In contrast, they are included in the complex THREETOX model. Therefore, it can be concluded that they do not play a significant role in the redistribution of contaminants within the Baltic Sea (see Figure 10). Of course, this may not be the case in a different marine area. In addition, given the relatively short simulated times (5 years) and water residence time in the Baltic Sea (some 10–30 years [15]), exchanges of radionuclides with the Atlantic Ocean do not play a significant role. While the THREETOX and USEV models only include deposition of radionuclides released from the Chernobyl accident as a ^{137}Cs source (added over a pre-Chernobyl accident background), Sellafield and La Hague releases are considered in the POSEIDON and NRPA models. From the intercomparison of model results and comparisons with observations shown in Figures 8 and 9, it is clear that Chernobyl fallout is the dominant source, as already noted in Section 2.3 above.

Significant work has been carried out concerning multi-model applications [37, 38]. It has been claimed that, given a certain level of process understanding, different model structures and parameter values can be equally acceptable. Traditionally it is supposed that an ‘ideal model’ exists, this being a unique model, inherent to nature. Thus, different models are different realizations of the ideal model in view of the specific applications for which they were developed. Consequently, a multi-model approach can be accepted if, and only if, the different models are developed to solve problems of various types, for which different realizations of the ideal model can be appropriate. However, it has been observed that this statement cannot be easily supported [37] and the results of the current work confirm this previous finding. Models with very different structures and parameters have been applied to the same environmental problem and no criteria can be found to decide which could be the most appropriate one. In this sense, it is interesting to point out that models may perform differently depending on the target variable. For instance, one model may predict radionuclide concentrations in bed sediments in good agreement with measurements, but it may provide not so good results for the water column. For another model, the situation may be the opposite.

For a correct model comparison, the appropriate question needs to be ‘asked’ to each model. This is particularly relevant when box and hydrodynamic models are compared and it has been documented previously that “different model approaches can lead to comparable results if these results are extracted in the correct way” [39].

Measurements of radionuclide concentrations in the Baltic Sea were already available within the framework of HELCOM¹⁰ when this study was carried out. Thus, a real blind-test exercise was not possible. However, as noted previously, no calibration was made for the POSEIDON, THREETOX and NRPA models. Only in the case of the USEV model was data on ^{137}Cs inventories in the water column and seabed used to calibrate uptake/release processes (see Annex V below). Thus, the results of the present exercise have not been significantly influenced by the prior knowledge of data.

¹⁰ <http://www.helcom.fi/>

2.5. CONCLUSIONS

Four radionuclide dispersion models have been applied to simulate the transport and distribution of ^{137}Cs fallout from the Chernobyl accident into the Baltic Sea. Models correspond to two categories: box models and hydrodynamic models. In all cases, interactions of dissolved radionuclides with suspended matter and bed sediments are included. Thus, models are very different in structure and parameters.

Model results have been compared with extensive field data obtained from the HELCOM database. Inventories in the water column and seabed, as well as ^{137}Cs activity concentrations over 5 years in water and sediments of several sub-basins of the Baltic, have been used for model comparisons.

Two main aspects are considered when comparing results: (i) the significant conceptual, numerical and parameterization differences between models; and (ii) the complexity of the Baltic Sea system. In spite of these two aspects, model results are consistent, even in the results observed in bed sediments which have been recognized as a significant source of model discrepancy. The same temporal trends are predicted by the models for ^{137}Cs inventories in water and bed sediments and for ^{137}Cs activity concentrations in these two phases in a number of sub-basins. Values predicted by the models for the target magnitudes are very similar and close to experimental values. There is an increase in activity concentrations in bed sediments as radionuclides are scavenged from the water column, where activity concentrations slowly decrease.

Results from this exercise suggest that some processes are not very relevant for radionuclide transport within the Baltic Sea, for instance the roles of ice cover and, surprisingly, water stratification by the halocline and thermocline. It is also clear that Chernobyl fallout is the dominant ^{137}Cs source into the Baltic Sea.

In addition, results confirm previous findings concerning multi-model applications. Because models with very different structures and parameters have been applied to the same environmental problem, no criteria can be found to decide which could be the most appropriate one. The recommended model to be applied, of course, depends on the modelling purpose, for instance, a fast assessment after an acute accidental release or a long term radiological study. The scale of the present exercise, i.e. timescale and spatial resolution of results (5 years and sub-basin level respectively), may be considered as an intermediate one. At this level, there is significant agreement between box and hydrodynamic models for the present scenario. The discrepancy would probably increase when moving towards smaller scales not properly solved by coarse box models. When moving towards longer timescales and larger domains, the situation can hardly be handled by complex hydrodynamic models, due to computational limitations, and box models might therefore be the best choice.

3. THE PACIFIC OCEAN RADIOLOGICAL SCENARIO

3.1. INTRODUCTION

Following the magnitude 9.0 earthquake and resulting tsunami which occurred on 11 March 2011, significant amounts of radioactive material were released into the environment from the Fukushima Daiichi NPP accident [2]. Radionuclides released to the atmosphere were transported eastward by a strong jet stream and reached the coast of North America in 4 days [40]. A portion of these radionuclides were deposited on the Pacific Ocean surface by wet and dry deposition processes. In addition, water used to cool the damaged nuclear reactor leaked into the ocean [41]. Thus, two radionuclides inputs into the Pacific Ocean from the Fukushima Daiichi NPP accident are considered: direct release of contaminated water and deposition of radionuclides on the sea surface from the atmosphere.

The general large scale marine circulation in this region of the western Pacific Ocean is dominated by the interaction between the Kuroshio current (western boundary current in the north Pacific) which flows along the coast of Japan towards the north and curves to the central Pacific Ocean and the Oyashio current, which is a cold current which flows from the north. These two current systems converge in the coastal waters off Fukushima and such convergence leads to the generation of unsteady eddies in the area. It is also known that the Kuroshio current acts as a barrier [42], which prevented the migration of radionuclides released from Fukushima towards the south beyond the latitude of Tokyo, instead they were transported towards the central Pacific.

3.1.1. Previous modelling studies

A significant number of modelling studies on the dispersion of radionuclides released from the Fukushima Daiichi NPP accident into the Pacific Ocean have been published in the scientific literature. The first studies were published soon after the accident, thus the spread of ^{131}I and ^{137}Cs was simulated using the Lagrangian model SEA-GEARN developed at JAEA [43]. Moreover, a Lagrangian code was also used to simulate the dispersion of ^{137}Cs and ^{134}Cs in the world ocean up to 30 years after the accident [44], where annually averaged water circulation was used for this purpose. ^{137}Cs dispersion was simulated using a high resolution (1 km) regional model during the first 3 months after the accident.

Another similar study found that radionuclides stay close to the coastline for relatively long times and suggested a role for freshwater discharges from land in offshore dispersion events [45]. Moreover, an Eulerian dispersion model for ^{137}Cs was used to carry out some sensitivity studies in order to highlight the relevant role of winds in the shelf region [46].

Simulations of ^{137}Cs dispersion over a 10 year period in the Pacific Ocean were made [47], where water circulation of the past 10 years was used. It was found that the initial current field is relevant for ^{137}Cs spreading in the first months after the accident, but this relevance fades in the long term. In addition, it was found by the same authors [47] that traces of ^{137}Cs would reach the coast of North America after about 5–6 years, and that very low concentrations would be nearly homogeneous over the whole Pacific after around 10 years. Simulations indicate a fast mixing over the upper 500 m of the water column [48] where it was also found that the radioactive caesium concentration due to the Fukushima Daiichi NPP accident was efficiently diluted in the North Pacific 2.5 years after the accident. The mesoscale eddies in the Kuroshio Extension played an important role in diluting the radioactive patch. The ^{137}Cs concentrations in the surface, intermediate, and deep layers reduce to the pre-Fukushima Daiichi NPP accident values over the North Pacific around 2.5 years after the occurrence of the Fukushima Daiichi NPP accident. Similar conclusions were obtained by modelling studies, i.e. the plume that

resulted from the Fukushima Daiichi NPP accident is rapidly diluted within the Kuroshio system over a timescale of a few months [49, 50]. Over the subsequent decades, radionuclides derived from the Fukushima Daiichi NPP accident will spread across the North Pacific basin. These model estimates have found that a component of ^{137}Cs radionuclides will be injected into the interior ocean via subduction, before eventually returning to the surface by coastal upwelling along the west coast of North America.

Other modelling results have found the residence time of ^{137}Cs in the continental shelf to be 43 ± 16 days [51]. The relevance of atmospheric deposition was studied, finding that relatively high ^{137}Cs concentrations detected in surface water north of 40°N and one month after the accident are due to atmospheric deposition [52].

More recently, a number of model sensitivity analyses have been made and have found that a tuning of the wind drag coefficient was required for a better reproduction of ^{137}Cs measurements [53]. However, for modelling purposes, a direct release source term of 27 PBq was used [54], which is considered a conservative high estimate [51].

In addition, some other modelling studies have had the objective of determining radionuclide releases from the Fukushima Daiichi NPP accident into the ocean, using inverse modelling [41, 45, 55].

All modelling studies mentioned previously, which is not a comprehensive list, present the common point that ^{137}Cs is treated as a tracer and is a perfectly conservative radionuclide which does not interact with sediments. The first models including ^{137}Cs contamination of bed sediments were described in Refs. [56, 57]. In the first case, a local study was carried out covering only the coastal region of Japan [56]. A larger domain was considered in the second study [57]. In both cases, calculated and measured ^{137}Cs concentrations in bed sediments were compared. Furthermore, water–sediment interactions were described in a dynamic way in both studies. Adsorption by bottom sediments have also been studied [58]. All of these papers agree that a significant adsorption occurs in the first months after the accident, with most of the radionuclides staying on the seabed once they have been adsorbed. More recently, a box model (POSEIDON-R) has been used to perform a radiological assessment of the accident over the period of 2011–2040 [59]. This model includes not only adsorption to sediments, but also the transfer of radionuclides through the marine food web, using a dynamic food-chain model, and subsequent doses to humans.

Some exercises comparing model performances when applied to simulate releases from the Fukushima Daiichi NPP accident have been carried out [60], with most of the discrepancies between the five participating models due to the different calculated current fields in the coastal waters of Japan, off Fukushima, which lead to different radionuclide distributions. Differences in current fields are caused by the different models and model settings used by the research groups. However, a systematic assessment aimed at investigating the reasons for differences was not carried out.

The Science Council of Japan carried out a similar intercomparison study, with eleven models involved [61]. Significant differences between models were found and the models used were different in concept (Eulerian versus Lagrangian), with different settings and even different source terms. Thus, it was concluded that a simple comparison of model results is not straightforward and that detailed systematic comparison studies, such as ones that use the same radionuclide forcing with different models and/or the same model with different forcing scenarios, are required. As described in the following sections, the objective of the work done in MODARIA consists of making such a systematic study [62].

3.1.2. Present modelling exercises and applied models

Generally speaking, a marine dispersion model consists of two submodels, i.e. a hydrodynamic model will provide the water circulation required to solve the advective transport of radionuclides and the dispersion model will use such currents to calculate transport including advection, mixing produced by turbulence and other processes like radioactive decay or interactions of dissolved radionuclides with suspended matter and bottom sediments.

A sequential chain of dispersion exercises was carried out within the MODARIA Programme in such a way that the reasons of the discrepancies between models could be assessed, i.e., if they are due to the hydrodynamic part, the dispersion part, and the ultimate reasons. The four modelling exercises are summarized in Table 9 below. The overall idea was to harmonize models, making them run with the same forcing in a step-by-step procedure, in such a way that the main agent in producing discrepancies between models could be found. This type of model intercomparison exercise has never been carried out before.

Initially, dispersion exercises were carried out with a “tracer” (which is taken to mean an entirely conservative radionuclide, i.e. no significant decay, no interaction with sediments), thereby ensuring that all parameters describing water–sediment interactions are avoided. In addition, a constant hypothetical source term was used by all models. Four exercises were carried out, although the final exercise was split into two parts. In Exercise 1 each model used its own water circulation and set of parameters, e.g. horizontal and vertical diffusion coefficients, after which all models used the same hydrodynamic description given in Exercise 2. All parameters were homogenized in Exercise 3 and, finally, a realistic source term both for direct releases into the ocean and atmospheric deposition on the sea surface was used in Exercise 4.

This method allows a comparison to be made between model results and measurements of ^{137}Cs in water and sediments. ^{137}Cs was introduced from Exercise 2 onwards. Exercise 3 was carried out with and without suspended matter particles in the water column. Exercise 4, was split into two exercises, 4a and 4b. A common model configuration was used in Exercise 4a. Each model was run with its own set-up and parameterization during Exercise 4b and a range of ^{137}Cs concentrations in water and sediments were produced which may be regarded as some kind of model uncertainty assessment.

The dispersion models used in the Pacific Ocean radiological scenario are summarized in Table 10. More detailed descriptions are given in the corresponding annexes and respective references. Some of these models make their own calculation of hydrodynamics (e.g. SELFE/IMMSP/KIOST, NTUA, Sisbahia (Sistema Base de Hidrodinamica Ambientál) models), while others import water circulation from operative ocean forecasting models (e.g. KAERI, JAEA and USEV models). The characteristics of these ocean circulation models are briefly described in Annex XI except for SELFE which is provided in Annex IV. A comparison of hydrodynamic model outputs was necessary to carry out Exercise 2, since a common hydrodynamic description to be used by all models had to be selected. Such a quantitative comparison of hydrodynamic model outputs is described in Section 3.3.2. The results of Exercises 1–4 described above are discussed in detail in sections 3.2 to 3.5

TABLE 9. MODELLING EXERCISES CARRIED OUT FOR THE PACIFIC OCEAN RADIOLOGICAL SCENARIO

Exercise	Features	Source	Radionuclide
1	Own circulation and parameters	Hypothetical	Tracer
2	Same circulation, own parameters	Hypothetical	Tracer; ¹³⁷ Cs
3	Same circulation and parameters	Hypothetical	Tracer; ¹³⁷ Cs
4a	Same circulation and parameters	Realistic	¹³⁷ Cs
4b	Own circulation and parameters	Realistic	¹³⁷ Cs

TABLE 10. MODELS APPLIED TO SIMULATE FUKUSHIMA RELEASES IN THE PACIFIC OCEAN

Model	Country	Circulation
SELFE/IMMSP/KIOST	Ukraine/Rep. of Korea	Own
KAERI LORAS* model	Rep. of Korea	NCOM** and JCOPE2***
NTUA	Greece	Own
JAEA SEA-GEARN model	Japan	Univ. of Kyoto
USEV 3-D model	Spain	JCOPE2
Sisbahia model	Brazil	Own

Notes: The origin of water circulation is also given. ‘Own’ means that the circulation is calculated by the model; in other cases the name of the ocean forecasting model is given.

* Lagrangian Oceanic Radiological Assessment System

** Navy Coastal Ocean Model

*** Japanese Coastal Ocean Predictability Experiment

3.2. EXERCISE 1: INITIAL MODEL COMPARISON

3.2.1. Modelling exercise

A very simple exercise was initially carried out to compare the performance of models under simple conditions. A constant source of a perfectly conservative radionuclide (tracer) was considered. The magnitude of the input/source term was arbitrarily defined as 1.0×10^6 Bq/s of a long lived radionuclide (i.e. radioactive decay can be omitted). The release is modelled to start on 26 March 2011, and the time frame of calculations extends until 30 May 2011.

Each model is run using varied water circulation as summarized in Table 10 and set or required parameters. The output of the models is a time series of tracer concentration in surface water at three points aligned with the Fukushima Daiichi NPP (P1, P2 and P3), and at various distances from it. The locations of these points are presented in Figure 11.

3.2.2. Results

The time series of calculated concentrations in the ocean surface for the three considered points are illustrated in Figures 12–14. JAEA has applied two models, i.e. a finite difference (JAEA FDM) and a particle-tracking model (JAEA PT). KAERI has run the same model using circulation from two hydrodynamic models, i.e. JCOPE2 and NCOM.

Point P1 is some tens of kilometres offshore from Fukushima. The arrival of the signal to P1 is similar for all models, although in the case of the SELFE/IMMSP/KIOST model (denoted by the abbreviation I/K or I/K-E when running in Eulerian form) there is a delay of approximately 20 days with respect to the others. Predicted concentrations extend over two to three orders of magnitude. Even at the closest point to Fukushima (P2, Figure 13), predictions expand over

several orders of magnitude. A very noisy signal is produced by all models at P2 and this is attributed to the very rapidly changing water speeds and directions, as is described below.

In the case of point P3 (see Figure 14), it is interesting to note that the arrival of the signal is similar for most models, i.e. approximately 40 days. Again, predictions expand over several orders of magnitude and differences between particle-tracking (i.e. KAERI, JAEA PT) and finite difference techniques (i.e. JAEA FDM, I/K-E) are clearly apparent in this figure. Finite differences introduce artificial (numerical) diffusion and thus, once the signal has arrived at the location of interest, a continuous line is obtained for the time series of concentrations. However, numerical diffusion is not introduced by particle-tracking methods. These models give a concentration above zero at a given location only if there is at least one particle there. Consequently, periods with zero concentration may alternate with periods during which some finite concentration is computed, as can be seen in the results of KAERI model (see Figure 14).

As an example, maps showing the distribution of the tracer for surface water at the end of the simulation for some models are presented in Figure 15. The two simulations of JAEA show similar dispersion patterns since they are using the same water circulation. Nevertheless, the more diffusive character of Eulerian models is clearly shown. In the case of the I/K model the dominant transport is directed to the northeast, while the KAERI model produces a rather isotropic pattern around Fukushima. All models predict a contaminated band along the coast, although with different values for the concentrations. A better agreement between the outputs of dispersion models is expected if the same water circulation is used by each model and this is carried out in Exercise 2. A previous step is to define which is the most appropriate hydrodynamic model to be used and a quantitative comparison between hydrodynamic models was carried out for this purpose and is described in Section 3.3.2. Essentially, calculated sea surface temperature fields have been compared with fields obtained from satellite observations, and differences between them have been evaluated.

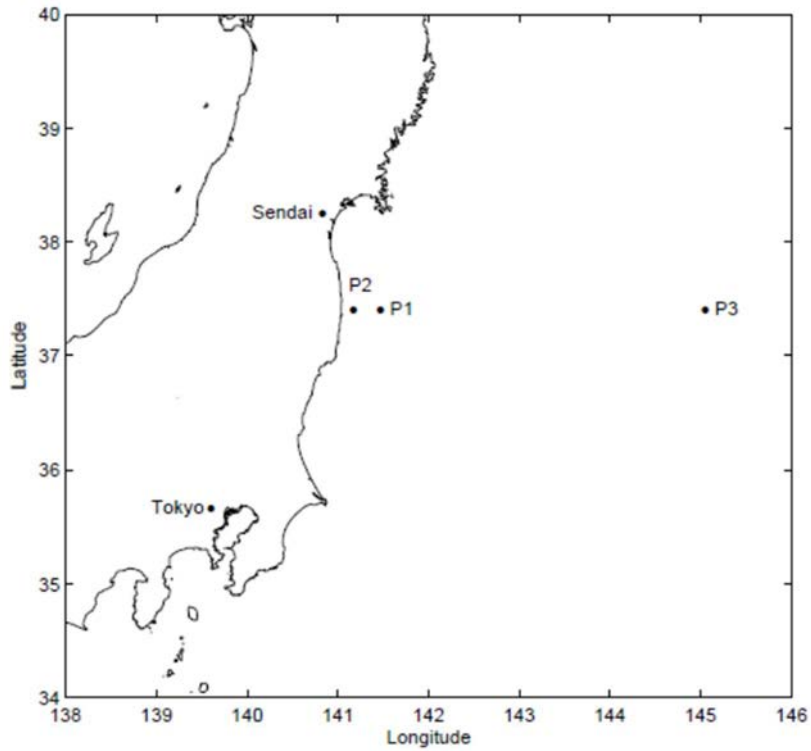


FIG. 11. Points (P1, P2 and P3) where the outputs from the applied dispersion models are provided.

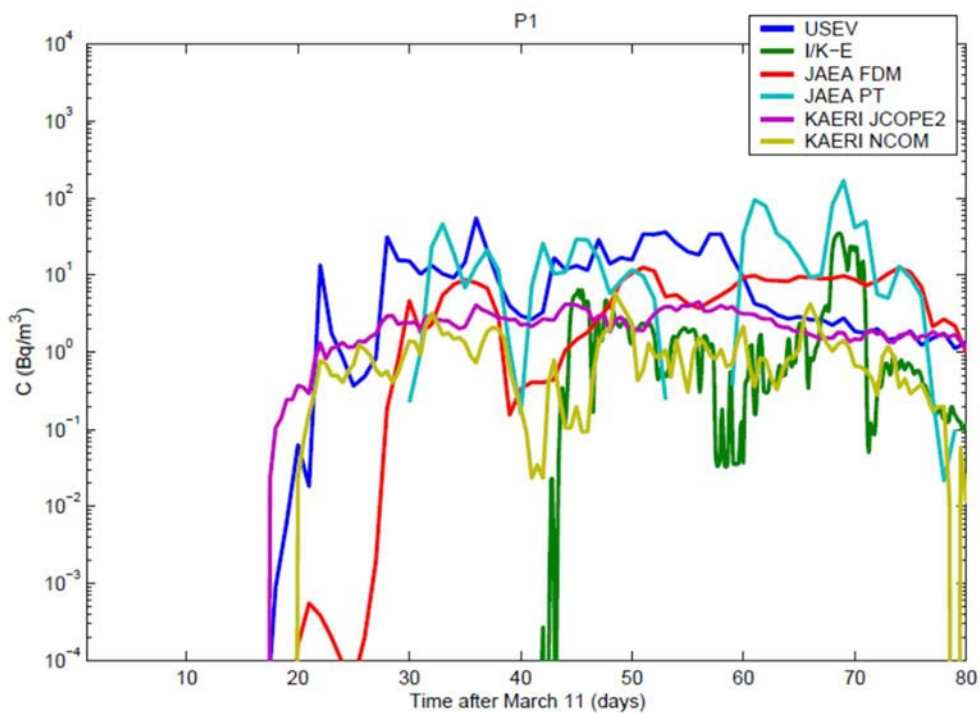


FIG. 12. Calculated concentrations (Bq/m³) for surface water at point P1 for Exercise 1. I/K-E means the IMMSP/KIOST model running in Eulerian form.

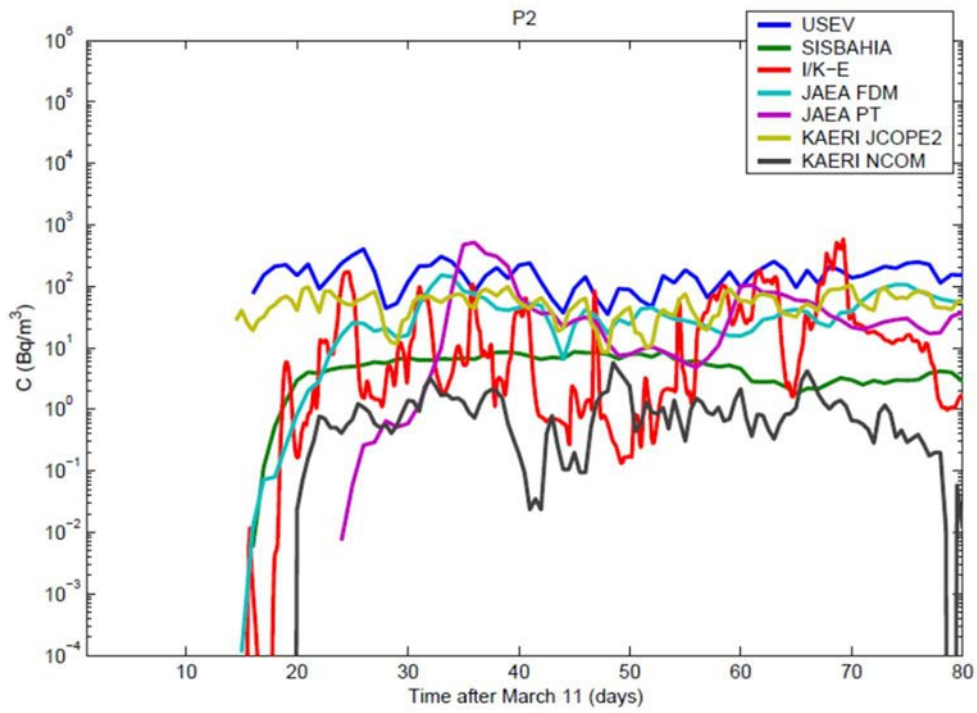


FIG. 13. Calculated concentrations (Bq/m³) for surface water at point P2 for Exercise 1.

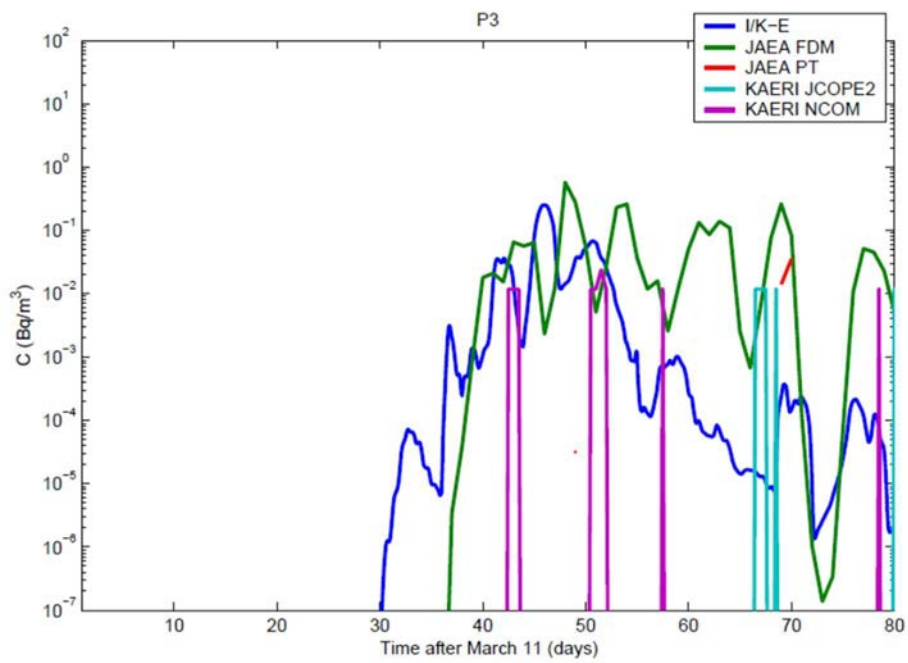


FIG. 14. Calculated concentrations (Bq/m³) for surface water at point P3 for Exercise 1.

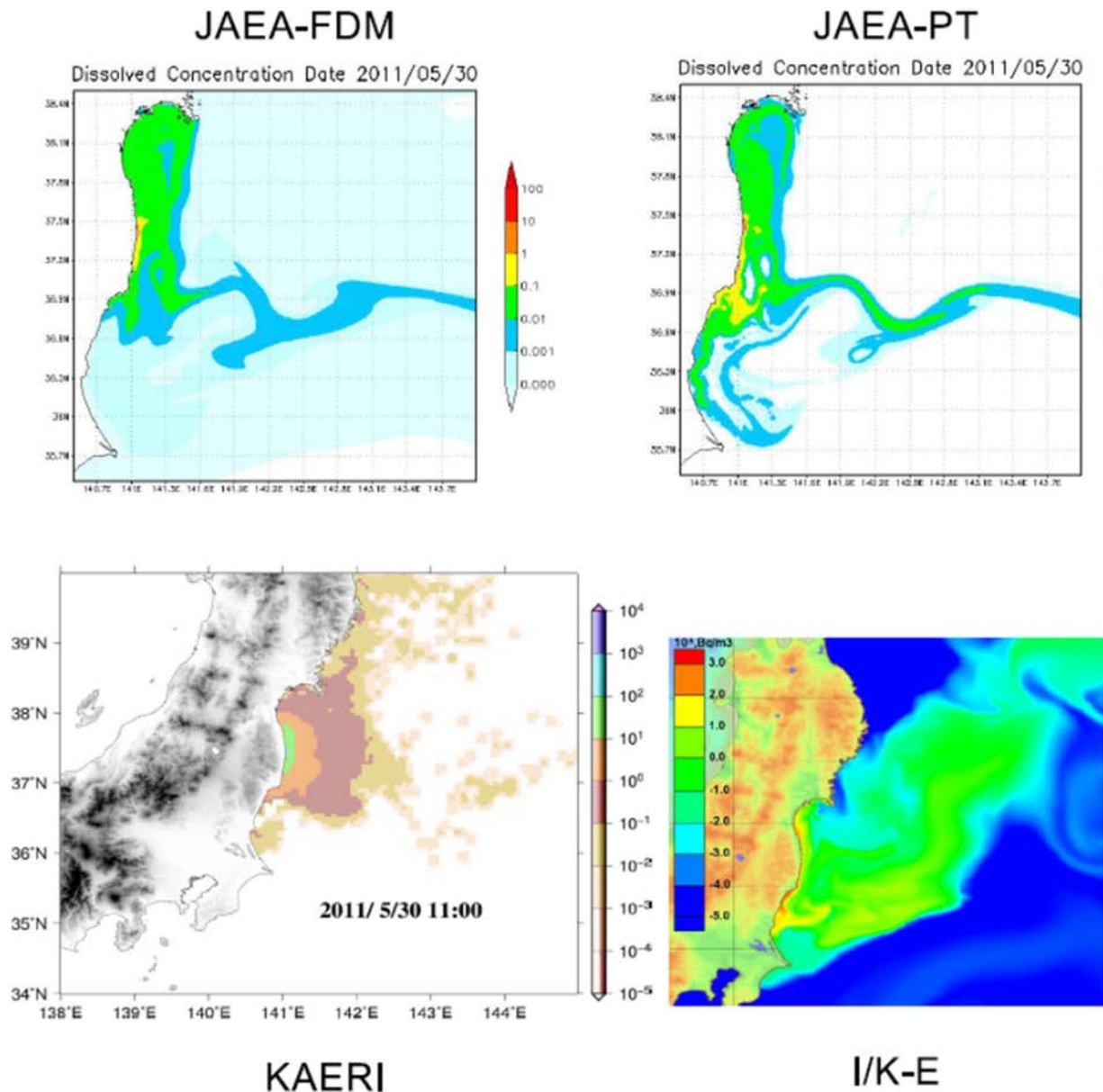


FIG. 15. Calculated concentrations (Bq/m^3) for surface water at the end of the simulation period.

3.3. EXERCISE 2: HOMOGENIZATION OF WATER CIRCULATION

3.3.1. Introduction

Exercise 2 was carried out using the same water circulation for all models. Water circulation computed by the hydrodynamic model JCOPE2 was used and, as in the case of Exercise 1, the magnitude of the input/source term is 1.0×10^6 Bq/s of a long lived radionuclide so that radioactive decay can be ignored. The release is modelled to start on 26 March 2011 and the time frame of calculations extends until 30 May 2011.

The exercise was carried out for two cases: a tracer (perfectly conservative radionuclide) and ¹³⁷Cs (including interactions with bed sediments). Thus, the first case is exactly the same as Exercise 1, but using the same water circulation for all models. Other model settings are left as

originally defined and each model also uses its own configuration and parameters to define water–sediment interactions.

As a result of the comparison of hydrodynamic fields described in sections 3.3.2 and 3.3.3, mean daily 3-D water currents computed by JCOPE2 were used and models were appropriately modified to import the data. In the case of the tracer, model end points are exactly the same as in Exercise 1, i.e. a time series of tracer concentration in the water surface for points P1, P2 and P3. Time series at the same points are provided for ^{137}Cs , but for surface water, bottom water (in the deepest layer, in contact with the seabed) and sediment.

3.3.2. Comparison of hydrodynamic fields

Given the significant discrepancies in model results, even in the very simple case of Exercise 1 with a perfectly conservative non-decaying radionuclide and a constant release, the first task consisted of comparing the output of the hydrodynamic models which were used to calculate dispersion. Following this comparison, the most adequate hydrodynamic model to be used in all the dispersion models was selected.

Water currents in the sea surface for 26 March 2011 calculated by some hydrodynamic models are presented in Figure 16. It is clear the overall picture provided by all models is similar, i.e. the Kuroshio current, flowing to the northeast is clearly visible. But clear differences can also be appreciated, with meanders and gyres which are produced by some models but not by others.

A closer inspection of hydrodynamic outputs was carried out by comparing the time series of current magnitude and direction. Water currents at the sea surface and also at mid-depth have been extracted from the models. The same points defined in Exercise 1 were used. As an example, these time series are presented in Figure 17 for P2 at the sea surface, with this being the closest point to the Fukushima Daiichi NPP for which model outputs were produced. The order of magnitude of the calculated currents is the same, but there are significant differences between models if the current magnitude and its direction are compared for a given instant of time. Consequently, it is not surprising there are significant differences in calculated radionuclide concentrations between the models, even in the simple case of Exercise 1. The different water velocities and directions in the vicinity of the release point lead to significantly different dispersion paths in the initial stages, which in turn implies that significantly different radionuclide concentrations are produced by the models.

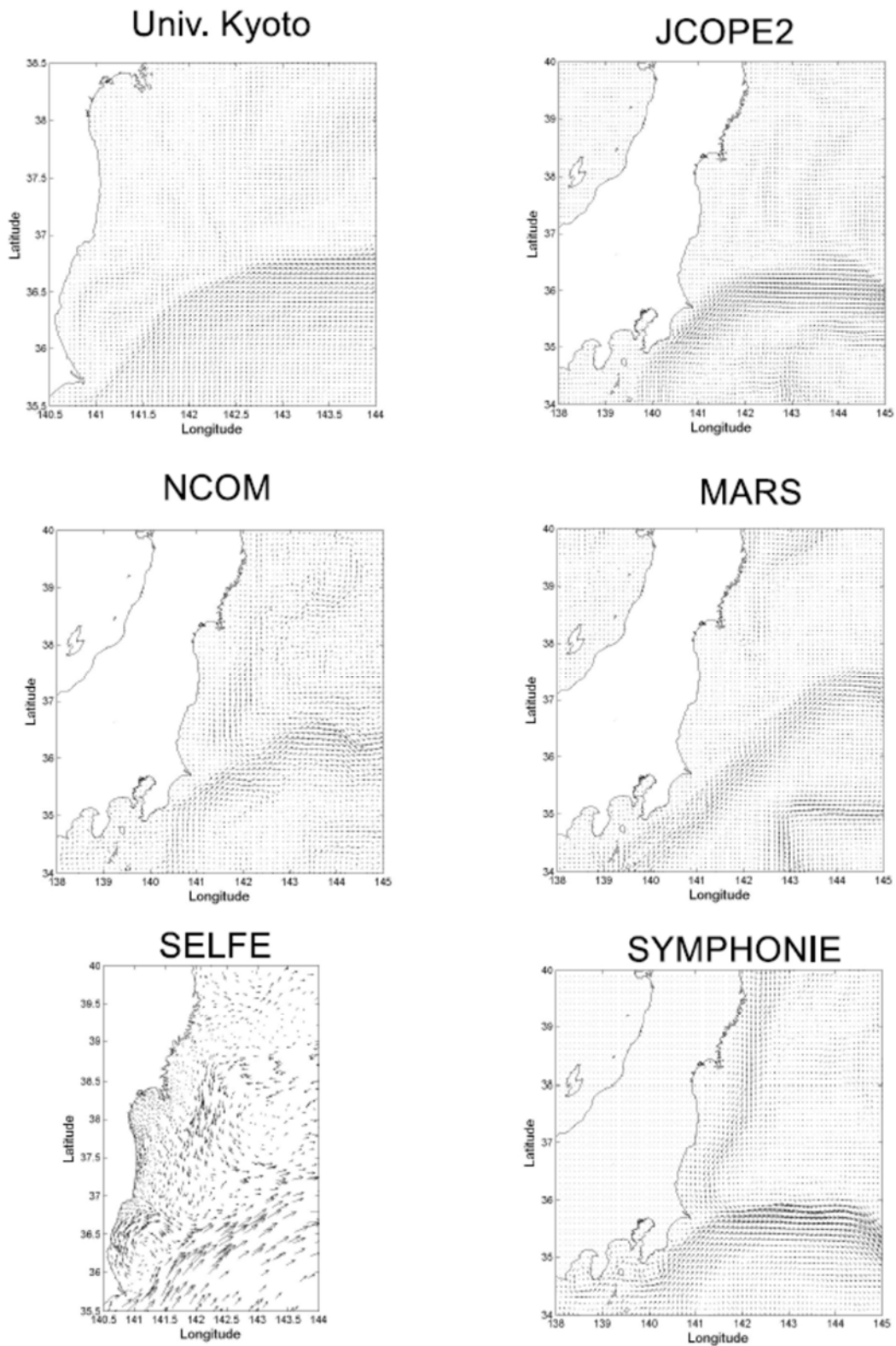


FIG. 16. Water currents in the sea surface for 26 March 2011 calculated by some hydrodynamic models.

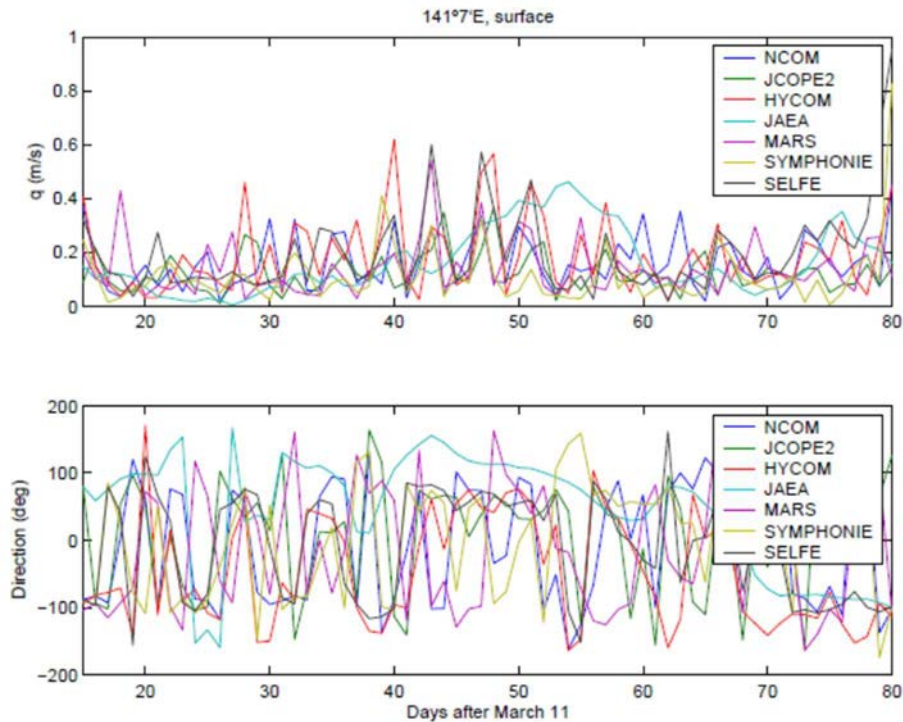


FIG. 17. Time series of surface current magnitude and direction calculated by the different hydrodynamic models in point P2. Current direction is measured in degrees counterclockwise from east.

3.3.3. Quantitative comparison

An objective comparison between calculated sea surface temperature (SST) fields and satellite observations was carried out to evaluate closeness between hydrodynamic model fields and to then assess which model may provide the most realistic picture of circulation. SST fields have been used since they can be more easily handled than current fields (i.e. it is a scalar instead of a vectorial field). Moreover, SST can be easily obtained from satellite observations. Finally, SST is essential in determining baroclinic circulation and a good SST description is required in order to have a realistic representation of circulation.

The SST gridded fields averaged for the first week of April 2011 were provided by 7 regional models and one local model. In this exercise only regional models are analysed. The models are:

- (1) HYCOM (Hybrid Coordinate Ocean Model);
- (2) JAEA (University of Kyoto);
- (3) JCOPE2;
- (4) MARS;
- (5) NCOM;
- (6) SELFE;
- (7) SYMPHONIE.

The hydrodynamic models used are briefly described in Annex XI, except for SELFE which is provided in Annex IV.

3.3.3.1. Methodology

The computed fields were interpolated on the same regular grid with 200×200 cells for a domain extending $140.5\text{--}144^\circ\text{E}$ in longitude and $35.5\text{--}38^\circ\text{N}$ in latitude. The same coastal line mask was applied to all data and the daily satellite SST fields were averaged, after which remaining gaps in observations were filled by linear interpolation from surrounding areas. The field was smoothed and interpolated into the same grid as computation data. The resulting observed SST field is shown in Figure 18, where the computed fields of SST are also shown in the same scale as the observed field and the ensemble averaged SST field is also given.

A simple method of classification (e.g. etalon-field [63]) was applied and, at a first step, the data matrix for SST anomalies was obtained by subtracting the model ensemble SST field from each model field. At a second step the geometric similarity between field pairs was identified using the criterion based on a sign of anomaly of two fields:

$$\rho = \frac{M_+ - M_-}{M}, -1 < \rho < 1 \quad (1)$$

where:

M_+ is the number of grid points in which sign of anomaly in the field pair coincides;
 M_- is the number of grid points in which sign of anomaly in the field pair is opposite;
 $M_+ + M_- = M$ is total number of grid points.

The square symmetric matrix R represents similarity between fields of anomalies:

$$R = \begin{pmatrix} \rho_{11} & \rho_{12} & K & \rho_{1j} & K & \rho_{1N} \\ K & K & K & K & K & K \\ \rho_{i1} & \rho_{i2} & K & \rho_{ij} & K & \rho_{iN} \\ K & K & K & K & K & K \\ \rho_{N1} & \rho_{N2} & K & \rho_{Nj} & K & \rho_{NN} \end{pmatrix} = \begin{pmatrix} 1 & \rho_{12} & K & \rho_{1j} & K & \rho_{1N} \\ K & K & K & K & K & K \\ \rho_{i1} & \rho_{i2} & K & \rho_{ij} & K & \rho_{iN} \\ K & K & K & K & K & K \\ \rho_{N1} & \rho_{N2} & K & \rho_{Nj} & K & 1 \end{pmatrix} \quad (2)$$

where:

N is number of fields in the ensemble.

At a third step the mean square distance between two fields is used as second criterion of similarity:

$$\eta_{i,j}^2 = \frac{1}{N} \sum_{k=1}^N (\Delta T_{i,k} - \Delta T_{j,k})^2 \quad (3)$$

where:

$\Delta T_{i,k}$ and $\Delta T_{j,k}$ are values of SST in point k of the grid from two fields i and j .

The square symmetric matrix η represents distance between fields of anomalies:

$$\eta = \begin{pmatrix} \eta_{11} & \rho_{12} & K & \eta_{1j} & K & \eta_{1N} \\ K & K & K & K & K & K \\ \eta_{i1} & \eta_{i2} & K & \eta_{ij} & K & \eta_{iN} \\ K & K & K & K & K & K \\ \eta_{N1} & \eta_{N2} & K & \eta_{Nj} & K & \eta_{NN} \end{pmatrix} = \begin{pmatrix} 0 & \eta_{12} & K & \eta_{1j} & K & \eta_{1N} \\ K & K & K & K & K & K \\ \eta_{i1} & \eta_{i2} & K & \eta_{ij} & K & \eta_{iN} \\ K & K & K & K & K & K \\ \eta_{N1} & \eta_{N2} & K & \eta_{Nj} & K & 0 \end{pmatrix} \quad (4)$$

The ρ and η criteria are used at a fourth step to divide fields on classes and to choose field-etalon representing fields in class.

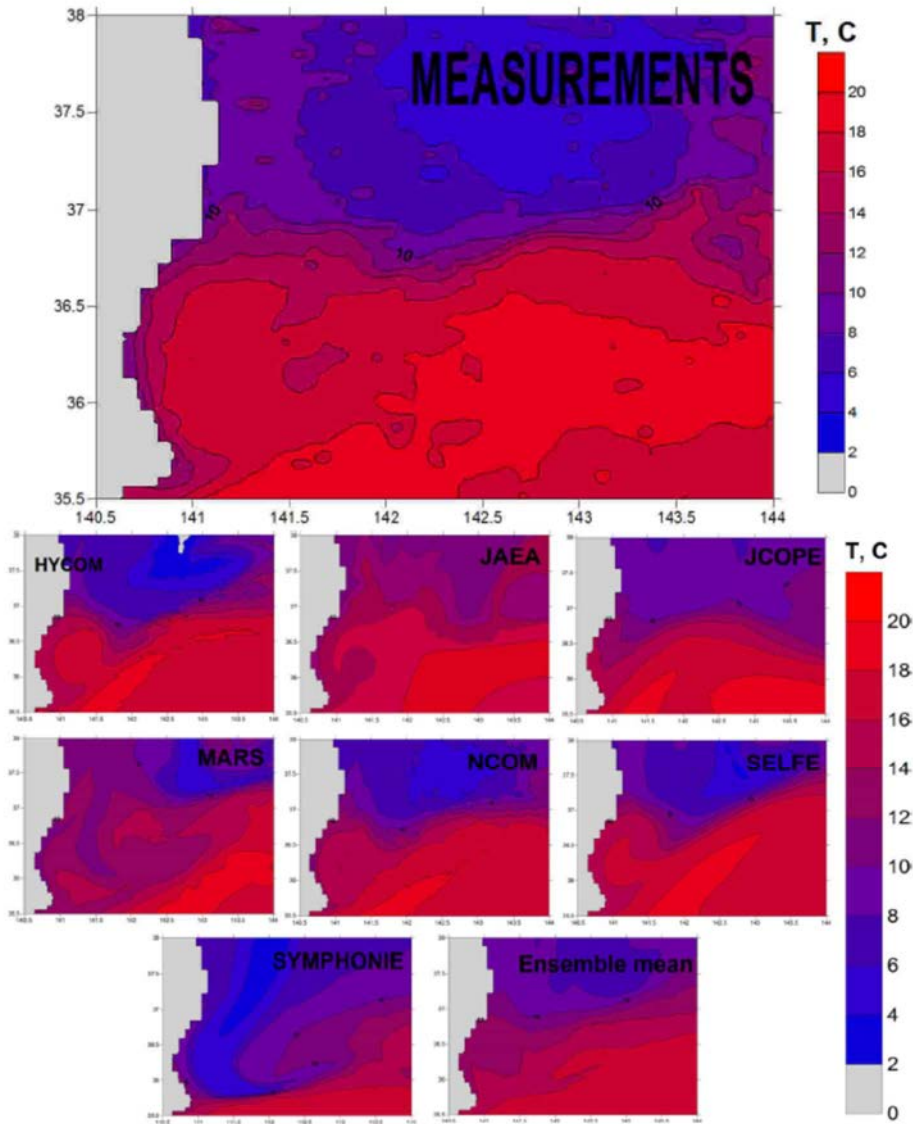


FIG. 18. SST field deduced from satellite observations and fields calculated by the different models. The ensemble averaged SST field is shown in the last panel.

3.3.3.2. Results and Conclusions

Initially seven model fields were compared. The matrices R and η are given in Tables 11 and 12, where the symmetric matrix R describes the correlation in range (-1; +1) between pairs of fields. Positive values mean that anomalies on more than 50% of the area have the same sign and the bottom row is the model averaged value, ρ_j , describing similarity of a given field to the rest of the fields. The overall averaged value for the matrix R is $\bar{\rho} = 0.21$. The matrix η is the mean square distance of a given field to the rest of fields and the overall averaged value is $\bar{\eta} = 2.95^\circ\text{C}$.

The first class of fields can be separated for $\rho_j > \bar{\rho}$. Five fields belong to the first class, i.e. HYCOM, JAEA, JCOPE2, NCOM and SELFE and all of these fields (except JAEA) also satisfy another condition, i.e. $\bar{\eta} > \eta_j$. The remaining fields belong to other classes. From the first class two fields can be chosen as etalon-fields, i.e. NCOM and SELFE.

Regarding similarity with the observed SST field, the modelled field and observed field were subtracted from the average of 8 fields and the matrices R and η are summarized in Tables 13 and 14. The overall averaged values are $\bar{\rho} = 0.222$ and $\bar{\eta} = 2.86^\circ\text{C}$. Table 13 shows that observed SST has the highest correlation with HYCOM, NCOM and SELFE fields and that the closest distance is again for the HYCOM, NCOM and SELFE fields.

The first class of fields can be separated by criterion $\rho_j > \bar{\rho}$, with five fields belonging to the first class, i.e. HYCOM, JAEA, NCOM, SELFE and observed SST, with JCOPE2 in the field $\rho_j = \bar{\rho}$. With the exception of JAEA, these fields also satisfy another condition, i.e. $\bar{\eta} > \eta_j$. The remaining fields belong to another class. From the first class, one field can be chosen as etalon-fields, i.e. NCOM.

Some general observations concluded from this study are as follows:

- Visual inspection and objective classification agree in the conclusions derived from the analysis of SST field similarity in the chosen domain;
- The presented results show the ability of the method of classification to determine field analogues;
- The set of fields can be used to obtain a statistically valid classification of ensemble results;
- The method of classification can also be applied to the analysis of fields of calculated radionuclide concentrations.

During previous modelling work concerning the Fukushima Daiichi NPP accidental releases into the Pacific Ocean [56, 57], it was found that a better agreement between model calculations and measured ^{137}Cs concentrations in water and sediment was obtained if JCOPE2 circulation was used than with NCOM or HYCOM. SELFE results for the first dispersion exercise are significantly noisy. Moreover, the JCOPE2 field is within the limit $\rho_j = \bar{\rho}$ and satisfies the additional condition $\bar{\eta} > \eta_j$. Consequently, it is concluded that JCOPE2 is a reasonable selection to carry out the dispersion exercises described in the following sections, in which all models will use the same hydrodynamics.

TABLE 11. MATRIX R FOR SEVEN MODELS

HYCOM	JAEA	JCOPE2	MARS	NCOM	SELFE	SYMPHONIE
1	0.191	0.064	-0.218	0.798	0.729	-0.289
0.191	1	0.62	0.212	0.145	0.368	-0.529
0.064	0.62	1	-0.028	0.086	0.139	-0.195
-0.218	0.212	-0.028	1	-0.246	-0.084	-0.155
0.798	0.145	0.086	-0.246	1	0.646	-0.192
0.729	0.368	0.139	-0.084	0.646	1	-0.41
-0.289	-0.529	-0.195	-0.155	-0.192	-0.41	1
0.325	0.287	0.241	0.069	0.32	0.341	-0.11

TABLE 12. MATRIX η FOR SEVEN MODELS

HYCOM	JAEA	JCOPE2	MARS	NCOM	SELFE	SYMPHONIE
0	4.053	2.614	3.262	1.043	1.455	5.12
4.053	0	2.912	3.162	3.757	3.577	6.445
2.614	2.912	0	2.845	2.135	2.723	4.836
3.262	3.162	2.845	0	2.982	3.012	4.54
1.043	3.757	2.135	2.982	0	1.696	4.741
1.455	3.577	2.723	3.012	1.696	0	5.453
5.12	6.445	4.836	4.54	4.741	5.453	0
2.507	3.415	2.581	2.829	2.336	2.559	4.448

TABLE 13. MATRIX R FOR SEVEN MODELS AND OBSERVED SST FIELD

HYCOM	JAEA	JCOPE2	MARS	NCOM	SELFE	SYMPH.	Obs
1	0.204	0.029	-0.237	0.777	0.716	-0.316	0.61
0.204	1	0.613	0.201	0.163	0.395	-0.512	0.201
0.029	0.613	1	-0.005	0.068	0.149	-0.176	0.1
-0.237	0.201	-0.005	1	-0.275	-0.108	-0.099	-0.251
0.777	0.163	0.068	-0.275	1	0.62	-0.219	0.629
0.716	0.395	0.149	-0.108	0.62	1	-0.43	0.526
-0.316	-0.512	-0.176	-0.099	-0.219	-0.43	1	-0.256
0.61	0.201	0.1	-0.251	0.629	0.526	-0.256	1
0.348	0.283	0.222	0.028	0.346	0.359	-0.126	0.32

TABLE 14. MATRIX η FOR SEVEN MODELS AND OBSERVED SST FIELD

HYCOM	JAEA	JCOPE2	MARS	NCOM	SELFE	SYMPH.	Obs
0	4.053	2.614	3.262	1.043	1.455	5.12	1.525
4.053	0	2.912	3.162	3.757	3.577	6.445	3.724
2.614	2.912	0	2.845	2.135	2.723	4.836	2.246
3.262	3.162	2.845	0	2.982	3.012	4.54	3.235
1.043	3.757	2.135	2.982	0	1.696	4.741	1.242
1.455	3.577	2.723	3.012	1.696	0	5.453	2.055
5.12	6.445	4.836	4.54	4.741	5.453	0	5.253
1.525	3.724	2.246	3.235	1.242	2.055	5.253	0
2.384	3.454	2.539	2.88	2.2	2.496	4.548	2.41

3.3.4. Tracer dispersion

Results for the tracer dispersion exercise are presented in Figure 19 where it can be observed that the agreement between models has been significantly improved. The shapes of the signals are much more similar than in Exercise 1. Results are within one order of magnitude with the exception of both the Sisbahia and NTUA models. The NTUA model is highly dispersive, since radionuclides reach point P3 essentially instantaneously after release, as can be observed in the lowest panel of Figure 19.

Although there are times and locations where some significant differences between models still remain (see for example point P1, some 30 days after 11 March 2011), most of the variability has been removed by use of the same water circulation when the transport of a tracer is simulated.

3.3.5. ^{137}Cs dispersion

The modelling of ^{137}Cs dispersion, which includes interactions with sediment, was also carried out for Exercise 2. To simplify the problem, it was assumed that bed sediments are uniform over all of the model domain and are composed entirely of fine material (clays) with a mean size of 10 μm . A uniform porosity of 0.6 was assumed and, finally, the thickness of the bed sediment which interacts with water was set to 10 cm. With this homogenization it is assured that differences between model outputs are due to intrinsic factors of the models, but not to input data. Thus, hypothetical, but realistic, values for some parameters may be used. Time series of ^{137}Cs concentrations for surface water, bottom water (deepest water layer, in contact with the seabed) are provided at points P1 to P3, as described above.

The results of these experiments are summarized in Figures 20–22. In the case of surface water, results from all models are similar, as per the tracer exercise. The reason for this is that surface water does not feel the presence of the bed sediment, especially when water depth increases. Exceptions are again the Sisbahia and NTUA models. Signal arrival at point P3 produced by the KAERI and JAEA models is in very good agreement, and the NTUA model produced very high concentrations too quickly.

In the case of bottom water, very low concentrations were calculated by all models at point P1 (see Figure 20). At P2, which is close to the Fukushima release point, higher concentrations were calculated in the bottom water, with the signal being similar for most models.

The majority of the variability between models now occurs for activity concentrations in sediment. At point P2 (see Figure 21), for instance, results vary over several orders of magnitude. In general, the JAEA model tends to produce lower concentrations in sediments than the other models. The NTUA model produces significant concentrations in bottom water and sediment at point P3, while zero concentrations are calculated by the other models.

Maps showing the computed distribution of ^{137}Cs in surface water and sediment are presented in Figures 23 and 24, respectively, for the JAEA and Sisbahia model as examples. The difference in scale of model domains makes a direct comparison difficult but, in general, it can be seen that the behaviour of the radionuclide patch is very similar, even in the case of sediment. In this case, there is an extension of contaminated sediment to the south of Fukushima and also along the shore of the Bay of Sendai to the north. These radionuclides appear as discrete spots in the case of the JAEA model, due to its Lagrangian nature, while a continuous patch is produced by the Sisbahia model.

In conclusion, it can be stated that when the dispersion of a tracer is simulated, a significant part of the variability between models is due to water circulation and that model agreement increases if the same circulation data is applied by all models.

In the case of ^{137}Cs , when water–sediment interactions are included, there are significant differences between models, with calculated concentrations in sediment expanding over several orders of magnitude. Nevertheless, agreement between models for water is similar to the tracer case. Each model used its own description for water–sediment interactions, as well as its own set of parameters for describing such processes. The next step is to homogenize the description of water–sediment interactions, using equivalent parameters in all models. This is the main objective of Exercise 3 which is described in the following section. Moreover, some additional harmonization between models was carried out which consisted of using the same topographic data and horizontal and vertical diffusion coefficients.

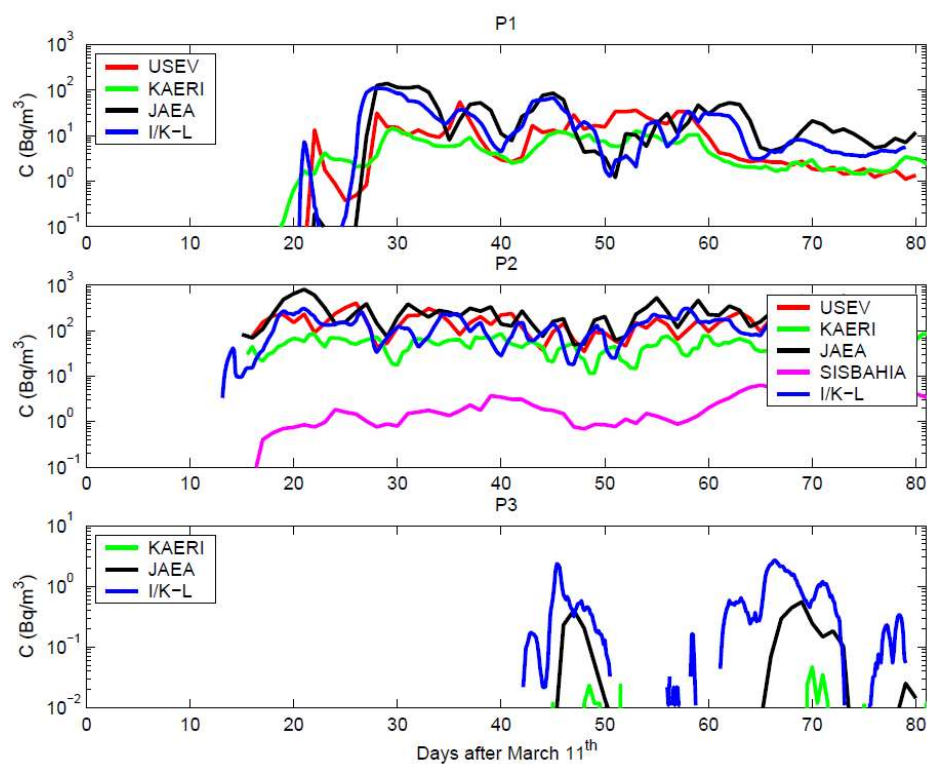


FIG. 19. Time series of radionuclide concentrations for surface water at points P1, P2 and P3 for Exercise 2, tracer dispersion. I/K-L denotes the IMMSP/KIOST model running in a Lagrangian framework.

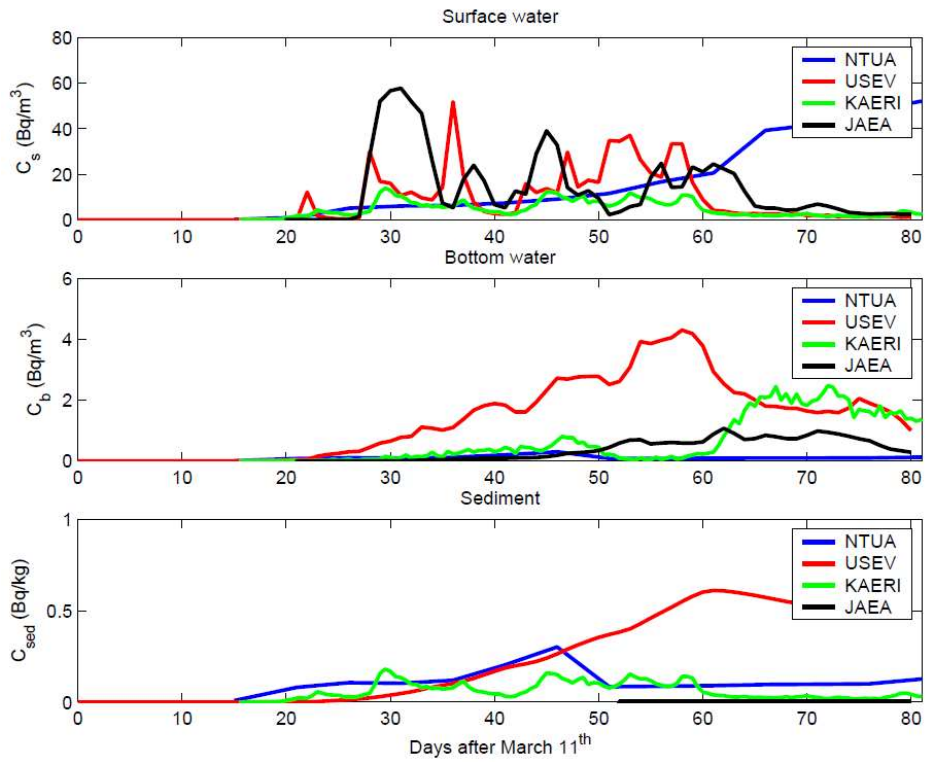


FIG. 20. Time series of radionuclide concentrations (^{137}Cs) at point P1 for surface water, bottom water and sediment for Exercise 2.

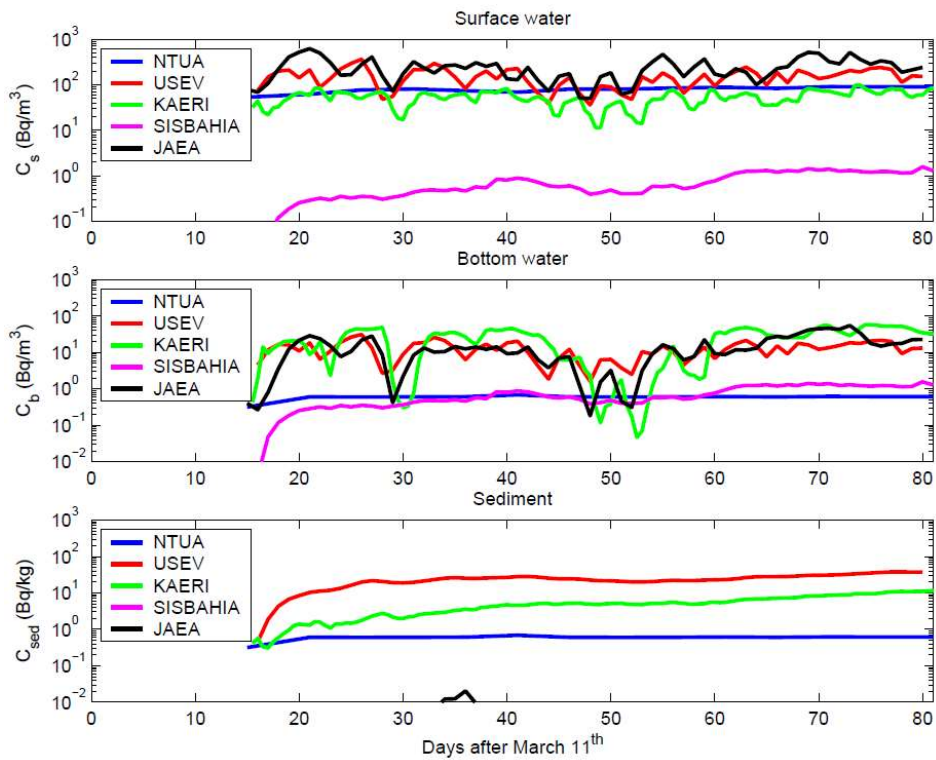


FIG. 21. Time series of radionuclide concentrations (^{137}Cs) at point P2 for surface water, bottom water and sediment for Exercise 2.

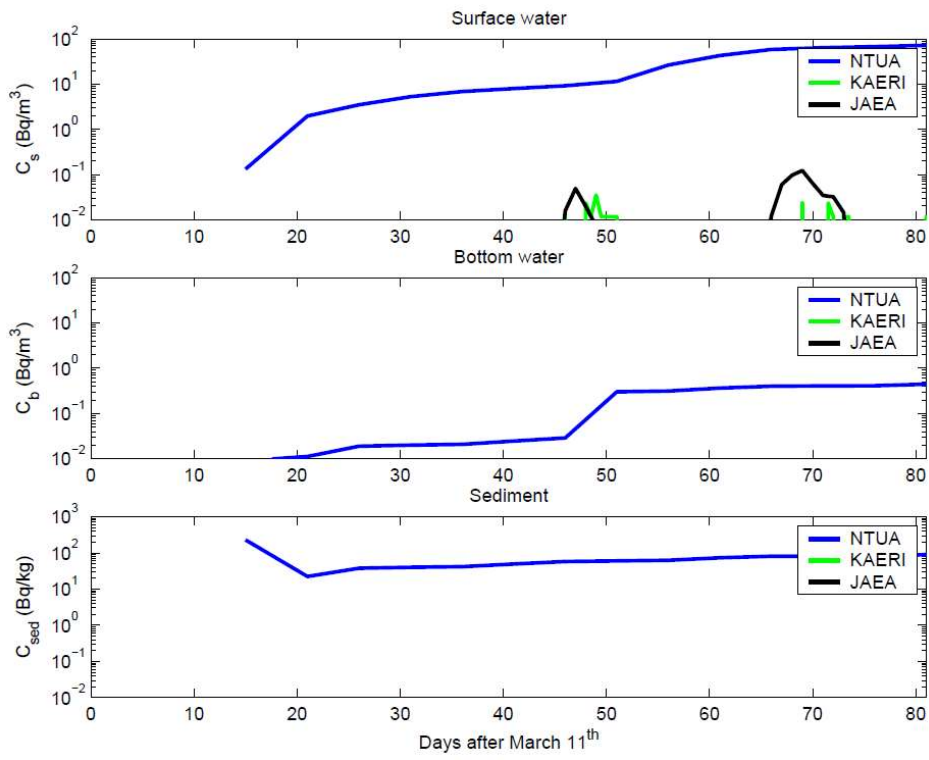


FIG. 22. Time series of radionuclide concentrations (^{137}Cs) at point P3 for surface water, bottom water and sediment for Exercise 2.

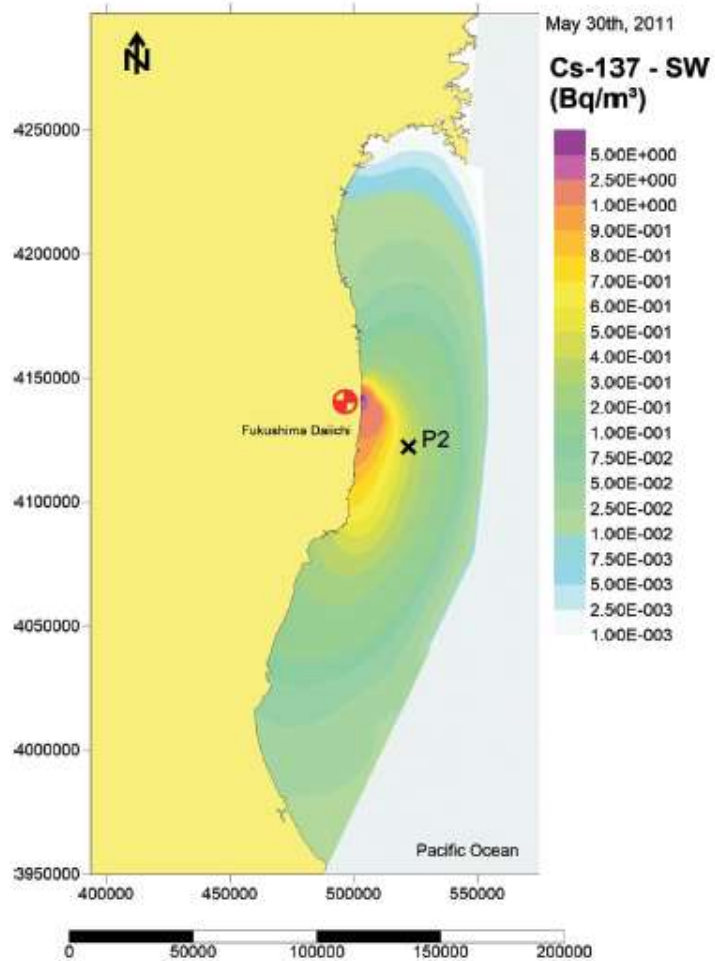
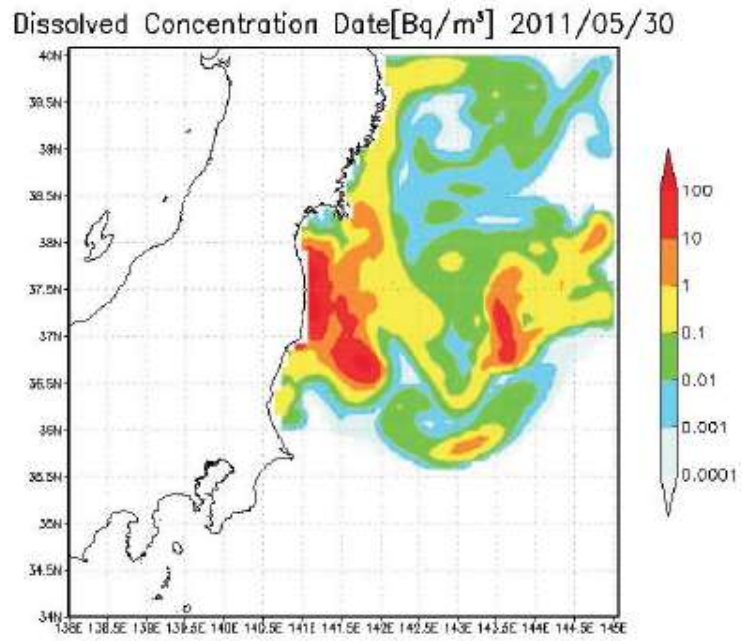


FIG. 23. Calculated ¹³⁷Cs distribution in surface water by JAEA (top) and Sisbahia (bottom) models.

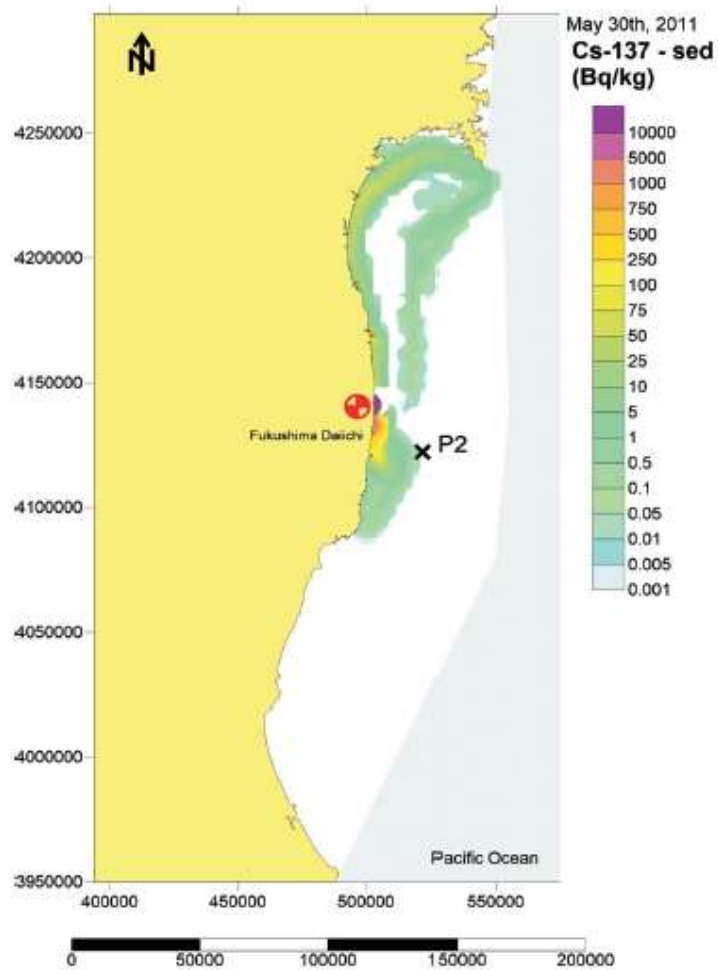
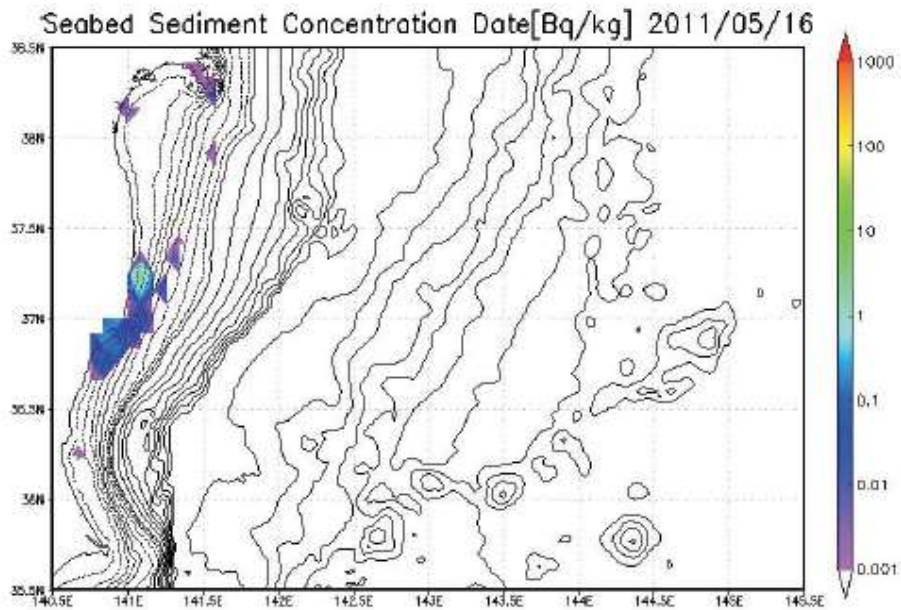


FIG. 24. Calculated ^{137}Cs distribution in sediment by JAEA (top) and Sisbahia (bottom) models.

3.4. EXERCISE 3: HOMOGENIZATION OF WATER–SEDIMENT INTERACTIONS

3.4.1. Introduction

This exercise is designed as in the previous cases. A constant release of 1.0×10^6 Bq/s of a long lived radionuclide (radioactive decay can be neglected) is used. The release starts on 26 March 2011 and the time frame of calculations extends until 30 May 2011. However, exactly the same bathymetric file was used for all models. The computational grid is presented in Figure 25. In addition, the same diffusion coefficients have been used. Constant and uniform reasonable values for diffusion coefficients have been defined. The purpose of using constant and uniform values is to remove additional variability between models which would be introduced if, for example, a Smagorinsky's scheme were to be used to compute the horizontal diffusion coefficient and/or any turbulence model were to be applied to calculate the vertical diffusivity. The fixed values for the horizontal and vertical diffusion coefficients, K_h and K_v , are:

$$K_h = 10 \text{ m}^2 / \text{s} \quad (5)$$

$$K_v = 1.0 \times 10^{-4} \text{ m}^2 / \text{s} \quad (6)$$

Exercise 3 consists of three parts, which are briefly summarized below and are described in more detail in the following sections.

- (1) Tracer: This considers the performance of models using a perfectly conservative radionuclide, as was done for Exercises 1 and 2.
- (2) ^{137}Cs and no SPM in the water column: It is equivalent to the ^{137}Cs case of Exercise 2. As previously, in order to simplify the problem, it was considered that bed sediments are uniform over the whole model domain and that they are composed entirely of fine material (clays) with mean size $10 \mu\text{m}$. A uniform porosity of 0.6 was assumed and, finally, the thickness of the sediment which interacts with water was set to 10 cm.

In addition, the same parameters were used to simulate uptake/release interactions with bed sediments. Models may use a distribution coefficient or, alternatively, kinetic transfer coefficients. Values for the two options have been defined and the equilibrium distribution coefficient is $2.0 \text{ m}^3/\text{kg}$. This is a mean value taken from Ref. [64] for open ocean water and in agreement with measurements taken off Fukushima [52]. The rate describing release from bed sediments is $k_2 = 1.16 \times 10^{-5} \text{ s}^{-1}$. The kinetic rate describing uptake (k_1) is derived from k_2 and the distribution coefficient [65].

- (3) ^{137}Cs with constant and uniform SPM in the water column: SPM concentration has been set as 5 mg/l and resuspension of particles from bed sediments back to the water column is not included in the calculations. Other parameters are required if SPM is included in the calculations. They are as follows:

- Particle diameter: $1 \mu\text{m}$;
- Particle density: 2600 kg/m^3 ;
- Settling velocity: derived from Stoke's law;
- Critical deposition stress: 0.5 N/m^2 .

End points of calculations are the same as defined previously, i.e. time series of radionuclide concentrations at points P1, P2 and P3. Radionuclide concentration for surface water is

provided for the tracer dispersion exercise and radionuclide concentration for the surface water, bottom water and sediment is provided for the ^{137}Cs exercises.

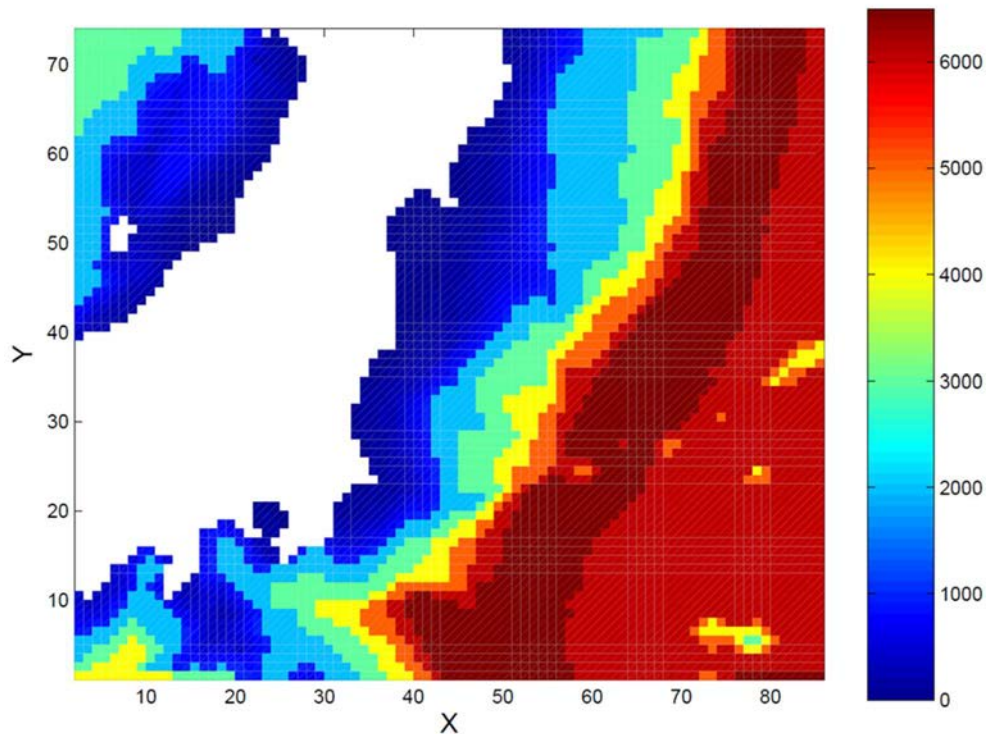


FIG. 25. Computational grid used by all models in Exercise 3. Water depths are given in m.

3.4.2. Tracer dispersion

Results for the tracer experiment are summarized in Figure 26 and are within the same order of magnitude for all models at points P1 and P2 (note that now a linear scale has been used for the y axis instead of a logarithmic one as previously). Thus, in general, the use of the same bathymetry and diffusion coefficients has slightly improved the agreement between models. Nevertheless, as can be seen from Exercises 1 and 2, the main factor in producing model discrepancies is water circulation. In other words, the agreement improvement is higher from Exercise 1 to 2 than from Exercise 2 to 3.

In the case of P3, results are similar to those of Exercise 2, where the agreement between models is relatively good for both the arrival of the signal and the calculated concentrations. The exception is the result of NTUA model which produces an instantaneous arrival of the signal and concentrations significantly higher than the other models.

3.4.3. ^{137}Cs dispersion and no SPM in the water column

Calculated time series for ^{137}Cs at points P1–P3 are presented in Figures 27–29. It can be seen that, for instance, at P2 the use of the same parameters has improved model agreement. Model results are, in general, within the same order of magnitude (note that logarithm scale is not used). In the case of sediment, the JAEA model produces lower concentrations than the KAERI

and USEV models at P1, which are more similar. In the case of P2, results from these three models are all similar. The NTUA model results do not seem consistent, since the model calculates very low concentrations in the bottom water and, simultaneously, concentrations in sediment are much higher than those of the other models (out of the scale range).

In the case of point P3, the new values defined for the diffusion coefficients lead to a very weak signal. ^{137}Cs does not seem to reach either the bottom water or the sediment. Again, the NTUA model predicts an instantaneous arrival of the radionuclide signal and very high concentrations in sediments at the initial time, which even reduce in time. These results again seem to be inconsistent.

3.4.4. ^{137}Cs dispersion and constant and uniform SPM distribution in the water column

As mentioned previously, this experiment was designed with a constant and uniform suspended matter concentration in the water column equal to 5 mg/l. Results for the three points are presented in Figures 30–32.

Essentially, the results are the same as in the previous exercise without SPM. This is not surprising given the relatively low affinity of ^{137}Cs to be fixed to solid particles. This affinity is quantified by the partition coefficient, which is defined as [65, 66]:

$$PC = \frac{1}{1 + k_d \cdot SPM} \quad (7)$$

where SPM is the suspended matter concentration and k_d the corresponding distribution coefficient of the radionuclide. This coefficient gives the fraction of radionuclides remaining dissolved, under equilibrium conditions, for a given k_d value and suspended matter concentration. For $SPM = 5 \text{ mg/L}$ and $k_d = 2 \times 10^3 \text{ L/kg}$, which are the values fixed for the exercise, a result of $PC = 0.99$ is obtained, indicating that most of ^{137}Cs remains in solution (99%), and is not significantly adsorbed on suspended particles. Hence, the contamination of bed sediments caused by deposition processes is also negligible. Contamination of bed sediments is mainly produced by direct adsorption of dissolved radionuclides present in the bottom water. The water–sediment interface may be considered as a high suspended matter environment [67]. Thus, the corresponding PC value would be significantly lower here and a significant fraction of ^{137}Cs would be adsorbed on bed sediments.

Maps showing the computed distribution of ^{137}Cs in surface water and sediment are presented in Figures 33 and 34, respectively, for the JAEA and KAERI models as examples. At a general level, it can be observed that the behaviour of the radionuclide patch is very similar, even in the case of sediment. For surface water, there is a remarkable agreement between both models. Essentially the same radionuclide patches are produced for surface water by these models.

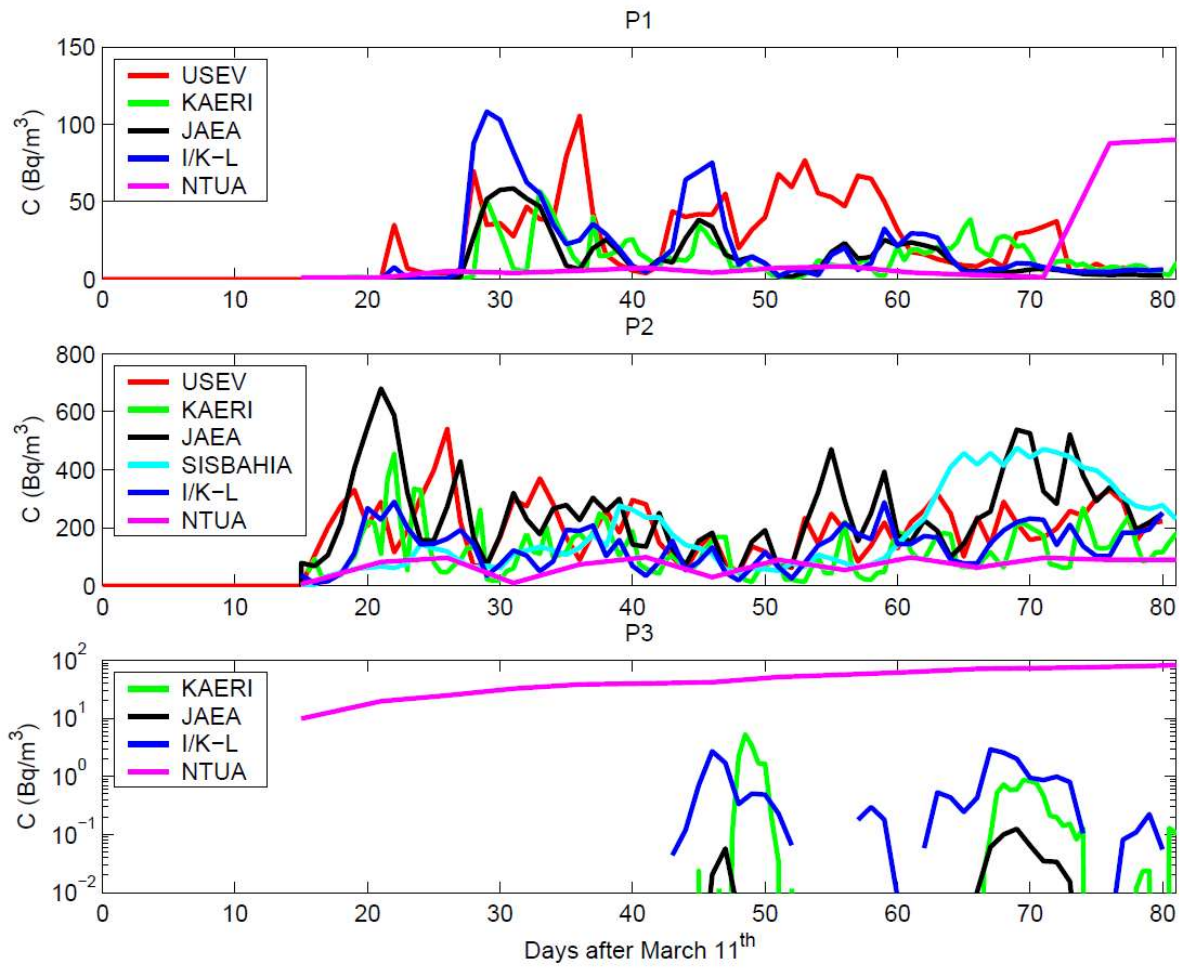


FIG. 26. Time series of radionuclide concentrations for surface water at points P1, P2 and P3 for Exercise 3, tracer dispersion.

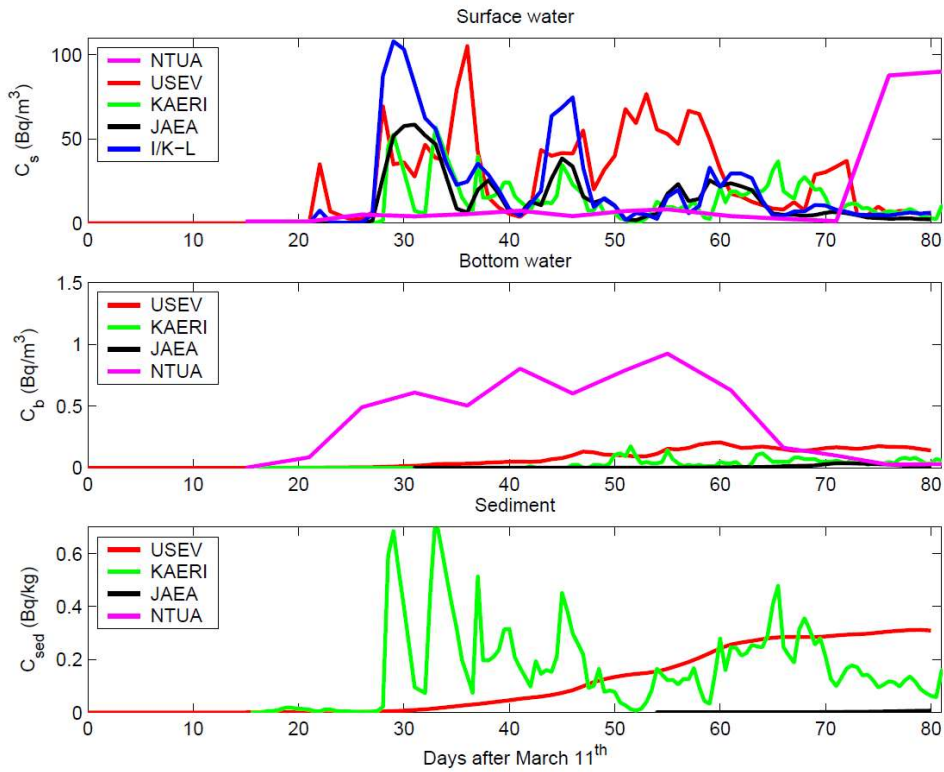


FIG. 27. Time series of radionuclide concentrations (^{137}Cs) at point P1 for surface water, bottom water and sediment. Exercise 3 without SPM.

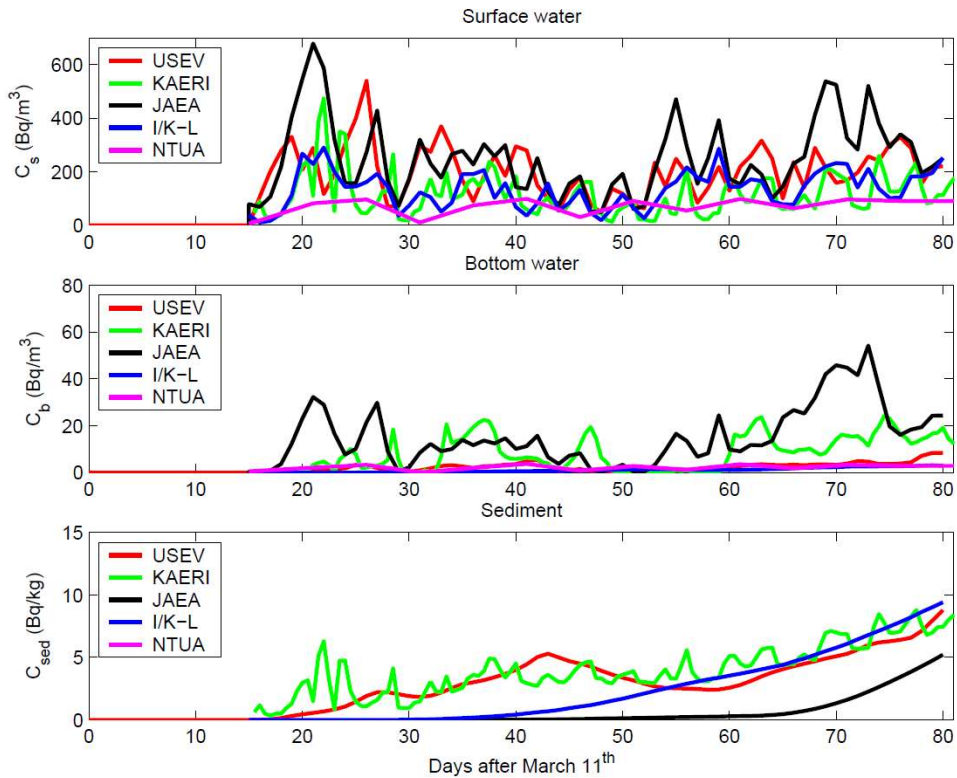


FIG. 28. Time series of radionuclide concentrations (^{137}Cs) at point P2 for surface water, bottom water and sediment. Exercise 3 without SPM.

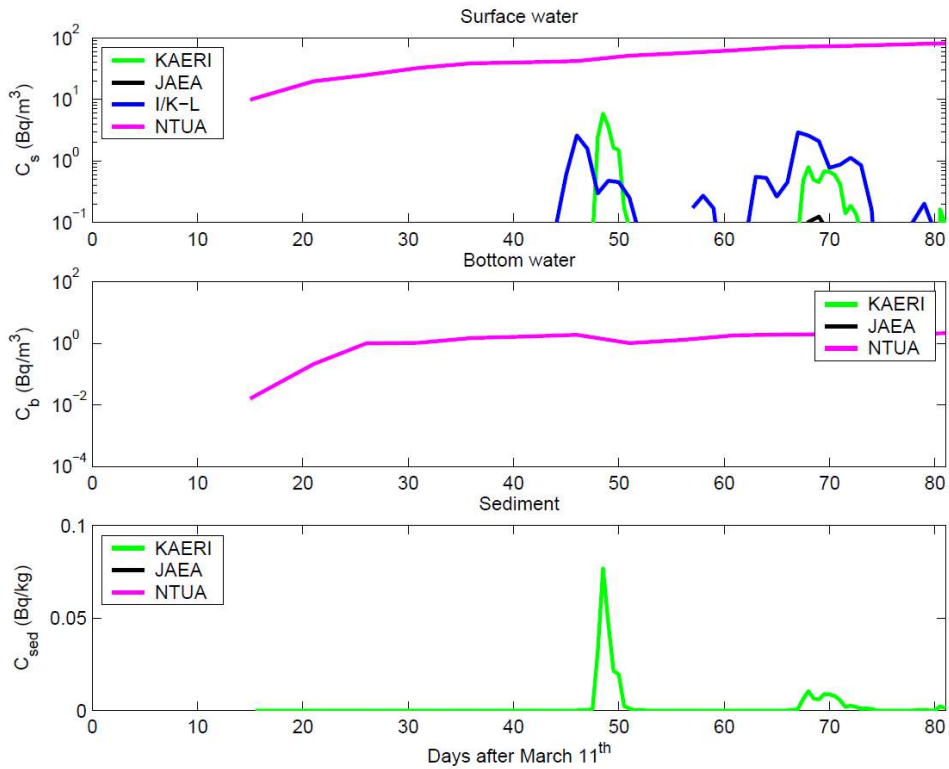


FIG. 29. Time series of radionuclide concentrations (^{137}Cs) at point P3 for surface water, bottom water and sediment. Exercise 3 without SPM.

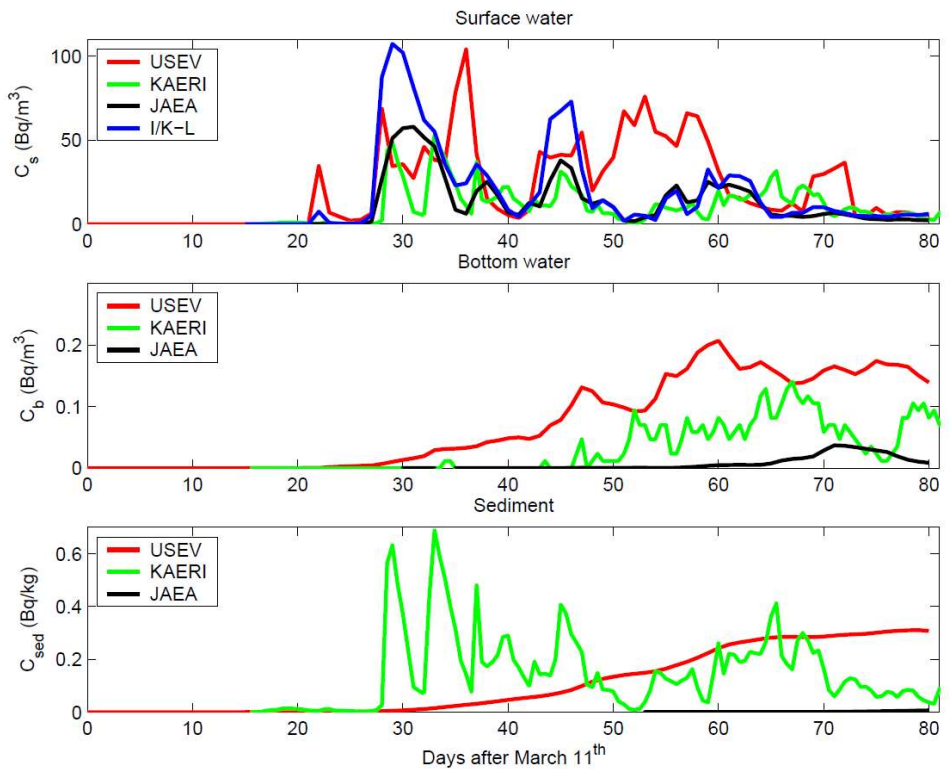


FIG. 30. Time series of radionuclide concentrations (^{137}Cs) at point P1 for surface water, bottom water and sediment. Exercise 3 with SPM.

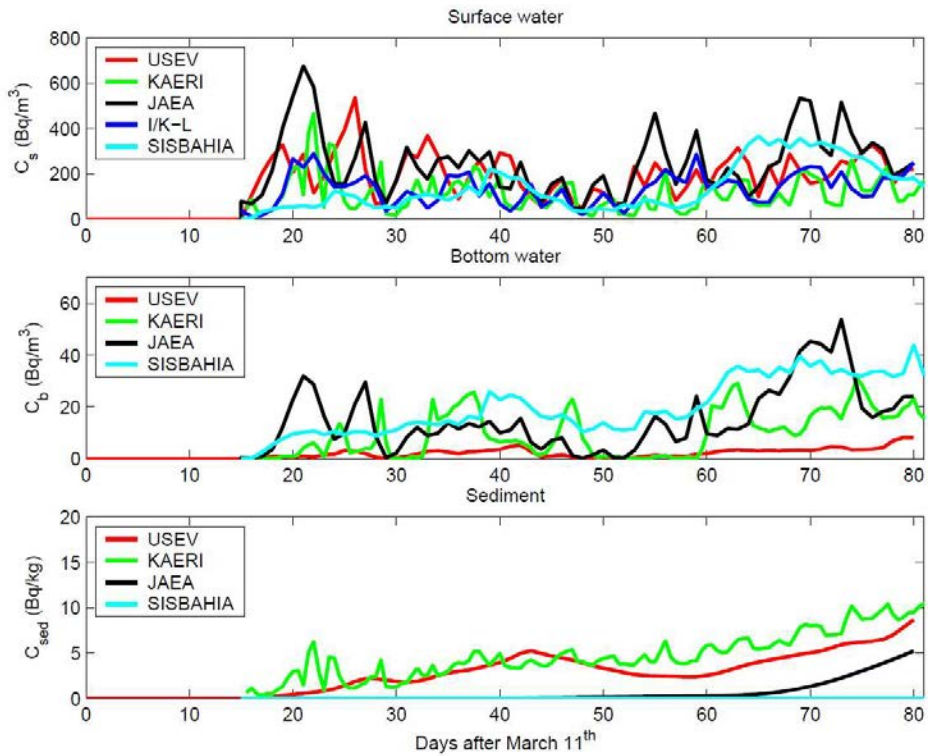


FIG. 31. Time series of radionuclide concentrations (^{137}Cs) at point P2 for surface water, bottom water and sediment. Exercise 3 with SPM.

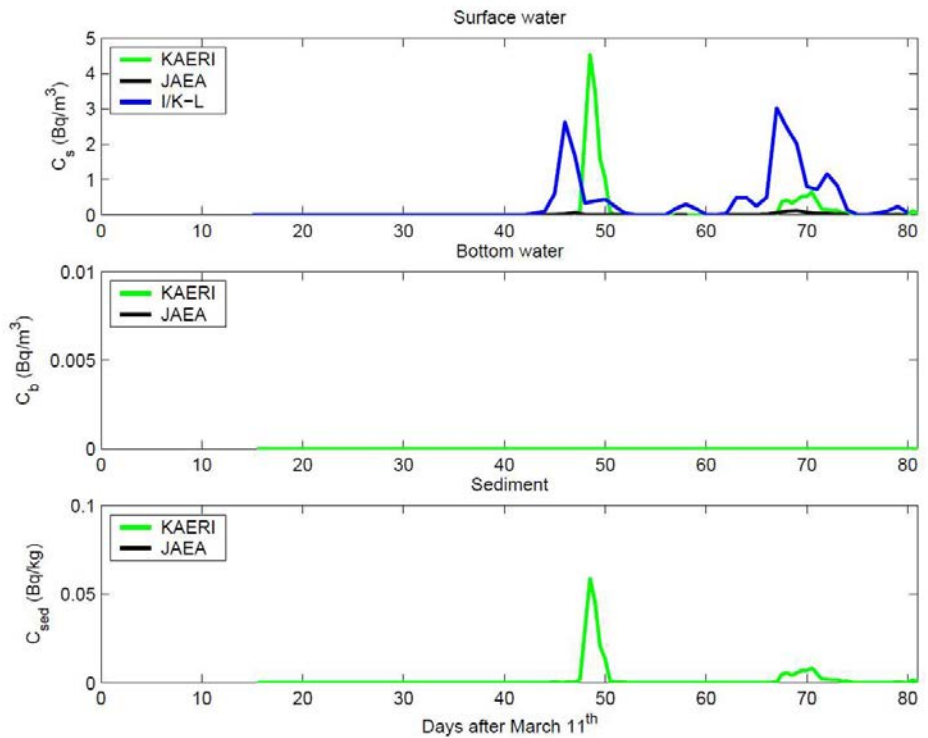


FIG. 32. Time series of radionuclide concentrations (^{137}Cs) at point P3 for surface water, bottom water and sediment. Exercise 3 with SPM.

Dissolved Concentration Date[Bq/m³] 2011/05/30

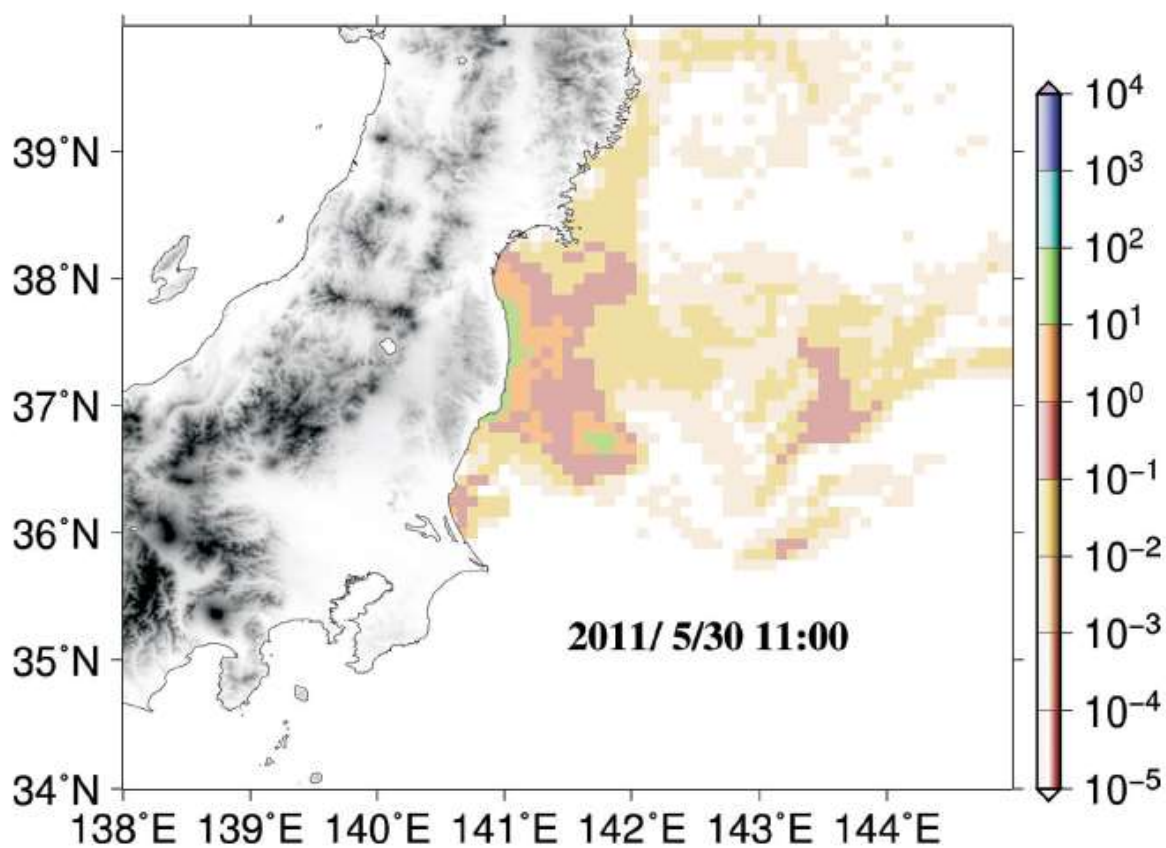
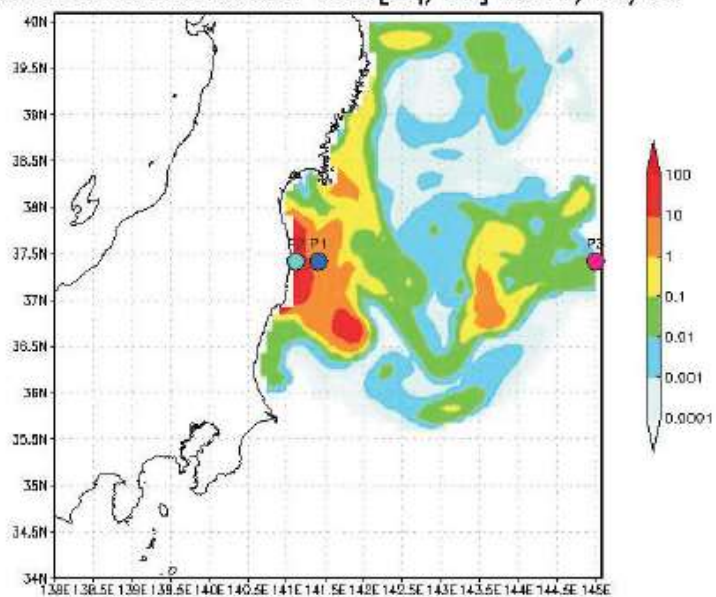


FIG. 33. Calculated ¹³⁷Cs distribution (Bq/m³) in surface water by JAEA (top) and KAERI (bottom) models for the ¹³⁷Cs experiment with SPM in the water column.

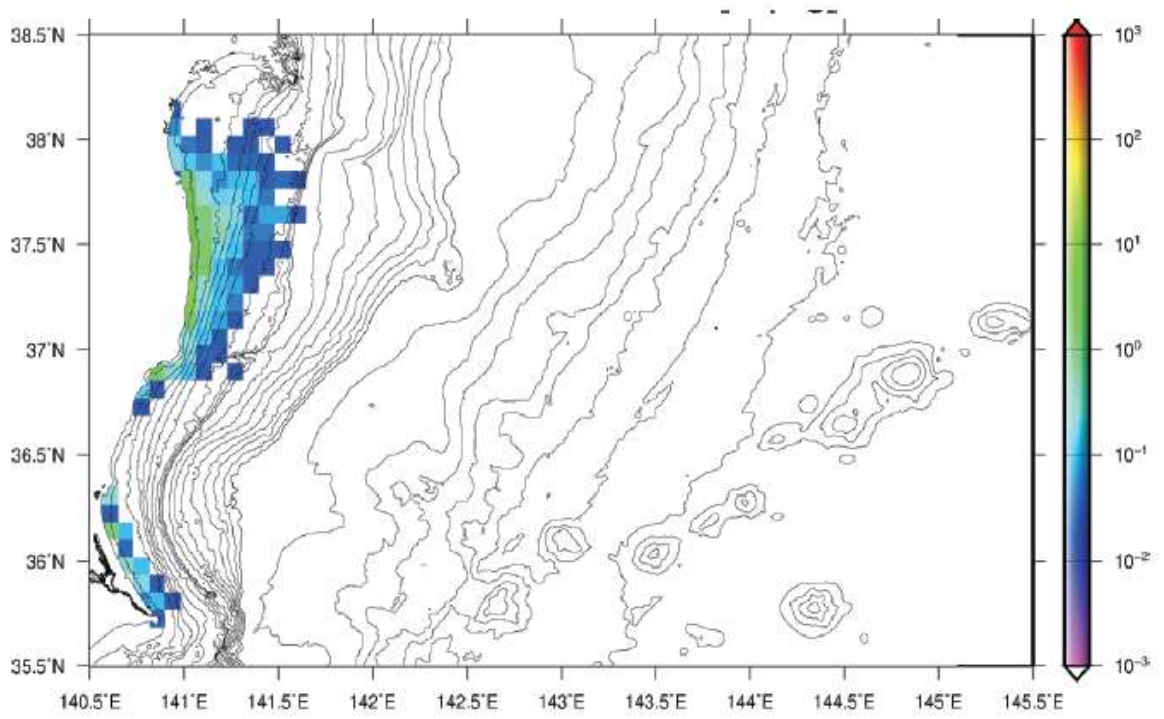
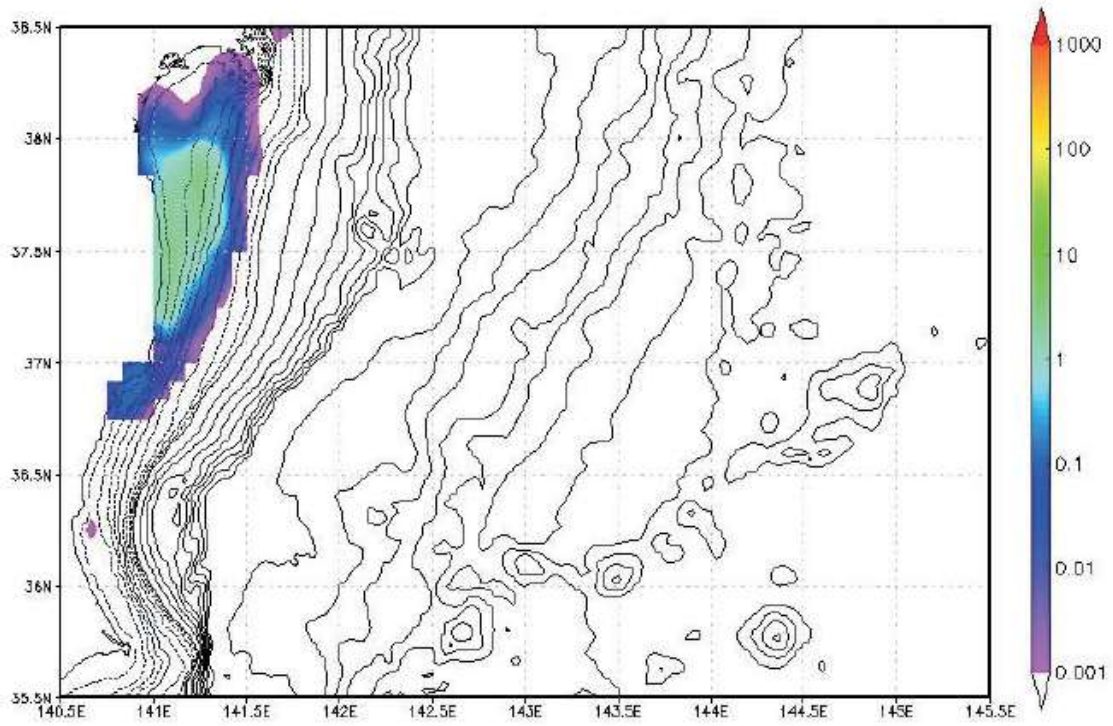


FIG. 34. Calculated ^{137}Cs distribution for sediment (Bq/kg) by JAEA (top) and KAERI (bottom) models for the ^{137}Cs experiment with SPM in the water column.

3.5. EXERCISE 4: COMPARISONS WITH FIELD DATA

3.5.1. Source term

In order to compare model predictions with radionuclide concentration measurements in the marine environment off Fukushima, a realistic ^{137}Cs source term needs to be used. During the Fukushima Daiichi NPP accident in 2011, radionuclides entered into the Pacific Ocean both from deposition on the sea surface of radionuclides previously released to the atmosphere and because of direct release of contaminated water into the sea. The reconstruction of these two source terms are described in the following two sub-sections.

3.5.1.1. Atmospheric deposition

Two atmospheric dispersion models were applied to simulate the dispersion of radionuclides released to the atmosphere and to evaluate the subsequent deposition to the sea surface. These models were developed by KAERI and JAEA. The output from both models were compared and the average from both taken as the best estimate of deposition.

Atmospheric dispersion models

The main characteristics of the applied atmospheric dispersion models are presented in Table 15 and both models are briefly described below:

- **KAERI model, LADAS (Long-range Accident Dose Assessment System):** After the accident, significant amounts of radioactivity were released to the air, which was transported inland and to the near shore of the Fukushima NPP between 12 March and 30 April 2011. During the early phase of the accident, i.e. 15–31 March 2011, radionuclides were deposited on the sea surface due to aeolian fallout, mainly in the northeast direction from Fukushima. Therefore, atmospheric deposition on the sea surface could affect dispersion patterns of radionuclides in water and sediment. The ^{137}Cs atmospheric fallout rate, as a function of time and space, was calculated from the long range atmospheric transport model LADAS developed by KEARI [68, 69].

The particle tracking method was used in LADAS for estimating the concentration distribution of radioactive material released into the atmosphere. The model was designed to estimate air concentrations and dry deposition, as well as wet deposition at distances of up to several thousands of kilometers from the release point in a horizontal direction. The turbulent motion of the particle is considered separately within and above the atmospheric mixing layer and particles are released in order to evaluate the transport and diffusion process of a pollutant in the atmosphere. The concentration is calculated by tracking the trajectory of each particle. Lagrangian type models can treat a rapid concentration gradient near a source point easily and do not introduce numerical dispersion. A particle is advected by the averaged wind components and dispersed by a turbulent motion in a 3-D space. The movement of the particle is represented by the sum of the movements due to the advection and the turbulence. This model was connected with 3-D meteorological forecasts from the KMA (Korea Meteorological Administration) in order to obtain the required wind fields [68, 69].

- **JAEA model, WSPEEDI-II (Worldwide Version of System for Prediction of Environmental Emergency Dose Information):** To simulate atmospheric dispersion of radionuclides released from the Fukushima NPP over eastern Japan, the WSPEEDI-II was used [70]. The simulation system WSPEEDI-II calculates air concentration and

surface deposition of radionuclides and radiological doses by successive use of the non-hydrostatic mesoscale meteorological prediction model MM5 and the Lagrangian particle dispersion model GEARN [70]. GEARN is a Lagrangian particle-tracking random walk model. The atmospheric dispersion of the released radionuclides is simulated by following the 3-D positions of many particles. Input data for GEARN are release condition of radionuclides and outputs from MM5 (e.g. 3-D wind fields, vertical diffusivity, mixing ratios of rain water, snow and graupel, cloud fractional cover, surface convective/non-convective precipitation and terrain height). By using 3-D and high resolution information on precipitation, GEARN can calculate deposition in detail. Output variables of GEARN are air concentration, accumulated surface deposition, air dose rate, external gamma dose and internal dose due to inhalation [71].

TABLE 15. MAIN CHARACTERISTICS OF ATMOSPHERIC DISPERSION MODELS

Model Parameter	WSPEEDI-II	LADAS
Meteorological Data	Japan Meteorological Agency and MM5	Korea Meteorological Administration
Domain	34–40°N, 138–145°E	34–40°N, 138–145°E
Horizontal resolution	6 km × 6 km	12 km × 12 km
Simulation period	2011.3.11, 23 h – 2011.5.30, 17 h (JST)	2011.3.12, 5 h – 2011.5.31, 0 h (KST)
¹³⁷ Cs source	Ref. [70]	Ref. [70]
Release height	20 m, 120 m	20 m
K_h	Ref. [72]	$2.5 \times 10^4 \text{ m}^2/\text{s}$
K_v	Mellor-Yamada level 2.5 [73]	$1.0 \text{ m}^2/\text{s}$
Dry deposition velocity	0.001 m/s 0.005 m/s on forests	0.001 m/s
Wet deposition scheme	$Sc = 5.0 \times 10^{-5} I^{0.8}$ I : precipitation (mm/h)	$Sc = 5.0 \times 10^{-5} I^{0.8}$ I : precipitation (mm/h)
Output interval	3 hours	3 hours

Notes: JST and KST are, respectively, Japan and Korea Standard Times. K_h and K_v are the horizontal and vertical diffusion coefficients and Sc means scavenging (s^{-1})

Calculated deposition patterns

A comparison of the time series of calculated deposition at points P1, P2 and P3 by both atmospheric dispersion models is presented in Figure 35. In general, there is a reasonable agreement between both models, which essentially produce the same deposition patterns. The main differences between model outputs are observed for point P2, due to the use of different meteorological data, especially precipitation data, in order to simulate wet deposition. The average between both models (the ensemble) is also illustrated in Figure 35. These average values, calculated over the whole domain of JCOPE2 circulation, will be used for the realistic Fukushima simulations and integrated deposition over time intervals of three hours will be applied.

As an example, average depositions over the domain for three time intervals during March are presented in Figure 36 where it can be seen that soon after the tsunami occurred the atmospheric plume is directed towards the north-east. On 16 March 2011 a significant deposition occurs inland and three days later, the plume curves towards the south, although deposition is reduced by one order of magnitude.

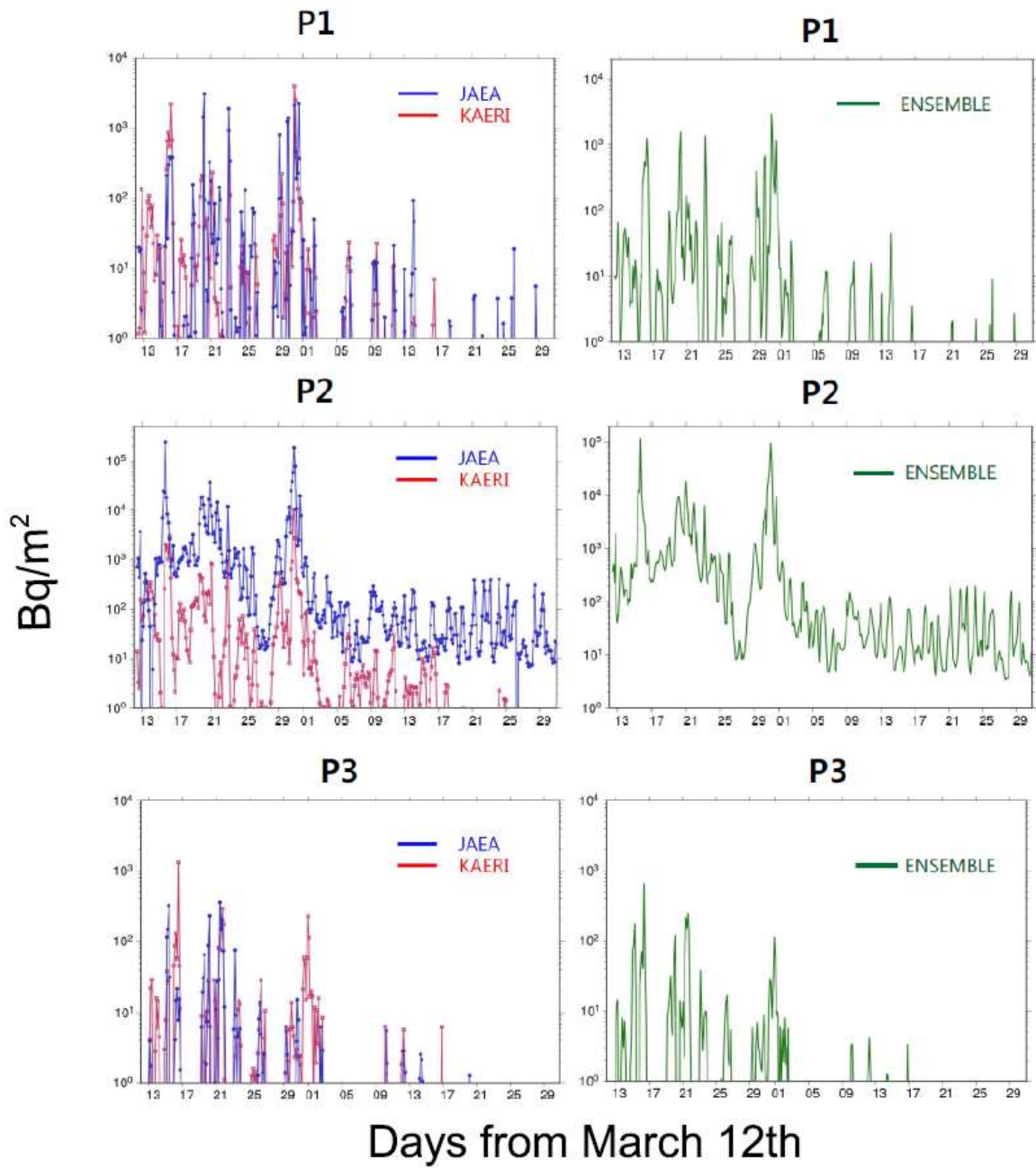


FIG. 35. Calculated ^{137}Cs depositions at points P1, P2 and P3 with the two atmospheric dispersion models. The average between both models is also shown.

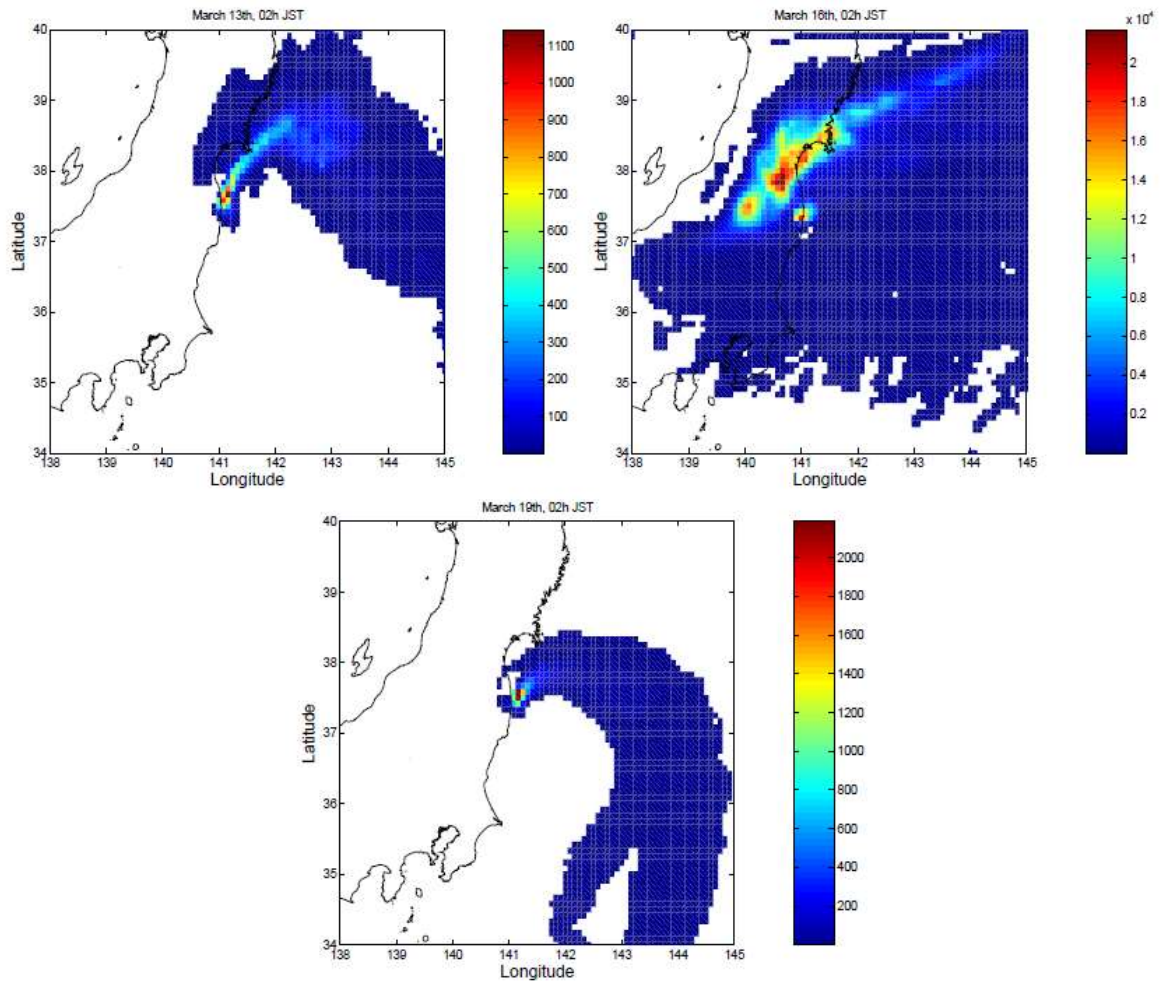


FIG. 36. Examples of calculated ^{137}Cs depositions (Bq/m^2) at three dates over the JCOPE2 domain. The average between both the KAERI and JAEA models is presented. Data correspond to integrated depositions over a three hour time interval (Japanese Standard Time (JST) is 9 hours ahead of Universal Coordinated Time (UTC)).

3.5.1.2. Direct releases to the Pacific Ocean

The source term of ^{137}Cs released directly into the ocean from the Fukushima Daiichi NPP accident was estimated as described below and in Ref. [41].

Monitoring data from the website of Tokyo Electric Power Company (TEPCO) regarding the area near to the northern and southern discharge channels of the Fukushima Daiichi NPP were used for this purpose [74]:

- (1) The release point was determined to be the middle point along the coast between the northern discharge channel and the southern discharge channel of the Fukushima Daiichi NPP;
- (2) With regard to the release duration, it was assumed that the direct release into the ocean from the Fukushima Daiichi NPP started on 26 March 2011. This was indicated by the analysis of the $^{131}\text{I}/^{137}\text{Cs}$ activity ratios [75] in ocean water. Discharges were assumed to continue until 30 June 2011;

- (3) The amount of ^{137}Cs released directly into the ocean was estimated based on the concentrations at the northern and southern discharge channels of the Fukushima Daiichi NPP, which were monitored approximately twice per day. Firstly the daily concentrations were averaged and then the amount of ^{137}Cs at the sea surface within a volume of $1.5 \text{ km} \times 1.5 \text{ km} \times 1 \text{ m}$ was calculated assuming that ^{137}Cs with averaged concentrations exists in the volume, because the distance between the northern and southern discharge channels is around 1.5 km. The calculated amounts were adjusted by multiplying the constant (7.5) obtained from a comparison of the total released amount of ^{137}Cs during 120 hours between 1–6 April 2011 with the values from TEPCO monitoring [74], which states that the total released amount of ^{137}Cs during this period was 0.94 PBq ($1 \text{ PBq} = 10^{15} \text{ Bq}$).

Figure 37 illustrates the resulting temporal variation of the released amount of ^{137}Cs to be used in the numerical simulations. This source term estimation leads to a total ^{137}Cs release of 3.5 PBq for the period 26 March–30 June 2011. Therefore, atmospheric deposition data, integrated over three hour intervals, together with the direct release source term presented in Figure 37, have been used in order to make realistic simulations on the dispersion of ^{137}Cs released from the Fukushima Daiichi NPP.

3.5.2. Results

The time frame of calculations extends from 12 March until 30 June 2011. Time series of calculated ^{137}Cs concentrations in surface water are provided by models for the points listed in Table 16, for which time series of measured concentrations were obtained by the Japanese company TEPCO (T1–T8). These measurements have been reported in regular press releases [76]. Three additional points were sampled [77] and have been included to compare model results with measurements taken at larger distances from Fukushima. The location of sampling points is shown in the map of Figure 38.

Two sets of calculations have been carried out:

- Exercise 4a, with common parameters (as in Exercise 3): circulation, bathymetry, diffusion coefficients, adsorption/desorption parameters and sediment characteristics. No suspended matter in the water column will be considered since, as has been shown before, it does not play a significant role;
- Exercise 4b, each model will use different water circulation and its own set of parameters. Thus, a range of expert estimations will be provided.

Results of these exercises are described in detail in the following sections.

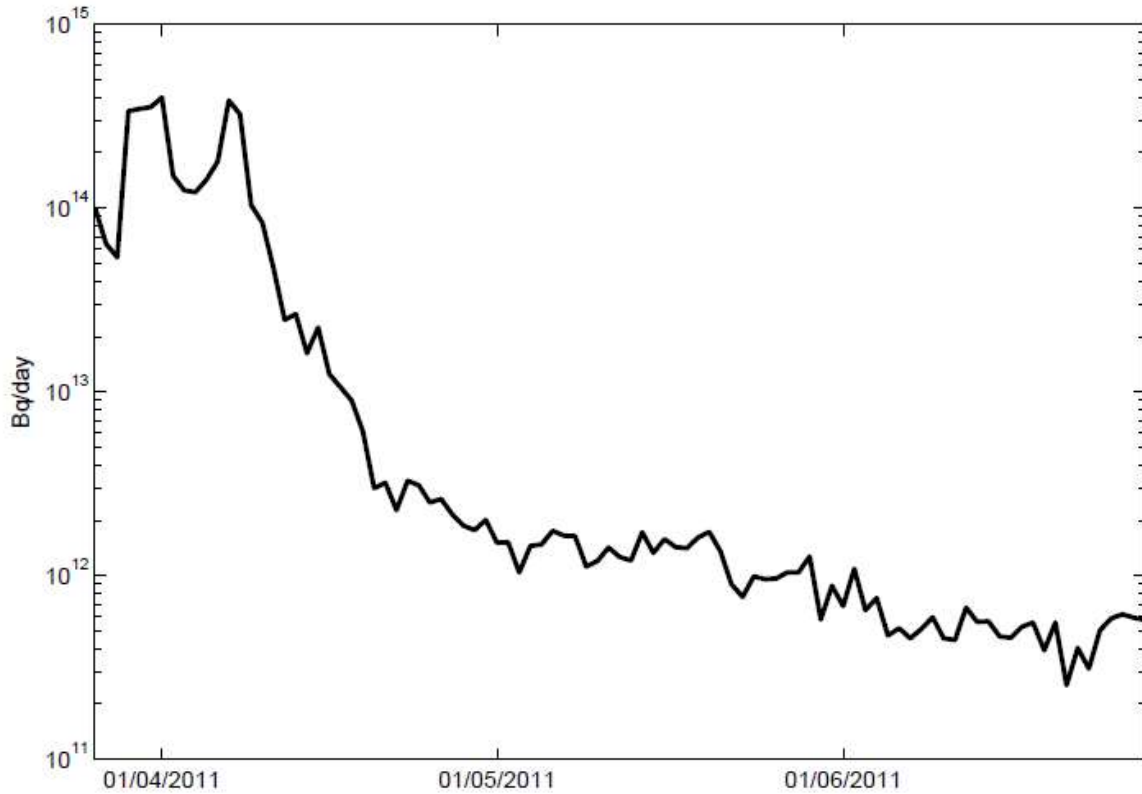


FIG. 37. ^{137}Cs daily direct releases to the Pacific Ocean from 26 March–30 June 2011.

TABLE 16. POSITIONS WHERE TIME SERIES OF ^{137}CS CONCENTRATIONS IN SURFACE WATER HAVE BEEN PRODUCED BY TEPCO (T1 TO T8) AND (B1, J1, E3)

Sampling Point	Longitude	Latitude
T1	141 02' 02"	37 24' 55"
T2	141 02' 04"	37 25' 52"
T3	141 01' 35"	37 19' 20"
T4	141 00' 50"	37 14' 30"
T5	141 12' 00"	37 35' 00"
T6	141 12' 00"	37 14' 00"
T7	141 12' 00"	37 10' 00"
T8	141 02' 15"	37 09' 00"
B1	141 15' 24"	38 05' 00"
J1	140 43' 00"	36 25' 00"
E3	141 36' 24"	37 25' 00"

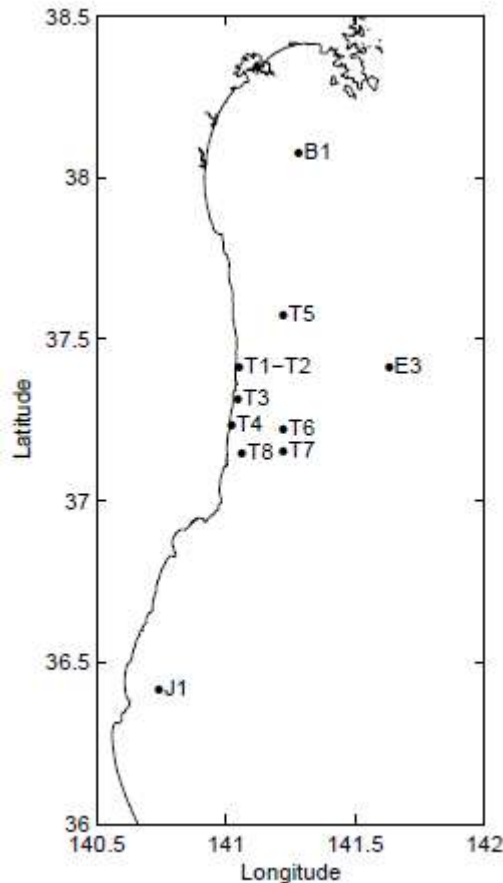


FIG. 38. Location of sampling points where calculated ^{137}Cs concentrations in surface water have been compared with measurements.

3.5.2.1. Exercise 4a: Common parameters

A comparison of model results with ^{137}Cs measurements in surface water for Exercise 4a (using JCOPE2 water circulation and common model parameters as in Exercise 3) is shown in Figures 39 and 40 for points T1–T8 and the three additional points at far distances from Fukushima, respectively. The general structure of the time series is very similar in all models since the same water circulation is being used and there is also an acceptable agreement with measured concentrations. At large distances from Fukushima, all models agree in producing concentrations below 10 Bq/L (except in E3). Additionally, peaks are generated at approximately the same time periods, except in B1, where a more noisy signal is produced by some models. Model results for sediment ^{137}Cs concentrations have also been compared with measurements and are presented in Figure 41. Modelled activity concentrations at the end of the simulation period (30 June 2011) are shown with TEPCO measurements. Given that the same water circulation was used in all models, the resulting ^{137}Cs distributions in sediment produce similar results, with the highest concentrations in the area nearest to Fukushima and some extension towards the south and northeast. There is consensus in the fact that most of the ^{137}Cs remains in a band along the coast and model results generally agree by order of magnitude with measurements.

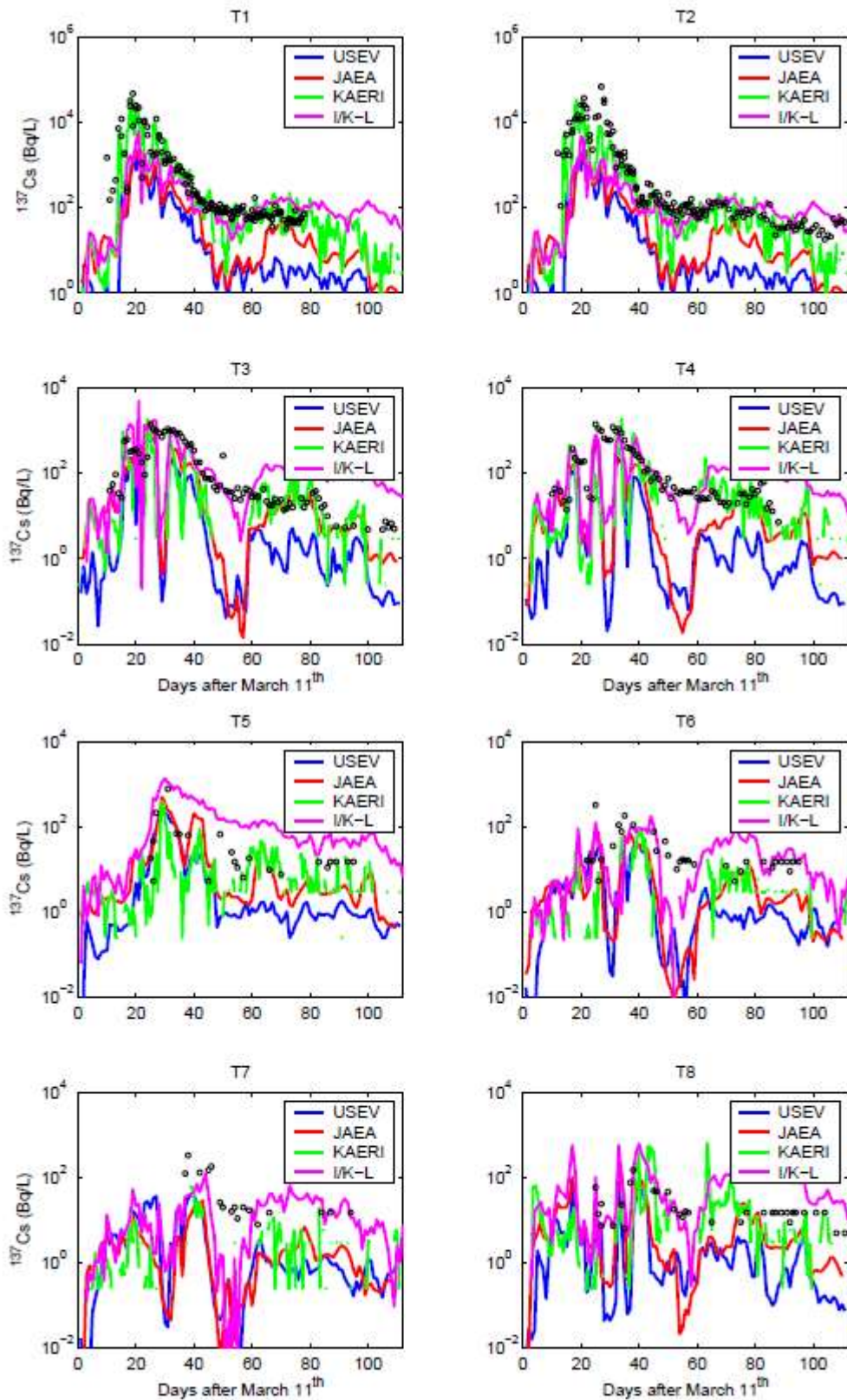


FIG. 39. Calculated and measured ^{137}Cs concentrations in surface water at points sampled by TEPCO. I/K model runs in a Lagrangian framework (Exercise 4a).

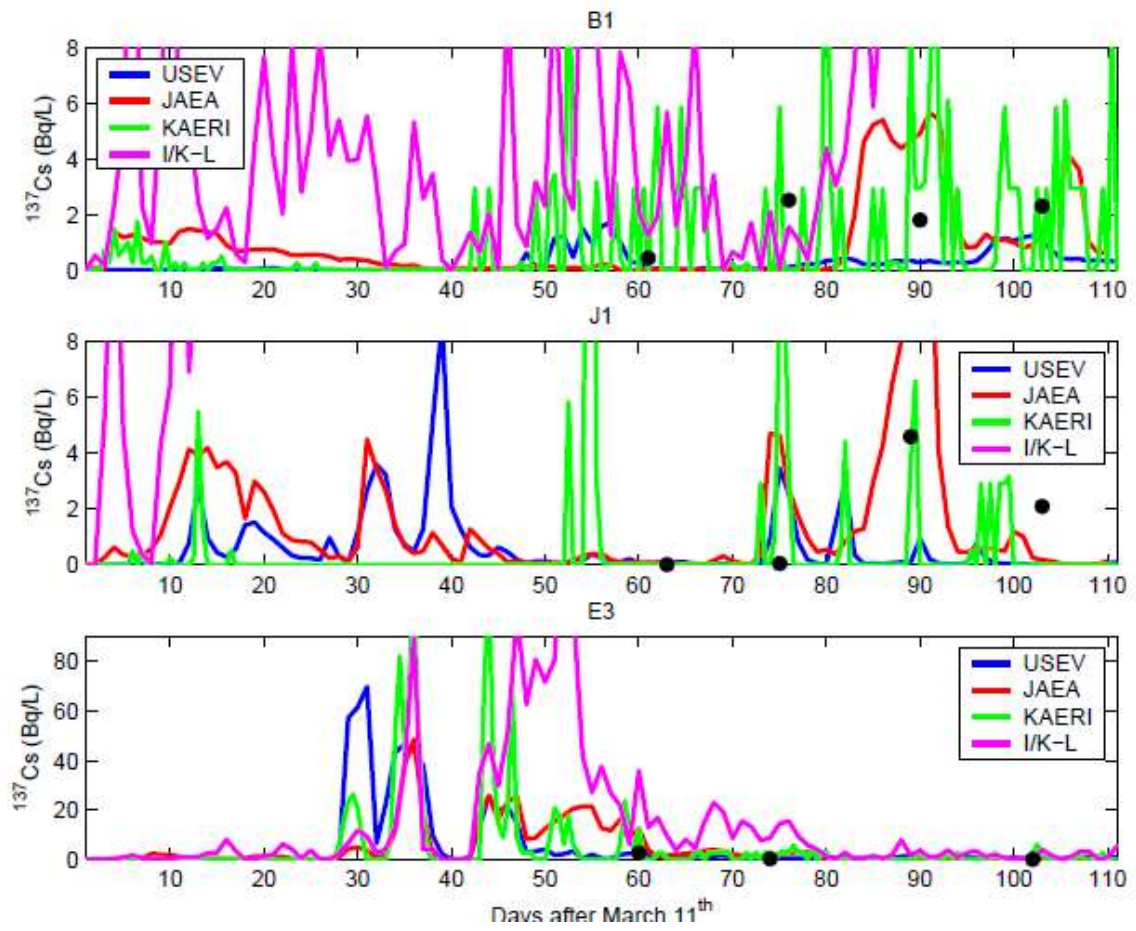


FIG. 40. Calculated and measured ^{137}Cs concentrations in surface water at points B1, J1 and E3 (Exercise 4a). I/K model runs in Lagrangian framework.

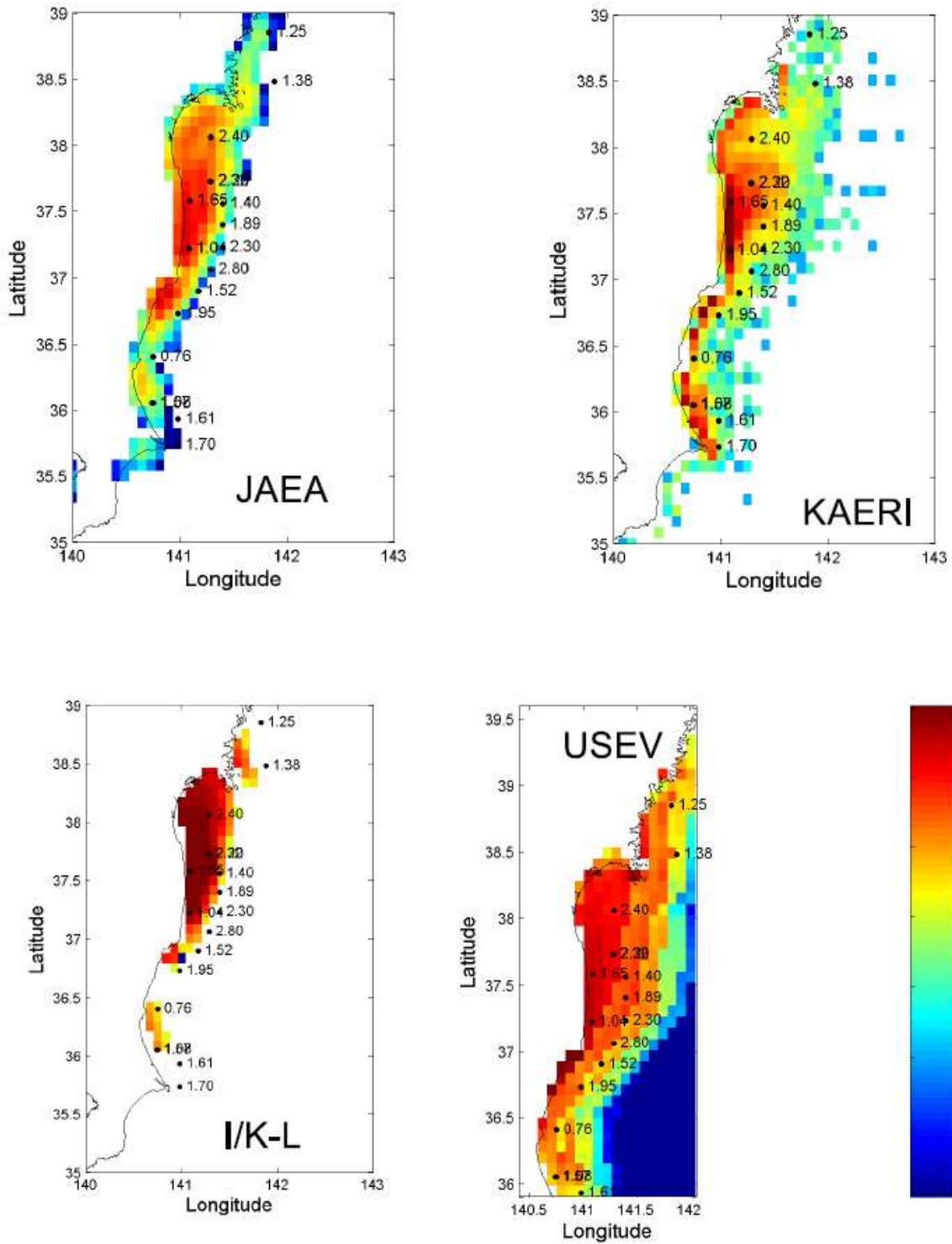


FIG. 41. ^{137}Cs in sediment (Bq/kg) at the end of the simulation period for Exercise 4a. Logarithms of calculated and measured concentrations are shown. The colour scale is the same for all maps.

3.5.2.2. Exercise 4b: A range of expert estimations

Results for Exercise 4b (with models using different water circulation and own set of parameters) are presented in Figures 42 and 43. The decrease in surface water ^{137}Cs concentrations produced by models in Exercise 4a around day 50 at some points (using JCOPE2 water circulation) is now not produced by the JAEA model (e.g. see Figure 42, T4), which reproduces the measured ^{137}Cs concentrations very well. This model uses water circulation from the University of Kyoto hydrodynamic model, which has a higher spatial resolution in the area of Fukushima than JCOPE2. This higher resolution may be leading to more accurate modelling of water circulation and a less noisy concentration time series. Except in the case of JAEA, models tend to underestimate water ^{137}Cs concentrations.

In the case of Exercise 4b, results for sediment are presented in Figure 44. The use of different water circulation by the models results in different distributions of ^{137}Cs activity concentration in sediment.

It is particularly interesting to observe that the University of Kyoto circulation (in the JAEA model) leads to a very narrow contaminated band along the coast and in the Bay of Sendai. There is not any extension of ^{137}Cs north of 38.5° latitude, which does not agree with measurements. However, water activity concentrations calculated with this model were in the best agreement with measurements. Thus, the JAEA model performs better than the others when calculating surface water concentrations, but worse than the others for sediment. This situation cannot be attributed to the water–sediment interaction description, since in the case of Exercise 4a (see Figure 41) output of this model was similar to the others. Instead, it seems that the University of Kyoto circulation model does not accurately reproduce deep circulation. In this sense, as mentioned previously [37], models may perform differently depending on the target variable. For instance, one model may predict radionuclide concentrations in sediment in good agreement with measurements, but it may provide not so close agreement for water. For another model, the situation may be the opposite.

The differences between the Eulerian (I/K-E and USEV) and Lagrangian (JAEA and KAERI) models may be clearly appreciated from the maps of sediment concentrations (see Figures 41 and 44). Eulerian models introduce artificial (numerical) diffusion which leads to smoother concentrations maps, with ^{137}Cs present over the whole domain.

It is noted that, while Exercises 1 to 3 are completely blind model tests, this is not entirely true for Exercise 4b due to the possible influence of model results by existing knowledge of measured data. In the case of the I/K model, the desorption rate from the sediment was fitted in order to reproduce measured concentrations in sediment. However, model results can be considered as blind for surface water. Exactly the same occurs in the case of the USEV model. The KAERI model was slightly modified with respect to Exercises 1–3 in order to obtain a better agreement with observations. This modification consisted of making the release in a single point instead of into an Eulerian grid cell. Moreover, it was also found that the best agreement with observations was obtained with parameters defined in Exercise 3. Consequently, results for KAERI model Exercises 4a and 4b are the same and the KAERI model results cannot be considered blind. Finally, the JAEA model application has been a blind exercise for both water and sediment.

In spite of some contamination of model results by knowledge of data, model results are in general consistent with observations. The range of computed values for a given variable may be regarded as an estimation of model uncertainty. Overall, ^{137}Cs concentrations in surface water tended to be underestimated, while a good representation of sediment was generally obtained.

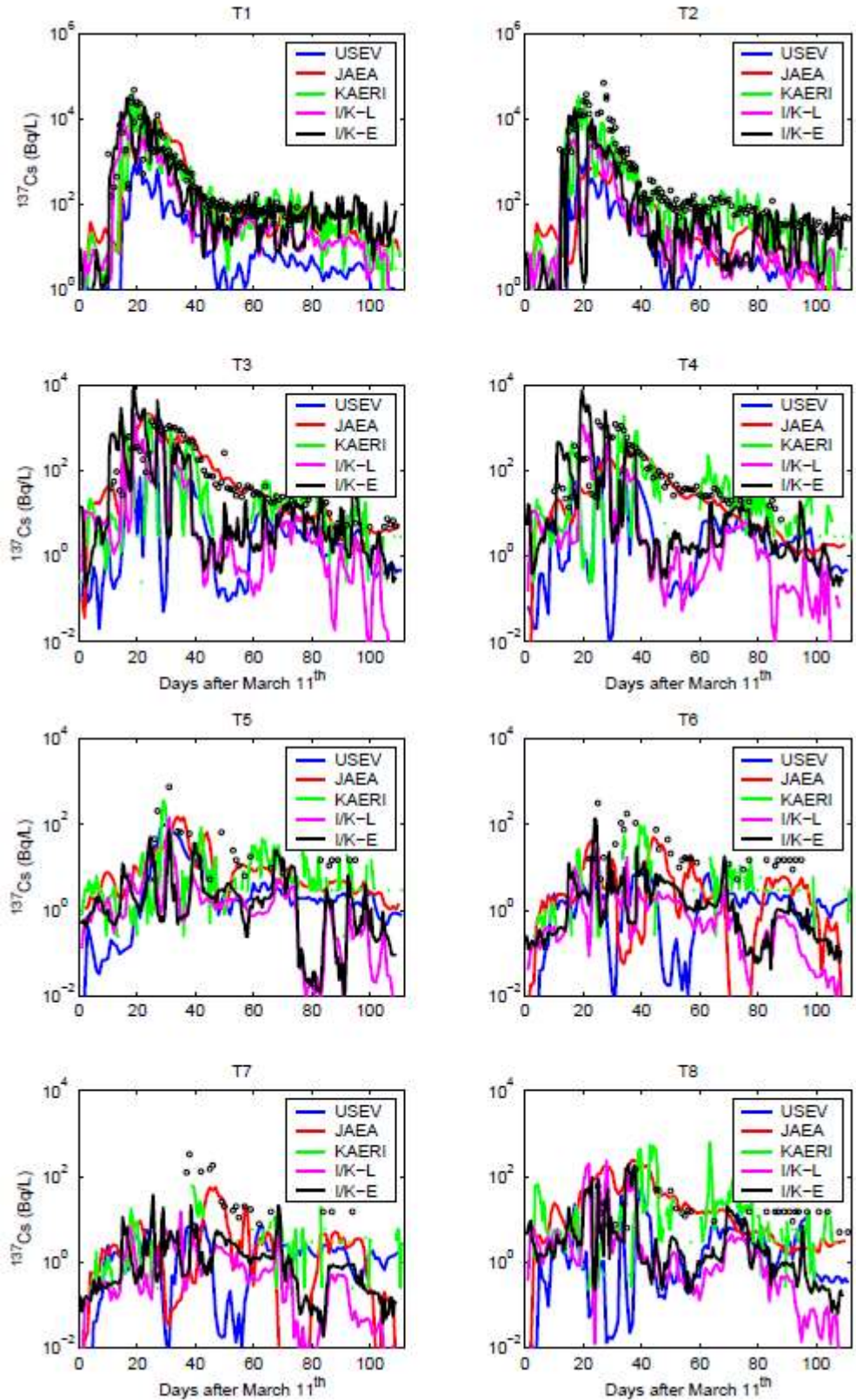


FIG. 42. Calculated and measured ^{137}Cs concentrations in surface water at points sampled by TEPCO. I/K model runs in Lagrangian (-L) and an Eulerian framework (-E) (Exercise 4b).

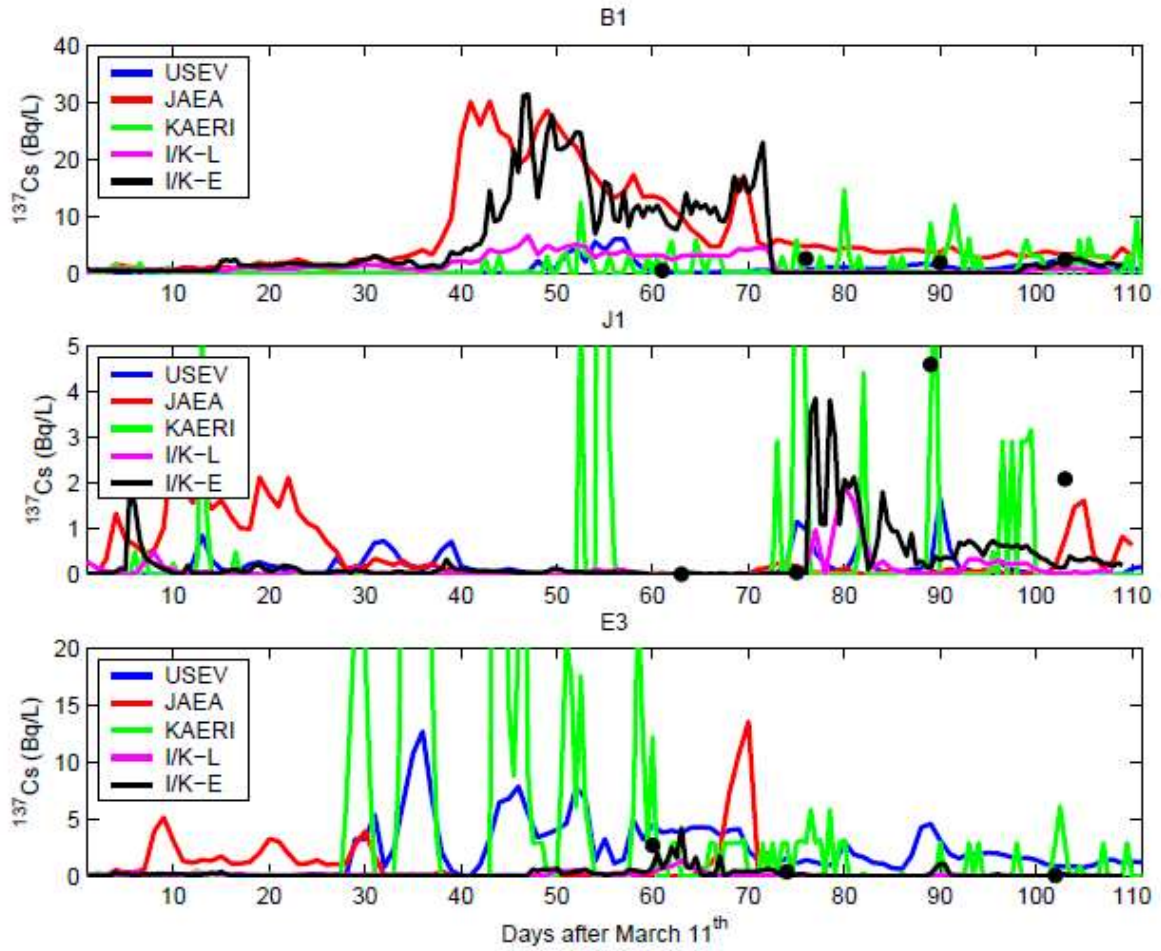


FIG. 43. Calculated and measured ^{137}Cs concentrations in surface water at points B1, J1 and E3 (Exercise 4b). I/K model runs in Lagrangian (-L) and an Eulerian (-E) framework.

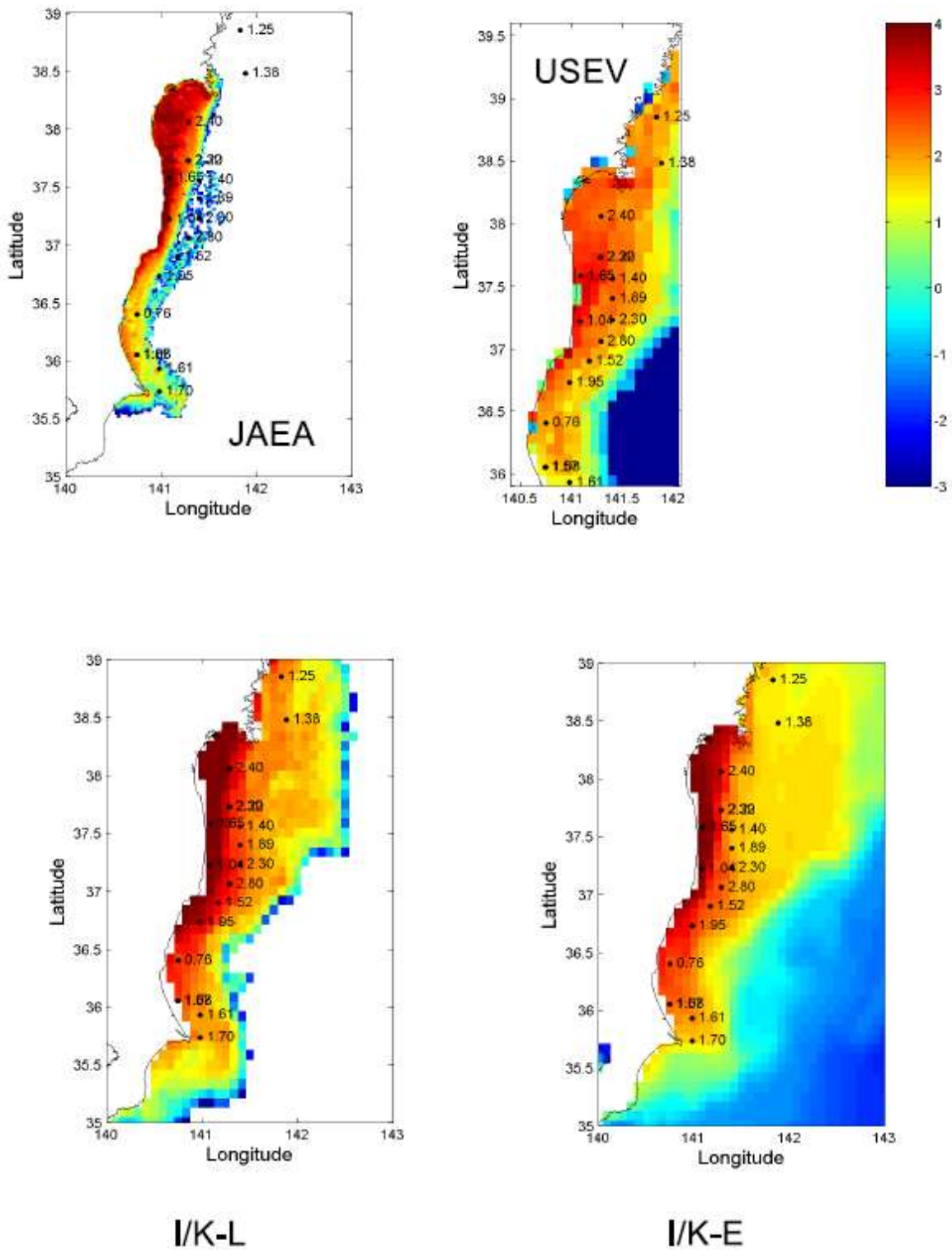


FIG. 44. ^{137}Cs in sediment (Bq/kg) at the end of the simulation period for Exercise 4b. Logarithms of calculated and measured concentrations are shown. The colour scale is the same for all maps.

3.6. CONCLUSIONS

Results obtained from modelling exercises regarding the dispersion of radionuclides released from the Fukushima Daiichi NPP accident into the Pacific Ocean are summarized below. The main objective of the exercises consisted of analysing the causes of variability between model results. A sequence of numerical experiments was carried out in which a progressive harmonization of model inputs – understood as using the same forcing and parameterizations – was performed.

Initially, Exercise 1 concerning a constant release of a perfectly conservative radionuclide (a non-decaying tracer) was carried out. For this exercise, each model was run with a different configuration for model setup, parameters, and water circulation in the Pacific Ocean. The water circulation could be calculated by the model itself in some cases or imported from operative ocean forecasting systems in others.

Results from this exercise presented significant variability of several orders of magnitude between model outputs, even at a point very close to the Fukushima Daiichi NPP. Moreover, maps of tracer concentrations in the water surface at the end of the simulated period also presented differences.

This variability in model results can be largely attributed to the different descriptions of hydrodynamics in each model. Water currents are the dominant factor in determining tracer dispersion in the marine environment. Consequently, model variability could be reduced if all the dispersion models are run with exactly the same description of water circulation for the period of interest.

To perform this task, the hydrodynamic description to be used was selected and a comparison of the hydrodynamics used by each model was carried out. The overall patterns of currents provided by the models are similar, showing the same general features, such as the Kuroshio current. However, a comparison of the time series of current magnitude and direction at a given point shows a strong variability in the signals produced by the models. Thus, it is not surprising that dispersion models produce such different results.

SST fields were used to compare the outputs of hydrodynamic models with observations in order to select the most appropriate hydrodynamic description to be used. The reasons are that SST is a scalar field (i.e. it's easier to handle than vector fields as currents), can easily be obtained for the domain of interest from satellite observations and, finally, baroclinic circulation is largely determined by SST.

The distances between calculated and measured SST fields were determined and the etalon-field methodology for their classification was applied. Following this procedure, it was concluded that a reasonable choice would be the JCOPE2 circulation. Thus, current fields produced by this hydrodynamic model were used in the subsequent exercises.

Exercise 2 was carried out using a tracer and ^{137}Cs (including water–sediment interactions) using JCOPE2 to simulate water currents. In the case of the tracer, model variability was significantly reduced and results are, in general, within one order of magnitude.

In the case of ^{137}Cs , results for surface water were similar to those of the tracer, since these waters do not feel the presence of the seabed. Most of the variability between models is therefore obtained for sediment. Here, in some points, results vary over several orders of magnitude. Nevertheless, maps of ^{137}Cs concentrations in water and sediment showed the same

general features. As a consequence, it could be concluded that a significant part of the variability between models is caused by the description of hydrodynamics. In the case of ^{137}Cs sediment concentrations, model variability is increased due to the different descriptions of water–sediment interactions used by each dispersion model.

Exercise 3 consisted of using the same description for water–sediment interactions in the case of ^{137}Cs . Thus, the same k_d , or equivalent kinetic ratios (to be used in cases of equilibrium or dynamic models respectively), were used. An additional harmonization of models in this exercise consisted of using exactly the same topographic data for the Pacific Ocean and the same values for the horizontal and vertical diffusion coefficients. This experiment was again carried out for a tracer and for ^{137}Cs . In the latter case, the effects of considering the presence of suspended matter in the water column were also investigated.

In the case of the tracer, agreement between models improved with respect to Exercise 2. The main factor in producing model discrepancies is water circulation since model agreement improvement is higher from Exercise 1 to 2 than from Exercise 2 to 3. This confirms a previous finding where differences between models are mainly due to hydrodynamics, although no systematic study was performed in order to assess this [60].

In the case of ^{137}Cs , the use of the same water–sediment parameterization also led to a better agreement between model outputs in sediment. Calculated ^{137}Cs concentration maps for water and sediment were also similar, with models producing the same behaviour. In this respect, it was also clear that a good description of contamination in the deepest water is essential for a good description of radionuclide adsorption by bed sediments.

The presence of suspended matter in the water column does not affect the calculated dissolved concentrations. This is not surprising given the relatively low affinity of ^{137}Cs to be fixed to the solid phase and the low suspended matter concentration in open ocean waters. Effectively, for the considered k_d of ^{137}Cs and suspended matter concentration (5 mg/L), the partition coefficient indicates that around 99% of this radionuclide remains in solution.

At this stage, given the model harmonization which was carried out, it does not seem possible to achieve a better agreement between models. Differences in model outputs were now due to intrinsic differences between models, i.e.:

- Lagrangian versus Eulerian models;
- Different numerical schemes which may be used for each model category mentioned above. In this sense, the method used to reconstruct concentrations from the density of particles in Lagrangian models may be relevant.

Nevertheless, the overall agreement between models which, generally, has been achieved, may be considered as satisfactory.

The first three exercises assumed a constant hypothetical source of radionuclides. The final exercise consisted of the use of a realistic source term, allowing the comparison of model outputs with ^{137}Cs measurements in water and sediment.

The source terms for both direct releases to the Pacific Ocean and atmospheric deposition on the sea surface had to be reconstructed. The direct release source term was reconstructed by the JAEA model based on ^{137}Cs measurements carried out by TEPCO at the southern and northern

discharge channels of the Fukushima Daiichi NPP. This source term implies a total release of 3.5 PBq of ^{137}Cs between 26 March and 30 June 2011.

For atmospheric deposition of ^{137}Cs on the sea surface, two atmospheric dispersion models were applied and their outputs compared. Since both outputs were similar, the average between the models was calculated by KAERI over 3 hour intervals.

Exercise 4 was carried out with these realistic source terms and consisted of two parts: calculations were performed with all common parameters and water circulation (as in Exercise 3) and, in addition, each model was run with its own configuration. This method allowed for a broad range of model expert estimation to be obtained and such a range may be considered an uncertainty estimation.

At a general level, model results were in good agreement with observations; although ^{137}Cs concentrations in surface water tended to be underestimated. It was also found that some models perform better for some target variables than for others. There was, however, agreement between all models in the sense that contamination of sediment extends over a banded area along the coast.

It may therefore be concluded that the dispersion models used are effective tools, although very sensitive to water circulation description in highly dynamic environments, such as the Fukushima coastal waters. If models for supporting decision making after emergencies are specially designed, great attention needs to be given to the forcing of the dispersion model by water circulation in this type of environment.

4. OVERALL SUMMARY AND CONCLUSIONS

Two marine dispersion scenarios were studied within the frame of MODARIA Working Group 10. The scenarios simulated dispersion of radionuclides in the Baltic Sea following the Chernobyl accident; and dispersion of radionuclides in the Pacific Ocean following the Fukushima Daiichi NPP accident.

For the Baltic Sea radiological scenario, ^{137}Cs dispersion was simulated by four models, which were either box or hydrodynamic models. In all cases, radionuclide transfer between water and suspended matter and bed sediments were included. Two main aspects are considered when comparing the results from each model:

- (1) the significant conceptual, numerical and parametric differences between models;
- (2) the complexity of the Baltic Sea hydrodynamics.

Despite these two aspects, radionuclide dispersion results from each model were relatively close, including for bed sediments. The observed temporal trends of ^{137}Cs activity concentrations taken from the HELCOM database are generally well reproduced by all models. The results of this study suggest that some processes do not significantly influence radionuclide transport within the Baltic Sea including winter ice cover and, surprisingly, water stratification by the halocline and thermocline.

For the Pacific Ocean radiological scenario, ^{137}Cs dispersion was simulated with six models. Box models were not used as they are unsuitable for the highly dynamic oceanographic conditions found off the Pacific Coast of Japan. A relatively good agreement between models could only be achieved after harmonization of model inputs, whereby all models were executed with the same hydrodynamic fields, the same parameters for describing water–sediment interactions, the same bathymetry and the same horizontal and vertical diffusion coefficients. A step-by-step reduction of variability between models was achieved through this harmonization process. It was found that the different water currents from the different hydrodynamic models were the main factor producing variability between models. Where each model was executed with its own water circulation and model parameterization (Exercise 4b), there was in general a very good agreement in model–model and model–data comparisons. The results of Exercise 4b are influenced by a previous knowledge of measured data. Thus, the final component of the study was not a genuine blind model test.

Two marine environments were studied: a semi-enclosed basin (Baltic Sea radiological scenario) and a highly dynamic system (Pacific Ocean radiological scenario). The description of hydrodynamics had a more significant impact on model results in the highly dynamic system. In the case of the Baltic Sea radiological scenario, results were in good agreement despite the different hydrodynamic modelling approaches and simplifications applied. In the case of the Pacific Ocean radiological scenario, even similar hydrodynamic models led to differing current fields which, in turn, lead to very different radionuclide dispersion patterns. Given the intensity and variability of currents in this area, as well as the presence of unsteady eddies due to current convergence, small differences in the hydrodynamics produced different dispersion patterns and these differences tended to be amplified with time.

This highlights the inherent difficulties in developing operational modelling systems for emergency decision support in this type of highly dynamic marine environment, i.e. the output of the system will be very dependent on the hydrodynamic model which has been used for the

prediction of water currents. Further research into this type of modelling for emergency preparedness and response purposes is therefore clearly required.

It may be concluded that the dispersion models used in the Baltic Sea and Pacific Ocean radiological scenarios are effective tools, but results are sensitive to the hydrodynamic forcing in energetic regions characterized by strong current variability. Where possible, it is clear that local forecasts of marine circulation ought to be used for emergency modelling [78].

A multi-model approach, as described here and in other international modelling projects [79], may be valuable when environmental processes are complex. Through this approach, the predictions that obtain the greatest degree of consensus among modellers are made evident and the aspects that are subject to disagreement, and which ought therefore to be handled carefully, also become clear.

REFERENCES

- [1] INTERNATIONAL ATOMIC ENERGY AGENCY, Environmental consequences of the Chernobyl accident and their remediation: twenty years of experience. Report of the Chernobyl forum expert group 'environment', IAEA, Vienna (2006).
- [2] INTERNATIONAL ATOMIC ENERGY AGENCY, The Fukushima Daiichi Accident, Report by the Director General, STI-PUB-1170, IAEA, Vienna (2015).
- [3] INTERNATIONAL ATOMIC ENERGY AGENCY, An overview of the BIOMOV5 II study and its findings, Technical Report No. 17, IAEA, Vienna (1996).
- [4] INTERNATIONAL ATOMIC ENERGY AGENCY, Modelling of the transfer of radiocaesium from deposition to lake ecosystems, Report of the VAMP Aquatic Working Group, IAEA-TECDOC-1143, IAEA, Vienna (2000).
- [5] INTERNATIONAL ATOMIC ENERGY AGENCY, Environmental Modelling for Radiation Safety (EMRAS) – A Summary Report of the Results of the EMRAS Programme (2003-2007), IAEA-TECDOC-1678, IAEA, Vienna (2012).
- [6] NUCLEAR ENERGY AGENCY OF THE OECD, Coordinated Research and Environmental Surveillance Programme Related to Sea Disposal of Radioactive Waste, CRESO Final Report 1981–1995, OECD, Paris (1996).
- [7] INTERNATIONAL ATOMIC ENERGY AGENCY, Modelling of the radiological impact of radioactive waste dumping in the Arctic Seas, IAEA-TECDOC-1330, IAEA, Vienna (2003).
- [8] INTERNATIONAL ATOMIC ENERGY AGENCY, The Radiological Situation at the Atolls of Mururoa and Fangataufa: Main Report, Radiological Assessment Reports Series, IAEA, Vienna (1998).
- [9] PERIÁÑEZ, R., BEZHENAR, R., IOSJPE, M., MADERICH, V., NIES, H., OSVATH, I., OUTOLA, I., DE WIT, G., A comparison of marine radionuclide dispersion models for the Baltic Sea in the frame of IAEA MODARIA program, *Journal of Environmental Radioactivity* **139** (2015) 66–77.
- [10] PUGH, D.T., Tides, Surges and Mean Sea Level, Wiley, Chichester (1987).
- [11] PICKARD, G.L., EMERY, W.J., Descriptive Physical Oceanography, Pergamon, Exeter (1982).
- [12] FEISTEL, R., NAUSCH, G., WASMUND, N., State and Evolution of the Baltic Sea 1952–2005, Wiley and Sons, Hoboken, New Jersey, USA (2008).
- [13] MATTHÄUS, W., The history of investigation of salt water inflows into the Baltic Sea – from the early beginning to recent results, Marine Science Reports No. 65, Baltic Sea Research Institute, Rostock-Warnemünde, Germany (2006).
- [14] NAUSCH, G., NAUMANN, M., UMLAUF, L., MOHRHOLZ, V., SIEGEL, H., Hydrographisch-hydrochemische Zustandseinschätzung der Ostsee, 2013, *Meereswiss. Ber., Warnemünde* **93** (2014) (in German).
- [15] LEPPÄRANTA, M., MYBERG, K., Physical Oceanography of the Baltic Sea, Springer, Berlin (2009).
- [16] OMSTEDT, A., NYBERG, L., Response of Baltic Sea ice to seasonal, inter-annual forcing and climate change, *Tellus* **48A** (1996) 644–662.
- [17] TOSCANO-JIMÉNEZ, M., Modelización tridimensional del transporte oceánico de ^{137}Cs forzado por vientos, Validación en el mar Báltico tras el accidente de Chernobyl, PhD Thesis, University of Seville (2013) (in Spanish).
- [18] HAKANSON, L., GYLLENHAMMAR, A., BROLIN, A., A dynamic compartment model to predict sedimentation and suspended particulate matter in coastal areas, *Ecological Modelling* **175** (2004) 353–384.

- [19] HELCOM, Baltic Sea Environmental Commission, Fourth Periodic Assessment of the State of the Marine Environment of the Baltic Sea, 1994–1998, *Baltic Sea Environment Proceedings* **82A** (2001) 26 pp.
- [20] ILUS, E, ILUS, T., Sources of Radioactivity. In: S.P. Nielsen (Ed.), The radiological exposure of the population of the European Community to radioactivity in the Baltic Sea, Marina-Balt project, *Radiation Protection* **110**, EUR 19200, European Commission, Luxembourg (2000) 9–76.
- [21] HELCOM, Thematic assessment of long-term changes in radioactivity in the Baltic Sea 2007–2010, *Baltic Sea Environment Proceedings* **135** (2013) 42 pp.
- [22] NIES, H., WEDEKIND, C., Die Kontamination von Nord- und Ostsee durch den Reaktorunfall von Tschernobyl, *German Journal of Hydrography* **40** (1987) 277–288 (in German).
- [23] GRITCHENKO, Z.G., IVANOVA, L.M., ORLOVA, T.E., TISHKOVA, N.A., TOPORKOV, V.P., TOCHILOV, I., Radiation situation in the Baltic Sea in 1986 in seawater and sediments, In: Three year observations of the levels of some radionuclides in the Baltic Sea after the Chernobyl accident, *Baltic Sea Environment Proceedings* **31**, Helsinki (1989) 10–30.
- [24] GRITCHENKO, Z.G., IVANOVA, L.M., ORLOVA, T.E., TISHKOVA, N.A., TOPORKOV, V.P., TOCHILOV, I., The results of determination of Sr-90, Cs-134 and Cs-137 in the water of the Baltic Sea, In: Three year observations of the levels of some radionuclides in the Baltic Sea after the Chernobyl accident, *Baltic Sea Environment Proceedings* **31**, Helsinki (1989) 52–61.
- [25] NIES, H., The distribution of Chernobyl fallout in the Baltic Sea and its change during 1987 and 1988, In: Three year observations of the levels of some radionuclides in the Baltic Sea after the Chernobyl accident, *Baltic Sea Environment Proceedings* **31**, Helsinki (1989) 10–30.
- [26] RIBBE, J., MÜLLER-NAVARRA, S.H., NIES, H., A one-dimensional dispersion model for radionuclides in the marine environment applied to the Chernobyl fallout over the Northern Baltic Sea, *Journal of Environmental Radioactivity* **14** (1991) 55–62.
- [27] NIELSEN, S.P., A comparison between predicted and observed levels of ¹³⁷Cs and ⁹⁰Sr in the Baltic Sea, *Radioprotection Colloques* **32** C2 (1997) 387–394.
- [28] KUMBLAD, L., GILEK, M., NÆSLUND, B., KAUTSKY, U., An ecosystem model of the environmental transport and fate of carbon-14 in a bay of the Baltic Sea, Sweden, *Ecological Modelling* **166** (2003) 193–210.
- [29] ERICHSEN, A.C., KONOVALENKO, L., MOHLENBERG, F., CLOSTER, R.M., BRADSHAW, C., AQUILONIUS, K., KAUTSKY, U., Radionuclide transport and uptake in coastal aquatic ecosystems: A comparison of a 3D dynamic model and a compartment model, *AMBIO* **42** (2013) 464–475.
- [30] TOSCANO-JIMÉNEZ, M., GARCÍA-TENORIO, R., A three dimensional model for dispersion of radioactive substances in marine ecosystems, Application to the Baltic Sea after the Chernobyl disaster, *Ocean Engineering* **31** (2004) 999–1018.
- [31] MONTE, L., Application of the migration models implemented in the decision system MOIRA-PLUS to assess the long term behaviour of ¹³⁷Cs in water and fish of the Baltic Sea, *Journal of Environmental Radioactivity* **134** (2014) 136–144.
- [32] IKÄHEIMONEN, T.K., OUTOLA, I., VARTTI, V.P., KOTILAINEN, P., Radioactivity in the Baltic Sea: Inventories and temporal trends of ¹³⁷Cs and ⁹⁰Sr in water and sediments, *Journal of Radioanalytical Nuclear Chemistry* **282** (2009) 419–425.

- [33] KARCHER, M.J., HARMS, I.H., Estimation of water and ice fluxes in the Arctic for an improved box structure of the NRPA box model, In: Iosjpe, M. (Ed.), *Transport and Fate of Contaminants in the Northern Seas*, Norwegian Radiation Protection Authority, NRPA, Østerås (2000).
- [34] NIES, H., GORONCY, I., HERRMANN, J., MICHEL, J., DARAOUI, A., GORNY, M., JAKOB, D., SACHSE, D., TOSCH, L., Kartierung von Tc-99, I-129 und I-127 im Oberflächenwasser der Nordsee, Bericht zum Vorhaben StSch 4481, Bundesamt für Seeschifffahrt und Hydrographie, Hamburg und Rostock (2009) (in German).
- [35] MICHEL, R., DARAOUI, A., GORNY M., JAKOB, D., SACHSE, R., TOSCH, L., NIES, H., GORONCY, I., HERRMANN, J., SYNAL, H.A., STOCKER, M., ALFIMOV, V., Iodine-129 and iodine-127 in European seawaters and in precipitation from Northern Germany. *Science of the Total Environment* **419** (2012) 151–169.
- [36] MONTE, L., BOYER, P., BRITTAIN, J.E., HAKANSON, L., LEPICARD, S., SMITH, J.T., Review and assessment of models for predicting the migration of radionuclides through rivers, *Journal of Environmental Radioactivity* **79** (2005) 273–296.
- [37] MONTE, L., HAKANSON, L., PERIÁÑEZ, R., LAPTEV, G., ZHELEZNYAK, M., MADERICH, V., KOSHEBUTSKY, V., Experiences from a case study of multi-model application to assess the behaviour of pollutants in the Dnieper-Bug estuary, *Ecological Modelling* **195** (2006) 247–263.
- [38] MONTE, L., Multi-model approach and evaluation of the uncertainty of model results, Rationale and applications to predict the behaviour of contaminants in the abiotic components of the fresh water environment, *Ecological Modelling* **220** (2009) 1469–1480.
- [39] IOSJPE, M., PERIÁÑEZ, R., Redissolution of cesium and plutonium from Irish Sea sediments: A comparison between different modelling approaches, *Radioprotection* **40** (2005) 607–612.
- [40] TAKEMURA, T., NAKAMURA, H., TAKIGAWA, M., KONDO, H., SATOMURA, T., MIYASAKA, T., NAKAJIMA, T., A numerical simulation of global transport of atmospheric particles emitted from the Fukushima Daiichi Nuclear Power Plant, *SOLA* **7** (2011) 101–104.
- [41] KOBAYASHI, T., NAGAI, H., CHINO, M., KAWAMURA, H., Source term estimation of atmospheric release due to the Fukushima Daiichi Nuclear Power Plant accident by atmospheric and oceanic dispersion simulations, *Journal of Nuclear Science and Technology* **50** (2013) 255–264.
- [42] JAYNE, S.R., HOGG, N.G., WATERMAN, S.N., RAINVILLE, L., DONOHUE, K.A., RANDOLPH WATTS, D., TRACEY, K.L., MCCLEAN, J.L., MALTRUD, M.E., QIU, B., CHEN, S., The Kuroshio extension and its recirculation gyres, *Deep Sea Research Part I*, **56**(12) (2009) 2088–2099.
- [43] KAWAMURA, H., KOBAYASHI, T., FURUNO, A., IN, T., ISHIKAWA, Y., NAKAYAMA, T., SHIMA, S., AWAJI, T., Preliminary numerical experiments on oceanic dispersion of ¹³¹I and ¹³⁷Cs discharged into the ocean because of the Fukushima Daiichi nuclear power plant disaster, *Journal of Nuclear Science and Technology* **48** (2011) 1349–1356.
- [44] NAKANO, M., POVINEC, P., Long-term simulations of the ¹³⁷Cs dispersion from the Fukushima accident in the world ocean, *Journal of Environmental Radioactivity* **111** (2012) 109–115.

- [45] ESTOURNEL, C., BOSC, E., BOCQUET, M., ULSES, C., MARSELAIX, P., WINIAREK, V., OSVATH, I., NGUYEN, C., DUHAUT, T., LYARD, F., MICHAUD, H., AUCLAIR, F., Assessment of the amount of ^{137}Cs released into the Pacific Ocean after the Fukushima accident and analysis of its dispersion in Japanese coastal waters, *Journal of Geophysical Research* **117** (2012) C1014.
- [46] MIYAZAWA, Y., MASUMOTO, Y., VARLAMOV, S.M., MIYAMA, T., Transport simulation of the radionuclide from the shelf to the open ocean around Fukushima, *Continental Shelf Research* **50–51** (2012) 16–29.
- [47] BEHRENS, E., SCHWARZKOPF, F.U., LUBBECKE, J., BONING, C.W., Model simulations on the long-term dispersal of ^{137}Cs released into the Pacific Ocean off Fukushima, *Environmental Research Letters* **7**, 034000 (2012) 10 pp.
- [48] KAWAMURA, H., KOBAYASHI, T., FURUNO, A., USUI, N., KAMACHI, M., Numerical simulation on the long-term variation of radioactive cesium concentration in the North Pacific due to the Fukushima disaster, *Journal of Environmental Radioactivity* **136** (2014) 64–75.
- [49] ROSSI, V., SEBILLE, E., GUPTA, A.E., GARÇON, V., ENGLAND, M.H., Multi-decadal projections of surface and interior pathways of the Fukushima Cesium-137 radioactive plume, *Deep-Sea Research I* **80** (2013) 37–46.
- [50] ROSSI, V., SEBILLE, E., GUPTA, A.E., GARC,ON, V., ENGLAND, M.H., Corrigendum to Multi-decadal projections of surface and interior pathways of the Fukushima Cesium-137 radioactive plume, *Deep-Sea Research I* **93** (2014) 162–164.
- [51] DIETZE, H., KRIEST, I., ^{137}Cs off Fukushima Daiichi, Japan, Model based estimates of dilution and fate, *Ocean Science* **8** (2012) 319–332.
- [52] HONDA M., AONO T., AOYAMA M., HAMAJIMA Y., KAWAKAMI H., KITAMURA M., MASUMOTO Y., MIYAZAWA Y., TAKIGAWA M., SAINO T., Dispersion of artificial caesium-134 and -137 in the western North Pacific one month after the Fukushima accident, *Geochemical Journal* **46** (2012) 1–9.
- [53] BAILLY DU BOIS, P., GARREAU, P., LAGUIONIE, P., KORSAKISSOK, I., Comparison between modelling and measurement of marine dispersion, environmental half-time and ^{137}Cs inventories after the Fukushima Daiichi accident, *Ocean Dynamics* **64** (2014) 361–383.
- [54] BAILLY DU BOIS, P., LAGUIONIE, P., BOUST, D., KORSAKISSOK, I., DIDIER, D., FIÉVE, B., Estimation of marine source-term following Fukushima Daiichi accident, *Journal of Environmental Radioactivity* **114** (2012) 2–9.
- [55] MIYAZAWA, Y., MASUMOTO, Y., VARLAMOV, S.M., MIYAMA, T., TAKIGAWA, M., HONDA, M., SAINO, T., Inverse estimation of source parameters of oceanic radioactivity dispersion models associated with the Fukushima accident, *Biogeosciences* **10** (2013) 2349–2363.
- [56] PERIÁÑEZ, R., SUH, K.S., MIN, B.I., Local scale marine modelling of Fukushima releases, Assessment of water and sediment contamination and sensitivity to water circulation description, *Marine Pollution Bulletin* **64** (2012) 2333–2339.
- [57] MIN, B.I., PERIÁÑEZ, R., KIM, I.G., SUH, K.S., Marine Dispersion Assessment of ^{137}Cs Released from the Fukushima Nuclear Accident, *Marine Pollution Bulletin* **72** (2013) 22–33.
- [58] CHOI, Y., KIDA, S., TAKAHASHI, K., The impact of oceanic circulation and phase transfer on the dispersion of radionuclides released from the Fukushima Daiichi Nuclear Power Plant, *Biogeosciences* **10** (2013) 4911–4925.

- [59] MADERICH, V., BEZHENAR, R., HELING, R., JUNG, K.T., MYOUNG, J.G., CHO, Y.-K., QIAO, F., ROBERTSON, L., Regional long-term model of radioactivity dispersion and fate in the Northwestern Pacific and adjacent seas: Application to the Fukushima Daiichi accident, *Journal of Environmental Radioactivity* **131** (2014) 4–18.
- [60] MASUMOTO, Y., MIYAZAWA, Y., TSUMUNE, D., TSUBONO, T., KOBAYASHI, T., KAWAMURA, H., ESTOURNEL, C., MARSELEIX, P., LANEROLLE, L., MEHRA, A., GARRAFFO, Z.D., Oceanic dispersion simulations of ^{137}Cs released from the Fukushima Daiichi nuclear power plant, *Elements* **8** (2012) 207–212.
- [61] SCIENCE COUNCIL OF JAPAN, A review of the model comparison of transportation and deposition of radioactive materials released to the environment as a result of the Tokyo Electric Power Company's Fukushima Daiichi Nuclear Power Plant accident, A Report by Sectional Committee on Nuclear Accident and Committee on Comprehensive Synthetic Engineering, SCJ (2014).
- [62] PERIÁÑEZ, R., BROVCHENKO, I., DUFFA, C., JUNG, K.T., KOBAYASHI, T., LAMEGO, F., MADERICH, V., MIN, B.I., NIES, H., OSVATH, I., PSALTAKI, M., SUH, K.S., A new comparison of marine dispersion model performances for Fukushima Daiichi releases in the frame of IAEA MODARIA program, *Journal of Environmental Radioactivity* **150** (2015) 247–269.
- [63] MARTAZINOVA, V., The classification of synoptic patterns by method of analogs, *Journal of Environmental Engineering* **7** (2005) 61–65.
- [64] INTERNATIONAL ATOMIC ENERGY AGENCY, Sediment distribution coefficients and concentration factors for biota in the marine environment, Technical Reports Series No. 422, IAEA, Vienna (2004).
- [65] PERIÁÑEZ, R., Modelling the dispersion of radionuclides in the marine environment: an introduction, Springer, Berlin (2005).
- [66] DUURSMA, E.K., CARROLL, J., Environmental Compartments. Springer, Berlin (1996).
- [67] LI, Y.H., BURKHARDT, L. BUCHHOLTZ, M., O'HARA, P., SANTSCHI, P.H., Partition of radiotracers between suspended particles and seawater, *Geochimica and Cosmochimica Acta* **48** (1984) 2011–2019.
- [68] SUH, K.S., JEONG, H.J., KIM, E.H., HWANG, W.T., HAN, M.H., Verification of the Lagrangian particle model using the ETEX experiment, *Annals of Nuclear Energy* **33** (2006) 1159–1163.
- [69] SUH, K.S., HAN, M.H., JUNG, S.H., LEE, C.W., Numerical simulation for a long-range dispersion of a pollutant using Chernobyl data, *Mathematical and Computer Modeling* **49** (2009) 337–343.
- [70] TERADA, H., KATATA, G., CHINO, M., NAGAI, H., Atmospheric discharge and dispersion of radionuclides during the Fukushima Daiichi Nuclear Power Plant accident, Part II: verification of the source term and analysis of regional-scale atmospheric dispersion, *Journal of Environmental Radioactivity* **112** (2012) 141–154.
- [71] TERADA, H., CHINO, M., Improvement of worldwide version of system for prediction of environmental emergency dose information (WSPEEDI-II), Evaluation of numerical models by ^{137}Cs deposition due to the Chernobyl nuclear accident, *Journal of Nuclear Science and Technology* **42**(7) (2005) 651–660.
- [72] GIFFORD, F.A., Horizontal diffusion in the atmosphere: A Lagrangian-dynamical theory, *Atmospheric Environment* **16** (1982) 505–512.

- [73] MELLOR, G.L., YAMADA, T., Development of a turbulence closure model for geophysical fluid problems, *Reviews of Geophysics* **20** (1982) 851–875.
- [74] TOKYO ELECTRIC POWER COMPANY, Influence to surrounding environment, TEPCO Archives, Tokyo, Japan (2011).
<http://www.tepco.co.jp/en/nu/fukushima-np/fl/index2-e.html>
- [75] TSUMUME, D., TSUBONO, T., AOYAMA M., HIROSE, K., Distribution of oceanic ^{137}Cs from the Fukushima Daiichi nuclear power plant simulated numerically by a regional ocean model, *Journal of Environmental Radioactivity* **111** (2012) 100–108.
- [76] TOKYO ELECTRIC POWER COMPANY, Press Releases Archive, TEPCO, Tokyo, Japan (2011).
<http://www.tepco.co.jp/en/press/corp-com/release/index1112-e.html>
- [77] OIKAWA, S., TAKATA, H., WATABE, T., MISONOO, J., KUSAKABE, M., Distribution of the Fukushima-derived radionuclides in seawater in the Pacific off the coast of Miyagi, Fukushima, and Ibaraki Prefectures, Japan, *Biogeosciences* **10** (2013) 5031–5047.
- [78] DUFFA, C., BAILLY DU BOIS, P., CAILLAUD, M., CHARMASSON, S., COUVEZ, C., DIDIER, D., DUMAS, F., FIEVET, B., MORILLON, M., RENAUD, P., THEBAULT, H., Development of emergency response tools for accidental radiological contamination of French coastal areas, *Journal of Environmental Radioactivity* **151**(2) (2016) 487–494.
- [79] MONTE, L., BOYER, P., BRITTAIN, J., GOUTAL, N., HELING, R., KRYSHEV, A., KRYSHEV, I., LAPTEV, G., LUCK, M., PERIÁÑEZ, R., SICLET, F., ZHELEZNYAK, M., Testing models for predicting the behaviour of radionuclides in aquatic systems, *Applied Radiation and Isotopes* **66** (2008) 1736–1740.

ANNEX I. DESCRIPTION OF THE NRPA BOX MODEL

The Norwegian Radiation Protection Authority's (NRPA) box model uses a modified approach for compartmental modelling [I-1–3] which allows for dispersion of radionuclides over time. The box structures for surface, mid-depth and deep water layers have been developed based on the description of polar, Atlantic and deep waters in the Arctic Ocean and the Northern Seas and site specific information for the boxes generated from the 3-D hydrodynamic model NAOSIM [I-4]. The structure of the NRPA's box model is presented in Figure I-1.

The NRPA box model includes the processes of advection of radioactivity between compartments, sedimentation, diffusion of radioactivity through pore water in sediments, particle mixing, pore water mixing and a burial process of radioactivity in deep sediment layers. Radioactive decay is calculated for all compartments and the contamination of biota is further calculated from the radionuclide concentrations in filtered seawater in the different water regions. Doses to humans are calculated on the basis of seafood consumption, in accordance with available data for seafood catches and assumptions about human diet in the respective areas. Dose rates to biota are developed on the basis of calculated radionuclide concentrations in marine organisms, water and sediment, using dose conversion factors. Its structure, for the Baltic Sea only, is presented in Figure I-2.

The equations of the transfer of radionuclides between the boxes are of the form:

$$\frac{dA_i}{dt} = \sum_{j=1}^N k_{j,i} A_j \gamma[t \geq (T_j + w_{j,i})] - \sum_{j=1}^N k_{i,j} A_i \gamma[t \geq (T_i + w_{i,j})] - k_i A_i \gamma(t \geq T_i) + Q_i; t \geq T_i \quad (\text{I-1})$$

$$A_i = 0; t \leq T_i \quad (\text{I-2})$$

where $k_{i,i} = 0$ for all i , A_i and A_j are activities (Bq) at time t in boxes i and j ; $k_{i,j}$ and $k_{j,i}$ are rates of transfer (y^{-1}) between boxes i and j ; k_i is an effective rate of transfer of activity (y^{-1}) from box i taking into account loss of material from the compartment without transfer to another, for example due to radioactive decay; Q_i is an input of radionuclides into box i (Bq/y); n is the number of boxes in the system, T_i is the time of availability for box i (the first time when box i is open for dispersion of radionuclides) and γ is a unit function:

$$\gamma(t) = \begin{cases} 1 & t \geq T_i \\ 0 & t < T_i \end{cases} \quad (\text{I-3})$$

The times of availability:

$$T_i = \min_{\mu_m(v_0, v_i) \in M_i} \sum_{j,k} w_{j,k} \quad (\text{I-4})$$

are calculated as a minimized weight summed for all paths $\mu_m(v_0, \dots, v_i)$ from the initial box (v_0) with discharge of radionuclides to the box i on the oriented graph $G = (V, E)$ with a set V of nodes v_j correspondent to boxes and a set E of arcs e_{jk} correspondent to the transfer possibility between the boxes j and k (graph elements as well as available paths are illustrated by Figure I-3).

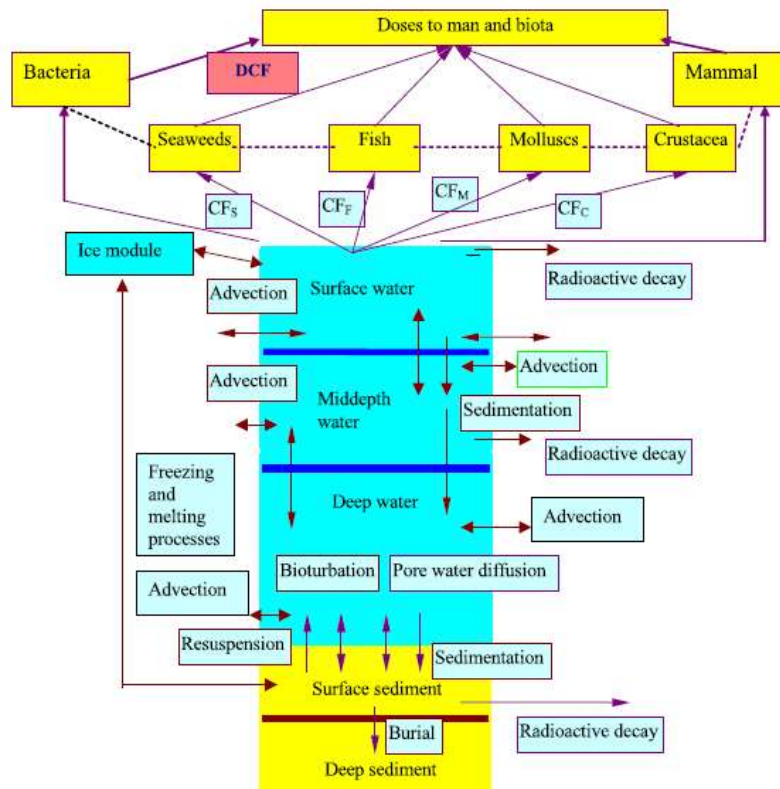


FIG.I-1. NRPA model structure. Reproduced courtesy of Elsevier [I-3].

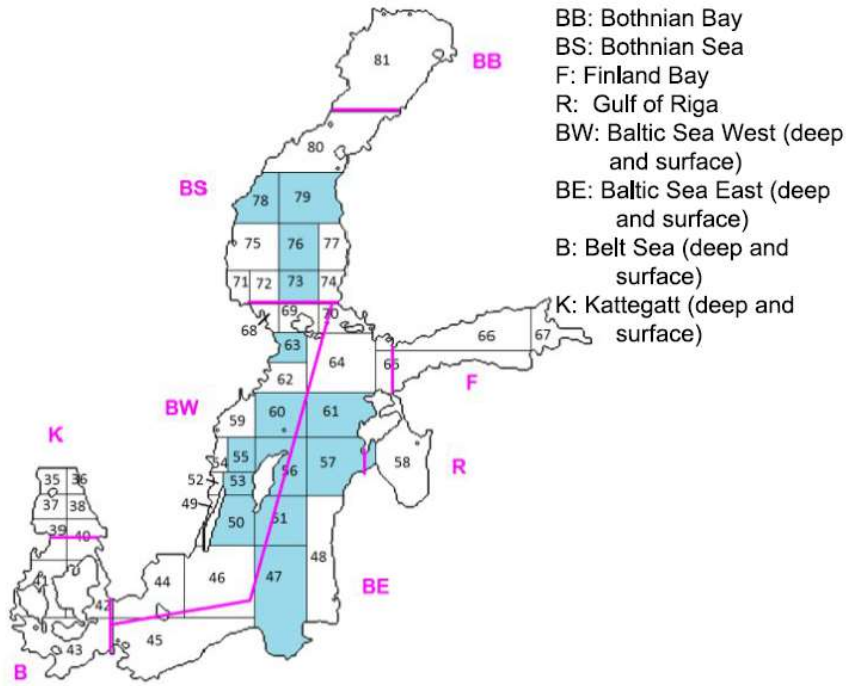


FIG. I-2. POSEIDON and NRPA model box structures. Pink lines define NRPA model boxes and numbered boxes correspond to POSEIDON. Blue boxes are those divided into two water layers.

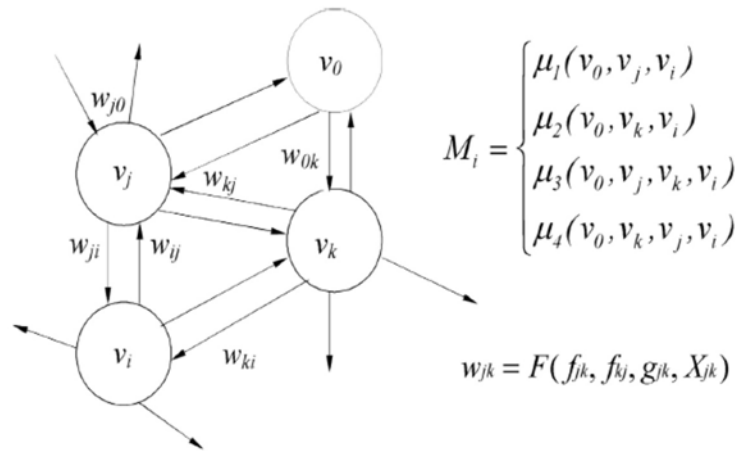


FIG. I-3. Graph elements. Reproduced courtesy of Elsevier [I-3].

Every arc e_{jk} has a weight w_{jk} which is defined as the time required before the transfer of radionuclides from box j to box k can begin (without any path through other boxes). Weight, w_{jk} , is considered as a discrete function F of the water fluxes f_{jk}, f_{kj} between boxes j and k , geographical information g_{jk} and expert evaluation E_{jk} . M_i is a set of feasible paths from the initial box (v_0) to the box i (v_i). It is interesting to note that traditional box modelling is a particular case of the present approach when all times of availability in Eq. I-1 are zero: $T_i = 0, \forall i$. Expressions for the transfer rates of radioactivity between the bottom water and

sediment compartments are useful in the present analysis (the transfer rates are shown in Figure I-4), i.e.:

$$k_{WS} = \frac{SR \cdot k_d}{d(1 + k_d \cdot SSL)} + \frac{D}{d \cdot h_s(1 + k_d \cdot SSL)} + \frac{R_T w \cdot h_s}{d(1 + k_d \cdot SSL)} + \frac{R_w \rho k_d(1-w)}{d(1 + k_d \cdot SSL)} \quad (I-5)$$

$$k_{SW} = \frac{D}{h_s^2[w + k_d \rho(1-w)]} + \frac{R_T w}{w + k_d \rho(1-w)} + \frac{R_w \rho k_d(1-w)}{h_s[w + k_d \rho(1-w)]} \quad (I-6)$$

$$k_{SM} = \frac{D \cdot w}{h_s^2[w + k_d \rho(1-w)]} + \frac{k_d \cdot SR}{h_s[w + k_d \rho(1-w)]} \quad (I-7)$$

$$k_{MS} = \frac{D \cdot w}{h_s h_{SM}[w + k_d \rho(1-w)]} \quad (I-8)$$

$$k_{MD} = \frac{k_d \cdot SR}{h_{SM}[w + k_d \rho(1-w)]} \quad (I-9)$$

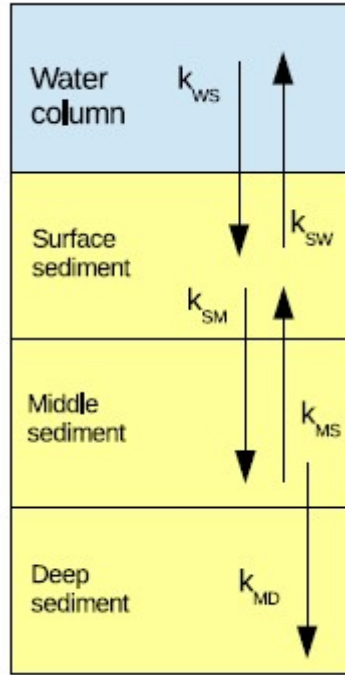


FIG. I-4. Generic vertical structure of the water-sediment compartments.

Here k_{SW} is composed of expressions describing the transfer of activity by sedimentation, molecular diffusion, pore water mixing and particle mixing, respectively. Similarly, k_{SW} is composed of expressions describing the transfer of radioactivity by molecular diffusion, pore water mixing and particle mixing. k_{SM} is composed of expressions describing the transfer of radioactivity by sedimentation and molecular diffusion. k_{MS} corresponds to the transfer by molecular diffusion. Finally, k_{MD} corresponds to the transfer of radioactivity by sedimentation. R_w (m/y) is the sediment reworking rate; R_T (y^{-1}) is the porewater turnover rate; k_d (m^3/t) is the sediment distribution coefficient; SSL (t/m^3) is the suspended sediment load in the water

column; SR (t/m^2y) is the sedimentation rate; D (m^2/y) is the molecular diffusion coefficient, h_S (m) and h_{SM} (m) are the surface and middle sediment thickness respectively; w is the porosity of the bottom sediment; ρ (t/m^3) is the density of the sediment material and d is the depth of the water column.

REFERENCES TO ANNEX I

- [I-1] IOSJPE, M., BROWN, J., STRAND, P., Modified approach to modelling of radiological consequences from releases into marine environment, *Journal of Environmental Radioactivity* **60** 1–2 (2002) 91–103.
- [I-2] IOSJPE, M., KARCHER, M., GWYNN, J., HARMS, I., GERDES, R., KAUKER, F., Improvement of the dose assessment tools on the basis of dispersion of the ⁹⁹Tc in the Nordic Seas and the Arctic Ocean. *Radioprotection* **44** (2009) 531–536.
- [I-3] IOSJPE, M., Environmental modelling: Modified approach for compartmental models, In: Povinec P.P., Sanchez-Cabeza J.A. (Eds.), *Radionuclides in the Environment, Radioactivity in the Environment* **8**, Series Ed.: M.S. Baxter (2006) 463–476.
- [I-4] KARCHER, M.J., HARMS, I.H., Estimation of water and ice fluxes in the Arctic for an improved box structure of the NRPA box model, In: Iosjpe, M. (Ed.), *Transport and Fate of Contaminants in the Northern Seas*, Norwegian Radiation Protection Authority, NRPA, Østerås (2000).

ANNEX II. POSEIDON BOX MODEL DESCRIPTION

The compartment model POSEIDON was developed and improved in several papers [II-1–3]. It is a model for radiological assessments of routine and accidental radioactivity releases into the sea and the software is based on a box modelling approach designed to cope with the need for large space and timescale calculations. The dispersion of radionuclides takes place via neighbouring boxes and across the vertical water column where the following dispersion mechanisms are considered:

- horizontal and vertical water exchanges from between boxes;
- adsorption on suspended sediments;
- depletion of activity in suspended materials in equilibrium with the water phase activity;
- exchange of radionuclides between water column and bottom through the molecular diffusion and bioturbation phenomena.

A more detailed representation of the water column and its sediment layers, as well as its interaction with neighbouring volumes, is shown in Figure II-1. The boxes describing the water column containing suspended matter are subdivided into a number of vertical layers. The radionuclide concentration for each water column layer is governed by a set of differential equations. These equations consider temporal variations in the nuclide concentration, the exchange with adjacent boxes due to advection, sediment settling and turbulent diffusion processes. Furthermore, the transfer of activity from suspended to bottom sediment due to suspended sediment settlement, radioactive sources and radioactive decay is considered. Temporal variations in the three sediment layers located under the water column are described by another set of equations. These equations consider the transfer of radioactivity between water column and sediment, and radioactive decay. The transfer of radioactivity from the upper sediment layer to the water column is described by diffusion in the interstitial water and by bioturbation. Radioactivity in the upper sediment layer migrates downwards by diffusion and by burial at a rate taken as the same at which particles settle from the overlying water. The upward transfer of radioactivity from the middle sediment layer to the top sediment layer occurs only by diffusion. Burial causes an effective loss of radioactivity from the middle to the deep sediment layers, from which no upward migration occurs.

II-1. TRANSPORT OF RADIONUCLIDES IN WATER AND SEDIMENTS

The mechanisms of radionuclide transfer are as follows: activity entering the water column is transported by currents and turbulent diffusion and lost to bottom sediments through sorption on suspended particles which then settle out. The exchange of activity between the upper layer of the sediment and the water column is described as diffusion and bioturbation (modelled as a diffusion process). Activity in the upper sediment layer may diffuse downward but there is also an effective downward transfer via the continued sedimentation at the top of the sediment layers. Return of activity from the middle sediment to the top sediment occurs only through diffusion. The effective loss of activity from middle sediment to deep sediment arises from the continued deposition of sediment.

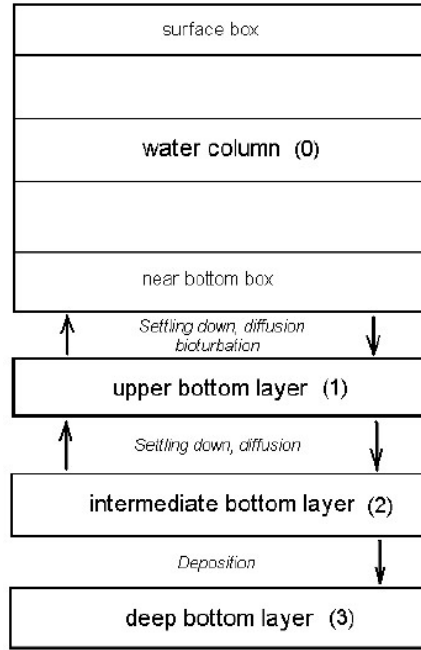


FIG. II-1. Schematic diagram of the activity transfer processes in POSEIDON model.

POSEIDON equations are obtained by averaging the 3-D transport equation for the dissolved radionuclide concentration C_w (Bq/m³) and the concentration in the three layers of the bottom sediment. It is assumed that the activity in the water column is partitioned between the water phase and the suspended sediment material, using the following relation:

$$C_s = k_d C_w \quad (\text{II-1})$$

where C_s (Bq/kg) is radioactivity concentration adsorbed in suspended sediment, k_d is the radionuclide distribution coefficient (m³/kg). The equation for the water column layers read as follows:

$$\frac{\partial C_{0,i}}{\partial t} = \sum_j \left(\frac{F_{j,i}}{V_{0,i}} C_{0,j} - \frac{F_{i,j}}{V_{0,i}} C_{0,i} \right) + \lambda_{0,i} C_{0(i,j,k-1)} - (\lambda_{1,i} + \lambda) C_{0,i} + \frac{L_{t,i}}{h_i} \lambda_2 C_1 + Q_{s,i} \quad (\text{II-2})$$

For the top sediment layer:

$$\frac{\partial C_1}{\partial t} = -(\lambda_2 + \lambda_3 + \lambda) C_1 + \frac{h_i}{L_{t,i}} \lambda_{1,i} C_{0,i} + \frac{L_{m,i}}{L_{t,i}} \lambda_4 C_2 \quad (\text{II-3})$$

and for the middle sediment layer:

$$\frac{\partial C_2}{\partial t} = -(\lambda_4 + \lambda_5 + \lambda) C_2 + \frac{L_{t,i}}{L_{m,i}} \lambda_3 C_1 \quad (\text{II-4})$$

where $F_{i,j}$ is the water flux from box i to box j ; V_0 is the box volume; h_i is the depth of the water compartment; L_t and L_m are the depth of top and middle sediment layers respectively; Q is the point source of the activity; $\lambda_1 \dots \lambda_5$ are the transfer coefficients, whose values depend on the characteristics of the radionuclide and sediments.

II-2. DESCRIPTION OF SOURCES OF ACTIVITY

The model POSEIDON can deal with three types of radioactive releases:

- (1) atmospheric fallout;
- (2) point sources associated with routine releases of nuclear facilities, located either directly at the coast or inland at river systems;
- (3) point sources associated with accidental releases.

For coastal discharges occurring into large ('regional') boxes, it may be useful to provide a more detailed description in the area close to the release point. For that purpose, 'coastal' release boxes can be added to the regional box system. These coastal boxes are nested into the regional boxes, and their physical characteristics (e.g. depth, sedimentation, etc.) can differ from those of the adjacent regional boxes.

POSEIDON also has the possibility to deal with offshore release points (e.g. for evaluation of the impact of sunken vessels, nuclear submarines, and offshore waste dumping). In that case, it is also possible to use a so-called 'local' box.

II-3. NUMERICAL SOLUTION

The problem is described by a set of ordinary differential equations (see Eqs. II-2–4 above), which may be written in a vector-matrix notation as:

$$\frac{dc}{dt} = AC + Q_{re} \quad (\text{II-5})$$

where C is the concentration vector; A is the coefficient matrix that includes water fluxes between boxes, parameters of sediments, etc., and Q_{re} is the vector for the release term. Step-like variations of the release in time are assumed and the Matrix Exponential Method [II-4] is used to solve this system.

II-4. APPLICATION TO THE BALTIC SEA

The model was customized for the Baltic Sea as shown in Figure I-2. Volume and average depth for each new box was calculated based on the bathymetry of the Baltic Sea, details of which were provided by the SMHI. The Baltic Sea compartments were connected with the North Sea compartments as described in the MARINA Project [II-5]. Boxes with depths larger than 60 m were divided into two layers (surface and bottom) for a rough description of stratification in the Baltic Sea. These boxes are shown in blue in Figure I-2 and water fluxes between boxes were calculated by averaging over 10 years the 3-D currents provided by the SMHI. River runoff was also taken into account for the largest 16 rivers and total river runoff was 484 km³/year [II-6].

The simulations were carried out for the period 1945–2010 and the sources of ¹³⁷Cs are global deposition from weapons testing, deposition from the Chernobyl accident and releases from the Sellafield and La Hague reprocessing plants. The global atmosphere deposition due to bomb tests was estimated for boxes 1–61 of Figure I-2 from Risø Research Reactor measurements and deposition due to fallout was estimated for boxes 62–81 taken from the Leningrad NPP measurements. The atmospheric deposition due to the Chernobyl accident was taken into account [II-7] and the release of ¹³⁷Cs from Sellafield (into box 15) and from La Hague (into box 26) was taken into account [II-8].

REFERENCES TO ANNEX II

- [II-1] MADERICH, V., BEZHENAR, R., HELING, R., JUNG, K.T., MYOUNG, J.G., CHO, Y.-K., QIAO, F., ROBERTSON, L., Regional long-term model of radioactivity dispersion and fate in the Northwestern Pacific and adjacent seas: Application to the Fukushima Daiichi accident, *Journal of Environmental Radioactivity* **131** (2014) 4–18.
- [II-2] LEPICARD, S., RAFFESTIN, D., RANCILLAC, F., POSEIDON: A dispersion computer code for assessing radiological impacts in European seawater environment, *Radiation Protection Dosimetry* **75** (1998) 79–83.
- [II-3] LEPICARD, S., HELING, R., MADERICH, V., POSEIDON/RODOS model for radiological assessment of marine environment after accidental releases: Application to coastal areas of the Baltic, Black and North seas, *Journal of Environmental Radioactivity* **72** 1–2 (2004) 153–161.
- [II-4] PATTEN, B.C., *Systems analysis and simulation in ecology*, Academic Press., V.1 (1971) 81–82.
- [II-5] COMMISSION OF THE EUROPEAN COMMUNITIES, *The radiological exposure of the population of the European Community from radioactivity in North European marine waters*, Project Marina, EUR 12483, CEC, Brussels (1990).
- [II-6] LEPPÄRANTA, M., MYBERG, K., *Physical Oceanography of the Baltic Sea*, Springer, Berlin (2009).
- [II-7] HELCOM, *Radioactivity in the Baltic Sea 1984–1991*, *Baltic Sea Environment Proceedings* **61** (1995) 182 pp.
- [II-8] HELCOM, *Radioactivity in the Baltic Sea, 1999–2006*, *Baltic Sea Environment Proceedings* **117** (2009) 60 pp.

ANNEX III. DESCRIPTION OF THE THREETOX MODEL

III-1. INTRODUCTION

The modelling system THREETOX was developed for simulating the dispersion of radionuclides and other contaminants at local and regional scales [III-1–3]. The system includes models for hydrodynamics, ice dynamics–thermodynamics and models for sediment and radionuclide transport (see Figure III-1). The prognostic variables of the hydrodynamic model are the three components of the velocity fields, temperature, salinity, water surface elevation and kinetic energy of turbulence and its dissipation rate. The ice model predicts the ice drift, thickness and ice concentration. The interactions between water, ice and atmosphere are parameterized by the bulk aerodynamic formulae, whereas the transport, deposition and resuspension of several fractions of sediments are calculated by the sediment transport model. The radionuclide concentration in solute, suspended sediments and the seabed is predicted by the radionuclide transport model and a one-step reversible model was used to describe the exchanges of radionuclides between water and sediments.

III-2. HYDRODYNAMICS

Hydrodynamics are simulated on the basis of the 3-D, time dependent, free surface, primitive equation model in the Boussinesq approximation. The model equations are written in curvilinear orthogonal coordinates. The governing Reynolds averaged equations of continuity, horizontal momentum, conservation equations for temperature T and salinity S , state equation and hydrostatic relation can be written in Cartesian coordinates as:

$$\nabla U = 0 \quad (\text{III-1})$$

$$\frac{\partial u}{\partial t} + U \cdot \nabla u - fv = -\frac{1}{\rho_0} \frac{\partial p}{\partial x} + \frac{\partial}{\partial z} \left(v_t \frac{\partial u}{\partial z} \right) + \frac{\partial}{\partial x} \left(K_M \frac{\partial u}{\partial x} \right) + \frac{\partial}{\partial y} \left(K_M \frac{\partial u}{\partial y} \right) \quad (\text{III-2})$$

$$\frac{\partial v}{\partial t} + U \cdot \nabla v - fu = -\frac{1}{\rho_0} \frac{\partial p}{\partial y} + \frac{\partial}{\partial z} \left(v_t \frac{\partial v}{\partial z} \right) + \frac{\partial}{\partial x} \left(K_M \frac{\partial v}{\partial x} \right) + \frac{\partial}{\partial y} \left(K_M \frac{\partial v}{\partial y} \right) \quad (\text{III-3})$$

$$\frac{\partial T}{\partial t} + U \cdot \nabla T = \frac{\partial}{\partial z} \left(v_t' \frac{\partial T}{\partial z} \right) + \frac{\partial}{\partial x} \left(K_T \frac{\partial T}{\partial x} \right) + \frac{\partial}{\partial y} \left(K_T \frac{\partial T}{\partial y} \right) + \frac{(1-A)I}{\rho_w c_{pw}} \frac{\partial I}{\partial z} \quad (\text{III-4})$$

$$\frac{\partial S}{\partial t} + U \cdot \nabla S = \frac{\partial}{\partial z} \left(v_t' \frac{\partial S}{\partial z} \right) + \frac{\partial}{\partial x} \left(K_T \frac{\partial S}{\partial x} \right) + \frac{\partial}{\partial y} \left(K_T \frac{\partial S}{\partial y} \right) \quad (\text{III-5})$$

$$\rho_w = \rho_w(T, S, p) \quad (\text{III-6})$$

$$p(x, y, z, t) = p_a + g \rho_0 \eta + g \int_z^0 \rho_w(x, y, z', t) dz' \quad (\text{III-7})$$

where t denotes time, $U = (u, v, w)$ is the velocity, η is surface elevation, f is the Coriolis parameter, p_a is the atmosphere pressure, ρ_w is the water density, ρ_0 is the undisturbed density, C_{pw} is the water heat capacity and $(1 - A)I$ is solar insolation absorbed in the water. Here ice concentration (compactivity) A is the fractional area covered by ice, whereas $(1 - A)$ is the fractional open water [III-4].

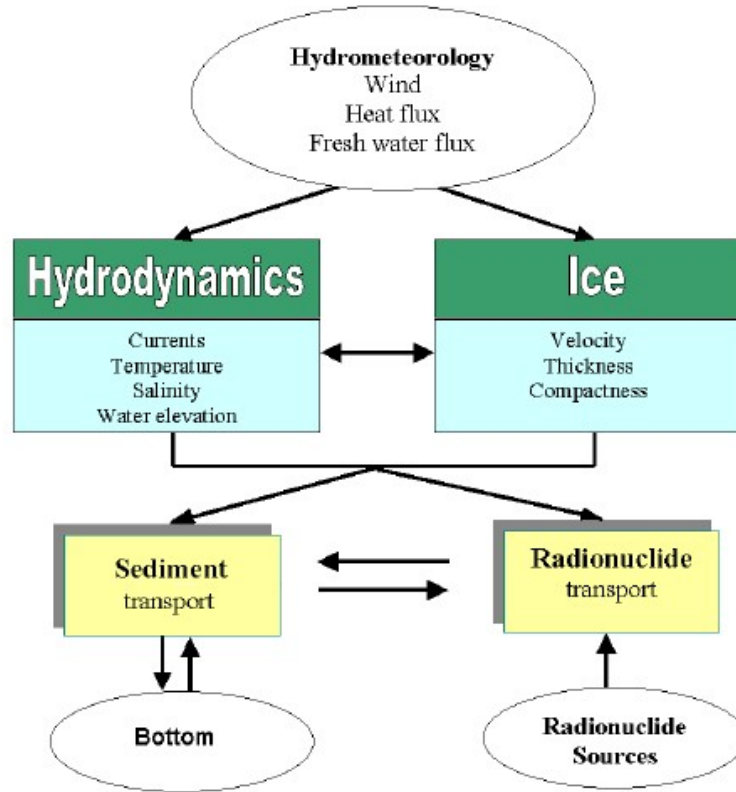


FIG. III-1. THREETOX modelling system.

The concept of eddy viscosity/diffusivity is used to determine the turbulent stresses. The vertical eddy viscosity $\nu_t \geq \nu_f$ and eddy diffusivity $\nu'_t \geq \nu_f$ are modelled as a product of turbulent velocity scale and turbulent length scale l , whereas ν_f is a constant background viscosity/diffusivity value when turbulence is suppressed by buoyancy forces at stable stratification. The turbulent velocity scale is proportional to the square root of kinetic turbulent energy k , therefore $\nu_t = c_\mu \sqrt{k}l$ and $\nu'_t = c'_\mu \sqrt{k}l$. Here c_μ and c'_μ are stability functions [III-5]. The United Nations Educational, Scientific, and Cultural Organization equation of state in the form proposed in Ref. [III-6] was used. The two-equation $k - \epsilon$ turbulence model is used to calculate k and its dissipation rate $\epsilon = (c_\mu^0)^3 k^{3/2} / l$. Here c_μ^0 is a constant. The horizontal turbulent viscosity/diffusivities are parameterized by a formula from [III-7].

At the free surface $z = \eta$ the kinematic boundary condition is:

$$\frac{\partial \eta}{\partial t} + u \frac{\partial \eta}{\partial x} + v \frac{\partial \eta}{\partial y} = w \quad (\text{III-8})$$

The surface fluxes required by the model are those of momentum, heat and salt. Turbulent fluxes of momentum at the surface are:

$$\nu_t \frac{\partial u}{\partial z} = (1 - A) \frac{\tau_{AW}^{(x)}}{\rho_w} + A \frac{\tau_{IW}^{(x)}}{\rho_w} \quad (\text{III-9})$$

$$v_t \frac{\partial v}{\partial z} = (1 - A) \frac{\tau_{AW}^{(y)}}{\rho_w} + A \frac{\tau_{IW}^{(y)}}{\rho_w} \quad (\text{III-10})$$

where τ_{AW} and τ_{IW} are atmospheric stresses directly imposed on water and stresses between ice and water, respectively. They have to be specified in the x and y directions.

The turbulent heat flux through water surface is:

$$v_t' \frac{\partial T}{\partial z} = \frac{F_T}{\rho_w c_{pw}} \quad (\text{III-11})$$

where F_T is the heat flux from the water and it includes long wave radiation [III-8], latent and sensible heat [III-9].

A simple ice dynamic–thermodynamic submodel that is applicable for simulation of the seasonal cycle of moving ice in the coastal seas is used by THREETOX [III-4, III-10]. The ice submodel describes momentum balance, ice rheology, mass balance, ice concentration and ice strength and is described in detail in Ref. [III-3].

III-3. SEDIMENT TRANSPORT

The model simulates the transport of non-cohesive and cohesive sediments, as well as a mixture of fractions of different sizes of cohesive/non-cohesive sediments. The sediments are transported in the water layer as suspended sediments. Suspended sediment transport is described by the advection–diffusion equation, taking into account settling velocity of sediment grains:

$$\frac{\partial S_{di}^w}{\partial t} + U \frac{\partial S_{di}^w}{\partial x} + V \frac{\partial S_{di}^w}{\partial y} + (W - W_{gi}) \frac{\partial S_{di}^w}{\partial z} = \frac{\partial}{\partial z} (v_t' \frac{\partial S_{di}^w}{\partial z}) + \frac{\partial}{\partial x} (K_T \frac{\partial S_{di}^w}{\partial x}) + \frac{\partial}{\partial y} (K_T \frac{\partial S_{di}^w}{\partial y}) \quad (\text{III-12})$$

where S_{di}^w is the concentration of i -th fraction of sediment in the water column, and W_{gi} is the settling velocity of solid particles. At the free surface $z = \eta$, zero vertical sediment flux is assumed, i.e.:

$$(W - W_{gi}) S_{di}^w = v_t' \frac{\partial S_{di}^w}{\partial z} \quad (\text{III-13})$$

The bottom boundary condition describes sediment resuspension or settling down depending on the ratio between equilibrium and actual near bottom suspended sediment concentration. The vertical flux of suspended sediments at the bottom $z = -H + z_b$ is equal to the difference of the resuspension and sedimentation rates:

$$v_t' \frac{\partial S_{di}^w}{\partial z} + W_{gi} S_{di}^w = q_i^w - q_i^b \quad (\text{III-14})$$

where q_i^w and q_i^b are sedimentation and resuspension rates, respectively. They are calculated according to empirical formulae for non-cohesive sediments [III-11] and cohesive sediments [III-12, III-13].

III-4. RADIONUCLIDE TRANSPORT

The submodel of radionuclide transport describes the specific water–sediment sorption processes. It includes the advection–diffusion equations for dissolved, C_s^w , and adsorbed by suspended sediment of i -th fraction, C_{pi}^w , radioactivity in the water column, and the equations for concentration of the dissolved, C_s^b , and adsorbed, C_{pi}^b , radioactivity in the bottom deposits:

$$\frac{\partial C_s^w}{\partial t} + \frac{\partial UC_s^w}{\partial x} + \frac{\partial VC_s^w}{\partial y} + \frac{\partial WC_s^w}{\partial z} = \frac{\partial}{\partial z} \left(v_t' \frac{\partial C_s^w}{\partial z} \right) + \frac{\partial}{\partial x} \left(K_T \frac{\partial C_s^w}{\partial x} \right) + \frac{\partial}{\partial y} \left(K_T \frac{\partial C_s^w}{\partial y} \right) - \lambda C_s^w - a_{12} (C_s^w \sum_{i=1}^n S_{di}^w K_{di}^w - C_p^w) \quad (\text{III-15})$$

$$\frac{\partial C_{pi}^w}{\partial t} + \frac{\partial UC_{pi}^w}{\partial x} + \frac{\partial VC_{pi}^w}{\partial y} + \frac{\partial (W - W_{gi}) C_{pi}^w}{\partial z} = \frac{\partial}{\partial z} \left(v_t' \frac{\partial C_{pi}^w}{\partial z} \right) + \frac{\partial}{\partial x} \left(K_T \frac{\partial C_{pi}^w}{\partial x} \right) + \frac{\partial}{\partial y} \left(K_T \frac{\partial C_{pi}^w}{\partial y} \right) - \lambda C_{pi}^w + a_{12} (C_s^w S_{di}^w K_{di}^w - C_{pi}^w) \quad (\text{III-16})$$

$$\frac{\partial (Z_* C_{pi}^b)}{\partial t} = a_{13} Z_* (K_{di}^b C_s^w - C_{pi}^b) - \frac{1}{\rho_s (1 - \epsilon)} (C_{pi}^w q_i^b - C_{pi}^b q_i^w) \quad (\text{III-17})$$

where $C_p^w = \sum_{i=1}^n C_{pi}^w$ and λ is the radionuclide decay constant. Adsorption and desorption of radionuclides between the liquid and solid phases are described by the radionuclide exchange rates, a_{12} and a_{13} , and by the distribution coefficients K_{di}^w and K_{di}^b [III-14, III-15, III-16], which are defined, under equilibrium conditions, as:

$$S_{di}^w K_{di}^w = \lim_{t \rightarrow \infty} \frac{C_{pi}^w}{C_s^w} \quad (\text{III-18})$$

$$\frac{S_{di}^b}{\epsilon} K_{di}^b = \lim_{t \rightarrow \infty} \frac{C_{pi}^b}{C_s^b} \quad (\text{III-19})$$

The dependence of the distribution coefficient on sediment particle size can be written for the water column as [III-17]:

$$K_{di}^w = \frac{\chi}{a_{12}} \frac{3}{R_i} \quad (\text{III-20})$$

and for bottom sediment as:

$$K_{di}^b = \frac{\chi}{a_{13}} \frac{3\theta}{\rho_s R_i} \quad (\text{III-21})$$

where R_i is sediment particle radius (m), χ is an exchange velocity (m/s), θ is a correction factor that takes into account that part of the sediment particle surface may be hidden by other sediment particles.

At the free surface $z = \eta$ the boundary conditions are:

$$v_t \frac{\partial C_s^w}{\partial z} = W C_s^w \quad (\text{III-22})$$

$$(W - W_{gi}) C_{pi}^w - v_t \frac{\partial C_{pi}^w}{\partial z} = 0 \quad (\text{III-23})$$

The fluxes into the bottom $z = -h + z_o$ are:

$$v_t \frac{\partial C_s^w}{\partial z} = 0 \quad (\text{III-24})$$

$$W_{gi} S_{di}^w C_{pi}^w + v_t \frac{\partial S_{di}^w C_{pi}^w}{\partial z} = C_{pi}^w q_{pi}^w - C_{pi}^b q_{pi}^b \quad (\text{III-25})$$

The numerical algorithm was implemented in a horizontal curvilinear orthogonal coordinate system. Fitting of the coordinate system to the bottom topography by means of mixed z -coordinate transformation allows the accurate description of shallow water flow and steep slopes [III-2]. The governing equations, together with the boundary conditions, are solved by finite difference techniques. The model equations are solved on an Arakawa C grid with all scalars located at the cell centroid, while velocity components are defined at the center of the faces of cells.

Temporal differencing is second order leap-frog scheme with the Asselin filter. The vertically integrated equations of continuity and momentum (external mode) are separated from the equations for the vertical structure of flow (internal mode). Splitting on the external and internal modes was applied [III-18]. The equations for the external mode were solved explicitly using a short time step to satisfy the Courant-Friedrichs-Lewy condition for fast barotropic long waves. The 3-D velocity and scalar fields (temperature, salinity, turbulent quantities) were computed semi-implicitly with a larger time step. An implicit treatment of the vertical viscosity and diffusion terms is used, whereas advective terms, horizontal viscosity and diffusion are computed on the previous time step. The advection of scalars is approximated by the high order Total Variation Diminishing scheme [III-19].

III-5. APPLICATION TO THE BALTIC SEA

The THREETOX model was customized for the Baltic Sea. The bathymetry was obtained from the GEODAS database [III-20] with 2 minute resolution, both in longitude and latitude. The bathymetry was extended to describe Kattegat and the transport of ^{137}Cs was modelled using spherical horizontal coordinates with a horizontal resolution of $1/15^\circ$ along the parallels and $1/30^\circ$ along the meridians, and by using 20 sigma layers in the vertical direction. Main rivers with seasonally varying discharge rates were included in the model, i.e, Neva, Vistula, Daugava, Oder, Neman, Kemijoki, Torne-Alv, Narva, Dalalven and other smaller rivers. The total freshwater discharge rate was $484 \text{ km}^3/\text{year}$. The atmospheric forcing was obtained from ERA-Interim reanalysis data [III-21] and air temperature, wind speed and direction, relative humidity, cloudiness and air pressure were interpolated from ERA-Interim data to the computational grid. Temperature, salinity, water velocity and surface elevation were prescribed along Kattegat from MyOcean reanalysis [III-22] for the North Sea. The sediment grain size was defined as $30 \mu\text{m}$.

The simulation started on 1 October 1985 when it was assumed that initially only a homogeneous background concentration of ^{137}Cs in water (15 Bq/m^3) exists. After one year, the concentration of ^{137}Cs in the surface layer after the Chernobyl accident was prescribed according to Figure 4 of the main report (see Section 2.2.2 of the main report) and calculations were performed for the period 31 October 1986 to 1 January 1991.

REFERENCES TO ANNEX III

- [III-1] MARGVELASHVILY, N., MADERICH, V., ZHELEZNYAK, M., THREETOX: Computer code to simulate three-dimensional dispersion of radionuclides in homogeneous and stratified water bodies, *Radiation Protection Dosimetry* **73** (1997) 177–180.
- [III-2] MADERICH, V., HELING, R., BEZHENAR, R., BROVCHENKO, I., JENNER, H., KOSHEBUTSKYY, V., KUSCHAN, A., TERLETSKA, K., Development and application of 3D numerical model THREETOX to the prediction of cooling water transport and mixing in the inland and coastal waters, *Hydrological Processes* **22** (2008) 1000–1013.
- [III-3] JOHANNESSEN, O.M., VOLKOV, V.A., PETTERSSON, L.M., MADERICH, V.S., ZHELEZNYAK, M.J., GAO, Y., BOBYLEV, L.P., STEPANOV, A.V., NEELOV, I.A., TISHKOV, V., NIELSEN, S.P., Radioactivity and Pollution in the Nordic Seas and Arctic Region, Observations, Modelling and Simulations, Springer, Series, Springer Praxis Books (2010) 408 pp.
- [III-4] MELLOR, G., KANTHA, L., An ice-ocean coupled model, *Journal of Geophysical Research* **94** (1989) 10837–10954.
- [III-5] CANUTO, V.M., HOWARD, A., CHENG, Y., DUBOVIKOV, M.S., Ocean Turbulence, Part I: One-point closure model-momentum and heat vertical diffusivities. *Journal of Physical Oceanography* **31** (2001) 1413–1426.
- [III-6] MELLOR, G.L., An equation of state for numerical models of ocean and estuaries, *Journal of Atmospheric and Ocean Technology* **8** (1991) 609–611.
- [III-7] SMAGORINSKY, J., General circulation experiments with primitive equations, I. The basic experiment, *Monthly Weather Review* **91** (1963) 99–164.
- [III-8] ZAPADKA, T., WOZNIAK, S.B., WOZNIAK, B., A simple formula for the net long-wave radiation flux in the southern Baltic Sea, *Oceanologia* **43** (2001) 265–277.
- [III-9] BLACKADAR, A., High resolution models of the planetary boundary layer, *Advances in Environmental Science and Engineering* 1, Pfafflin and Ziegler, Eds. Gordon and Breich, NY (1979) 50–85.
- [III-10] HIBLER W.D. III, A dynamic thermodynamic sea ice model. *Journal of Physical Oceanography* **9** (1979) 815–846.
- [III-11] VAN RIJN, L.C., Sediment transport, Part II: Suspended load transport, *Journal of Hydraulic Engineering* **110** (1984) 1613–1641.
- [III-12] KRONE, R.B., Flume Studies of the Transport of Sediment in Estuarial Processes, Final Report, Hydraulic Engineering Laboratory and Sanitary Engineering Research Laboratory, University of California, Berkeley (1962).
- [III-13] PARTHENIADES, E., Erosion and deposition of cohesive soil, *Journal of Hydraulic Division* **91** (1965) 105–139.
- [III-14] INTERNATIONAL ATOMIC ENERGY AGENCY, Sediment distribution coefficients and concentration factors for biota in the marine environment, Technical Reports Series No. 422, IAEA, Vienna (2004).
- [III-15] SANTSCI, P.H., HONEYMAN, B.D., Radionuclides in aquatic environments, *Radiation Physics and Chemistry* **34** (1989) 2213–2407.
- [III-16] CARROLL, J., HARMS, I.H., Uncertainty analysis of partition coefficients in a radionuclide transport model, *Water Research* **33**(11) (1999) 2617–2626.
- [III-17] PERIÁÑEZ, R., A modelling study on ¹³⁷Cs and ^{239/240}Pu behaviour in the Al-borán Sea, western Mediterranean, *Journal of Environmental Radioactivity* **99** (2008) 694–715.

- [III-18] BLUMBERG, A.F., MELLOR, G.L., A description of a three-dimensional coastal ocean circulation model, Three-Dimensional Coastal Ocean Models, N. Heaps (Ed.), Am. Geoph. Union (1987) 1–16.
- [III-19] VAN LEER, B., Toward the ultimate conservative difference scheme, V: A second order sequel to Godunov’s method, Journal of Computational Physics **32** (1979) 101–136.
- [III-20] <https://www.ngdc.noaa.gov/mgg/geodas/>
- [III-21] http://apps.ecmwf.int/datasets/data/interim_full_daily/
- [III-22] <http://www.copernicus.eu/projects/myocean>

ANNEX IV. DESCRIPTION OF THE SELFE/IMMSP/KIOST MODEL

IV-1. INTRODUCTION

The model developed by IMMSP/KIOST for radionuclide transport is based on the finite element hydrodynamic model SELFE [IV-1, IV-2]. The radionuclide transport model describes the key exchange processes shown in Figure IV-1. In the water column, radionuclides in dissolved and particulate phases are transported by currents (advection processes) with the simultaneous influence of the turbulent diffusion processes. The radionuclides in the dissolved phase interact with the particulate phase (suspended sediments and bottom deposits). The transfer of activity between the dissolved and particulate phases is described by adsorption–desorption processes. The settling of contaminated suspended sediments and the bottom erosion are important pathways of radionuclide exchanges between bottom and suspended sediments. The transfer of activity between the water column and the pore water in the upper layer of the bottom sediment is governed by diffusion processes. For a correct simulation of radionuclide dispersion 3-D current fields, suspended sediment concentrations, sediment fluxes of bottom erosion and deposition, as well as composition of bed sediments should be known. In order to carry out the required simulations a set of models, including a 3-D hydrodynamic model, 3-D sediment transport model and the radioactivity transport model were set up. The Eulerian and Lagrangian versions of radioactivity transport models are used.

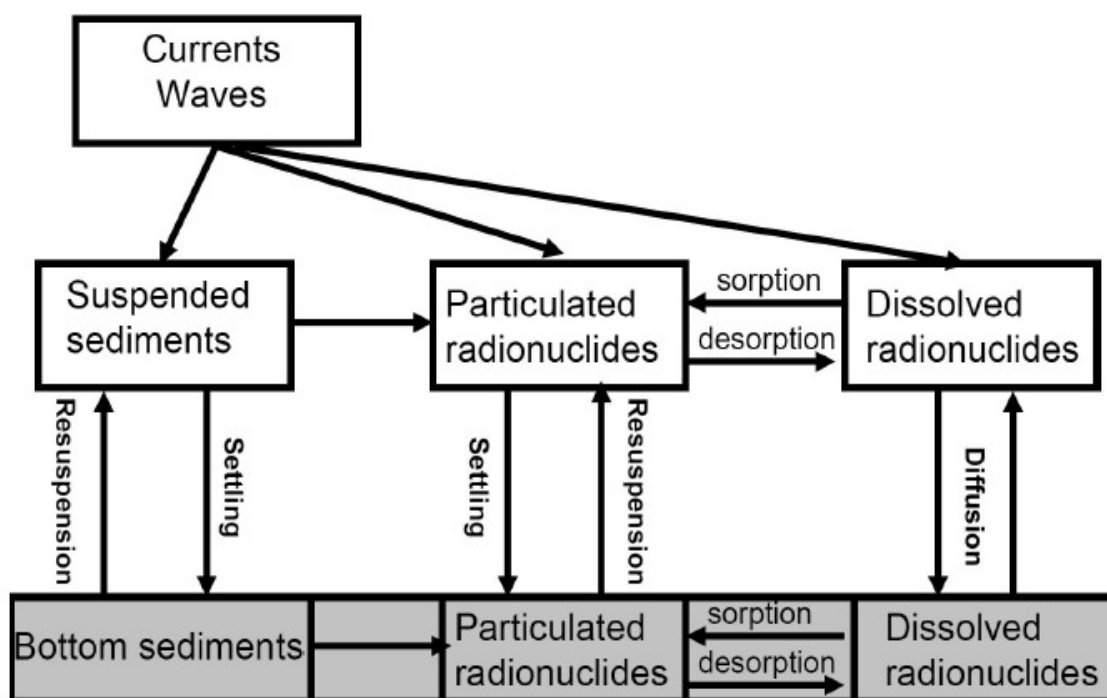


FIG. IV-1. Main processes affecting the radionuclide transport in marine environment.

IV-2. SELFE 3-D CIRCULATION MODEL

The 3-D circulation hydrostatic model SELFE [IV-1, IV-2] solves Reynolds-stress averaged Navier–Stokes (RANS) equations using a finite element approach and unstructured grids. The governing equations are conservation of mass, momentum, salt and heat with hydrostatic and Boussinesq approximations:

$$\nabla \cdot \vec{u} + \frac{\partial w}{\partial z} = 0 \quad (\text{IV-1})$$

$$\frac{\partial \eta}{\partial t} + \nabla \cdot \int_{-h}^h \vec{u} dz = 0 \quad (\text{IV-2})$$

$$\frac{D\vec{u}}{Dt} = -f\vec{k} \times \vec{u} + \alpha g \nabla \Psi - \frac{1}{\rho_0} \nabla p_a - \frac{g}{\rho_0} \int_{-h}^h \nabla \rho dz + \nabla \cdot (K_M \nabla \vec{u}) - g \nabla \eta + \frac{\partial}{\partial z} (v_t \frac{\partial \vec{u}}{\partial z}) \quad (\text{IV-3})$$

$$\frac{DS}{Dt} = \frac{\partial}{\partial z} (v_t' \frac{\partial S}{\partial z}) + F_s \quad (\text{IV-4})$$

$$\frac{DT}{Dt} = \frac{\partial}{\partial z} (v_t' \frac{\partial T}{\partial z}) + \frac{Q}{\rho_0 c_p} + F_t \quad (\text{IV-5})$$

Here (x, y) are horizontal Cartesian coordinates, in [m]; z is the vertical coordinate, positive upwards, in [m]; t is time [s]; η is the free-surface elevation, in [m]; h is bathymetric depth, in [m]; $D = h + \eta$ is the water column total depth [m]; \vec{u} is the horizontal velocity, with Cartesian components (u, v) , in [m/s]; w is the vertical velocity, in [m/s]; f is the Coriolis parameter, in [s^{-1}]; g is acceleration of gravity, in [m/s^2]; Ψ is the Earth tidal potential, in [m]; α is the effective Earth elasticity factor; ρ is water density; its reference value is $\rho_0 = 1025 \text{ kg/m}^3$; p_a is atmospheric pressure at the free surface, in [Pa]; S, T are salinity and temperature of the water [practical salinity units (psu), $^{\circ}\text{C}$]; v_t is vertical eddy viscosity, in [m^2/s]; K_M is horizontal eddy viscosity, in [m^2/s]; v_t' is vertical eddy diffusivity for salt and heat, in [m^2/s]; F_s and F_t are horizontal diffusion operators for transport equations. SELFE uses the Generic Length Scale (GLS) turbulence closure [IV-3]. The following operators appear in the equations above:

$$\nabla = \left(\frac{\partial}{\partial x}, \frac{\partial}{\partial y} \right) \quad (\text{IV-6})$$

$$\frac{D}{Dt} = \frac{\partial}{\partial t} + \vec{u} \nabla + w \frac{\partial}{\partial z} \quad (\text{IV-7})$$

In the horizontal direction SELFE uses unstructured triangular grids, while in the vertical direction the model uses hybrid coordinates, i.e. terrain following σ -coordinates and partly Z-coordinates. However, inside the numerical code all model equations are written in a Z-coordinate system. The valid representation of horizontal derivatives in σ -system is achieved by vertical interpolation of required variables.

The calculation mesh for the Pacific Ocean simulations contains 49 700 nodes and 97 989 triangular elements and has resolution from approximately 500 m near the Fukushima Daiichi NPP to 10 km in the Northwest Pacific. The surface forcing is obtained from ERA-Interim reanalysis. The lateral boundary conditions for KIOST/IMMSP calculations were obtained from HYCOM nowcast/forecast system. The KIOST/IMMSP temperature was nudged towards the HYCOM fields. The tidal forcing is imposed at open boundaries using the NAO.99b tidal prediction system.

IV-3. 3-D SEDIMENT TRANSPORT MODEL

Sediment transport in the water column is described by an advection–diffusion equation:

$$\frac{\partial C_j}{\partial t} + \frac{\partial}{\partial x_i} (u_i C_j) = \frac{\partial}{\partial x_i} \left(k_i \frac{\partial C_j}{\partial x_i} \right) + W_{sj} \frac{\partial C_j}{\partial x_3} \quad (\text{IV-8})$$

where C_j is the volume concentration of suspended sediment of class j ; u_i are velocity components, k_i are eddy diffusivity coefficients and W_{sj} is the settling velocity of suspended sediment of class j . The exchange of sediment between the bed and the flow is modelled using sink and source terms acting on the bottom computational cell. These terms represent the processes of sediment entering the flow due to erosion flux and the sediment settling down due to the depositional flux. Total flux is the difference between erosion and deposition fluxes and it is required to define them for each sediment size class.

Bottom boundary conditions are:

$$k_3 \frac{\partial C_j}{\partial z} = -D_j + E_j \quad (\text{IV-9})$$

where D_j and E_j are, respectively, the deposition and erosion flux of sediments of class j .

Non-cohesive sediment flux due to sediment deposition is simulated as a flux of particles that fall down with settling velocity W_{sj} :

$$D_i = W_{sj} C_{j,bottom} \quad (\text{IV-10})$$

where $C_{j,bottom}$ is the concentration, in the bottom computational cell, of sediments of class j . The erosion flux is calculated [IV-4, IV-5]:

$$E_j = E_{0,j}(d_j)(1-p)f_j \left(\frac{\tau_b}{\tau_{cr,j}(1+f_0)} - 1 \right)^{1.5} \text{ if } \tau_b > \tau_{cr,j} \quad (\text{IV-11})$$

where d_j is the sediment particle diameter; p is porosity; f_j is the volume fraction of sediments of class j in the bed; τ_b is the bottom shear stress; $\tau_{cr,j}$ is the critical shear stress for the sediments of class j ; f_0 is the volume fraction of cohesive sediments in bed composition and $a = 3d_j$ is a reference level above the bottom. The erosion rate is defined as:

$$E_{0,j}(d_j) = \frac{\rho_s}{a} \frac{0.015 d_j}{D_*^{0.3}} \quad (\text{IV-12})$$

with:

$$D_* = \left(\frac{g(\rho_s/\rho_w - 1)}{v^2} \right)^{1/3} \quad (\text{IV-13})$$

For the cohesive sediments, a deposition flux appears only if the shear stress is lower than the critical shear stress for deposition:

$$D_0 = -W_{sj} C_j \left(1 - \frac{\tau_b}{\tau_{cd}} \right) \text{ if } \tau_b < \tau_{cd} \quad (\text{IV-14})$$

The erosion flux for cohesive sediments is formulated using [IV-6]:

$$E_0 = E_0(1 - p)f_0 \left(\frac{\tau_b}{\tau_{cr,0}} - 1 \right) \text{ if } \tau_b > \tau_{cr,0} \quad (\text{IV-15})$$

where τ_{cd} is the critical shear stress for the deposition of cohesive sediments and $\tau_{cr,0}$ is the critical shear stress for the erosion of cohesive sediments.

For the mixture of cohesive and non-cohesive sediments the assumptions made by [IV-7] were followed. This is based on the parameter of critical cohesive sediment fraction in the seabed. Erosion of mixtures of cohesive (mud) and non-cohesive sediments (sand) is independent if clay content is below critical. Above critical clay content, the bed behaves cohesively. In the non-cohesive regime, exchange of sand and mud with bottom is independent, whereas in a cohesive regime an erosion of mud and sand occurs simultaneously as cohesive sediment. The deposition is an independent process for cohesive and non-cohesive sediments.

Cohesive sediments are able to form flocs that may have a larger effective diameter than primary particle size and, therefore, larger settling velocity. The equilibrium model is used to calculate floc size and settling velocity [IV-8]:

$$W_s = \frac{(\rho_s - \rho_w)g}{\rho_w 18\nu} D \cdot D_F \frac{1}{1 + 0.15Re^{0.687}} \quad (\text{IV-16})$$

where $Re = W_s D / \nu$ is the Reynolds number, ν is water kinematic viscosity, D_F is the diameter of original particles and:

$$D = D_F + \frac{k_A C}{k_B G^{1/2}} \quad (\text{IV-17})$$

with $G = \sqrt{\epsilon/\nu}$, where ϵ is dissipation rate, k_A and k_B are parameters describing aggregation and floc break-up respectively.

IV-4. 3-D RADIONUCLIDE DISPERSION MODEL

IV-4.1. Eulerian model

The equations for the temporal variations of dissolved radionuclide concentrations in the water column (Bq/m^3), for the concentration of particulate phase radionuclides for each sediment size class i in the water column (Bq/m^3), for the bottom layer averaged concentration of radionuclide in the pore water (Bq/m^3) and for concentration of particulate phase of radionuclide for each sediment size class i in the sediment (Bq/kg of sediments) are written in Cartesian coordinates as:

$$\frac{C_d^w}{\partial t} + \vec{U} \nabla C_d^w = -a_{12} (C_d^w \sum_{i=1}^n S_{p,i} K_{d,i} - C_p^w) - \lambda C_d^w + \text{DIFF}(C_d^w) \quad (\text{IV-18})$$

$$\frac{C_{p,i}^w}{\partial t} + \vec{U} \nabla C_{p,i}^w = W_{p,i} \frac{\partial C_{p,i}^w}{\partial z} + a_{12} (C_d^w S_{p,i} K_{d,i}^w - C_{p,i}^w) - \lambda C_{p,i}^w + \text{DIFF}(C_{p,i}^w) \quad (\text{IV-19})$$

$$\frac{\partial Z_* C_d^b}{\partial t} = W_{pw} (C_d^w (-H) - C_d^b) - a_{12} Z_* \rho_s (1 - \epsilon) (C_d^b \sum_{i=1}^n K_{d,i}^b \phi_i - C_s^b) \lambda C_d^b \quad (\text{IV-20})$$

$$\frac{\partial Z_* C_{s,i}^b}{\partial t} = a_{12} Z_* (K_{d,i}^b C_d^b - C_{s,i}^b) + \frac{D_i C_{s,i}^w}{\rho_s (1-\epsilon)} - \frac{E_i C_{s,i}^b}{\phi_i \rho_s (1-\epsilon)} - \lambda Z_* C_{s,i}^b \quad (\text{IV-21})$$

Here t is time; z is the vertical coordinate directed upwards; $\vec{U} = (U, V, W)$ is water velocity; ρ_s is the density of the sediments (kg/m^3); i is the index of sediment size class; n is total number of sediment classes; $S_{p,i}$ is the concentration of i -th class of suspended sediment (kg/m^3); $W_{p,i}$ is settling velocity of sediment class i (m/s); D_i is sediment deposition rate ($\text{kg/m}^2\text{s}$); E_i is sediment erosion rate ($\text{kg/m}^2\text{s}$); Z_* is the thickness of the upper layer of sediment (m); ϕ_i is the fraction of particles of i -th class in the bottom sediment ($\sum \phi_i = 1$); ϵ is porosity; W_{pw} is water exchange rate between the water column and pore water (m/s), related with the diffusion coefficient v_D and the thickness of upper layer of sediment as $W_{pw} = v_D Z_*^{-1}$ and λ is the radioactive decay rate. The total concentration of the particulate phase of radionuclides in water column is $C_p^w = \sum C_{p,i}^w$ and the total concentration of particulate phase of radionuclide in bottom sediment is $C_s^b = \sum \phi_i C_{s,i}^b$. The term *DIFF* presents vertical and horizontal turbulent diffusion. The phase exchange between dissolved and particulate radionuclides is written in terms of the desorption rate a_{12} (s^{-1}) and the distribution coefficients $K_{d,i}^w$ and $K_{d,i}^b$ for the water column and for the bottom deposit, respectively. The dependence of the distribution coefficient on sediment particle size can be written for the water column as [IV-9]:

$$K_{d,i}^w = \frac{3\chi}{a_{12} R_i} \quad (\text{IV-22})$$

and for bottom sediment as:

$$K_{d,i}^b = \frac{3\chi\theta}{a_{12} \rho_s R_i} \quad (\text{IV-23})$$

where R_i is sediment particle radius (m), χ is an exchange velocity (m/s) and θ is a correction factor that takes into account that part of the sediment particle surface may be hidden by other sediment particles.

At the free surface $z = \eta$ the boundary conditions for Eqs. IV-18 and IV-19 are:

$$v_T \frac{\partial C_d^w}{\partial z} - W C_d^w = -q_d \quad (\text{IV-24})$$

$$v_T \frac{\partial C_{p,i}^w}{\partial z} + (W - W_{p,i}) C_{p,i}^w = -q_{p,i} \quad (\text{IV-25})$$

where η is sea level elevation, and q_d and $q_{p,i}$ are atmospheric deposition fluxes ($\text{Bq/m}^2\text{s}$) of dissolved and particulate radionuclide, respectively. The fluxes into the bottom at $z = -H + z_o$ are:

$$v_T \frac{\partial C_d^w}{\partial z} = W_{pw} (C_d^w - C_d^b) \quad (\text{IV-26})$$

$$v_T \frac{\partial C_{p,i}^w}{\partial z} + (W - W_{p,i}) C_{p,i}^w = C_{s,i}^w D_i - C_{s,i}^b E_i \quad (\text{IV-27})$$

where z_o is roughness height of the seabed.

Assuming that the exchange of the sediment pore water with water column is balanced by redistribution of activity in bottom sediments, the pore water concentration can be obtained as:

$$C_d^b = \frac{W_{pw} C_d^w (-H) + a_{12} Z_* \rho_s (1-\epsilon) C_s^b}{W_{pw} + a_{12} Z_* \rho_s (1-\epsilon) \sum_i K_{d,i} \phi_i} \quad (\text{IV-28})$$

Using Eq. IV-22, Eq. IV-21 is simplified as:

$$\frac{\partial Z_* C_{s,i}^b}{\partial t} = a_{13} Z_* (K_{d,i}^b C_d^w - C_{s,i}^b) + \frac{D_i C_{s,i}^w}{\rho_s (1-\epsilon)} - \frac{E_i C_{s,i}^b}{\phi_i \rho_s (1-\epsilon)} - \lambda Z_* C_{s,i}^b \quad (\text{IV-29})$$

where:

$$a_{13} = \frac{a_{12} W_{pw}}{W_{pw} + a_{12} Z_* \rho_s (1-\epsilon) \sum_i K_{di} \phi_i} \approx \frac{W_{pw}}{Z_* \rho_s (1-\epsilon) \sum_i K_{di} \phi_i} \quad (\text{IV-30})$$

IV-4.2. Lagrangian model

In the Lagrangian model a release of radioactivity is simulated by a large number of particles, with each of them transporting an equal amount of activity. The same equations were used as for the Eulerian model but for only one characteristic fraction of sediments. The particles are transported by currents, turbulent diffusion and they can settle with sediment particles. The turbulent diffusion, transfer of activity between solute, particulate and bottom phases and decay are described by stochastic methods [IV-10].

In order to simulate radioactivity transport a Random Dispersion Model (RDM) was used where positions of particles are simulated as a random Markov process. The equations describing increment of particle position over each time increment dt are given by:

$$dx = u dt + \frac{\partial K}{\partial x} dt + \sqrt{2K} R_x \quad (\text{IV-31})$$

$$dy = v dt + \frac{\partial K}{\partial y} dt + \sqrt{2K} R_y \quad (\text{IV-32})$$

$$dz = w dt + w_s dt + \frac{\partial K_z}{\partial z} dt + \sqrt{2K_z} R_z \quad (\text{IV-33})$$

where u , v and w are velocity components on coordinate axis (x, y, z) , and (R_x, R_y, R_z) are random variables with zero mean and variance dt .

REFERENCES TO ANNEX IV

- [IV-1] ZHANG, Y., BAPTISTA, A.M., SELFE: A semi-implicit Eulerian-Lagrangian finite-element model for cross-scale ocean circulation, *Ocean Modelling* **21**(3–4) (2008) 71–96.
- [IV-2] ROLAND, A., ZHANG, Y.J., WANG, H.V., MENG, Y., TENG, Y.C., MADERICH, V., BROVCHENKO, I., DUTOUR-SIKIRIC, M., ZANKE, U., A fully coupled 3D wave-current interaction model on unstructured grids, *Journal of Geophysical Research* **117**, C00J33 (2012) 1–18.
- [IV-3] UMLAUF, L., BURCHARD, H., A generic length-scale equation for geophysical turbulence models, *Journal of Marine Research* **61**(2) (2003) 235–265.
- [IV-4] VAN RIJN, L.C., Sediment transport, Part II: Suspended load transport, *Journal of Hydraulic Engineering* **110** (1984) 1613–1641.
- [IV-5] VAN RIJN, L.C., Sediment transport, Part I: Bed load transport, *Journal of Hydraulic Engineering* **110** (1984) 1431–1456.
- [IV-6] ARIATHURAI, R., ARULANANDAN, K., Erosion rates of cohesive soils, *Journal of Hydraulic Division* **104**(2), 279–283 (1978).
- [IV-7] VAN LEDDEN, M., Sand-mud segregation in estuaries and tidal basins PhD Thesis: Delft University of Technology, Delft (2003) 221 p.
- [IV-8] WINTERWERP, J.C., VAN KESTEREN, W.G.M., Introduction to the Physics of Cohesive Sediment Dynamics in the Marine Environment, Elsevier (2004) 576 p.
- [IV-9] PERIÁÑEZ, R., A modelling study on ^{137}Cs and $^{239/240}\text{Pu}$ behaviour in the Al-borán Sea, western Mediterranean, *Journal of Environmental Radioactivity* **99** (2008) 694–715.
- [IV-10] PERIÁÑEZ, R., ELLIOTT, A.J., A particle-tracking method for simulating the dispersion of non-conservative radionuclides in coastal waters, *Journal of Environmental Radioactivity* **58**(1) (2002) 13–33.

ANNEX V. DESCRIPTION OF THE UNIVERSITY OF SEVILLE (USEV) 2-D DEPTH AVERAGED MODEL (BALTIC SEA APPLICATION)

V-1. HYDRODYNAMICS

USEV applied a 2-D depth averaged model forced by the annual mean winds (southwest wind, 6 m/s) to solve the annual mean circulation in the Baltic Sea. Ice cover and water density differences were not considered. A steady mean circulation was obtained, which was used in order to simulate the transport of radionuclides. The model spatial resolution is 2 minutes of arc, both in longitude and latitude and bathymetry was obtained from the GEODAS database [V-1].

Hydrodynamic calculations were based on the following equations [V-2]:

$$\frac{\partial \zeta}{\partial t} + \frac{\partial}{\partial x}(Hu) + \frac{\partial}{\partial y}(Hv) = 0 \quad (V-1)$$

$$\frac{\partial u}{\partial t} + u \frac{\partial u}{\partial x} + v \frac{\partial u}{\partial y} + g \frac{\partial \zeta}{\partial x} - fv + \frac{\tau_u}{\rho_w H} = A \left(\frac{\partial^2 u}{\partial x^2} + \frac{\partial^2 u}{\partial y^2} \right) \quad (V-2)$$

$$\frac{\partial v}{\partial t} + u \frac{\partial v}{\partial x} + v \frac{\partial v}{\partial y} + g \frac{\partial \zeta}{\partial y} + fu + \frac{\tau_v}{\rho_w H} = A \left(\frac{\partial^2 v}{\partial x^2} + \frac{\partial^2 v}{\partial y^2} \right) \quad (V-3)$$

where u and v are the depth averaged water velocities along the x and y axis, h is the depth of water below the mean sea level, ζ is the displacement of the water surface above the mean sea level (positive upwards), $H = h + \zeta$ is the total water depth, f is the Coriolis parameter ($f = 2\Omega \sin \lambda$, where Ω is the Earth rotational angular velocity and λ is latitude), g is acceleration due to gravity, ρ_w is water density and A is the horizontal eddy viscosity. Friction stresses τ_u and τ_v are written in terms of a quadratic law:

$$\begin{aligned} \tau_u &= k\rho_w u \sqrt{u^2 + v^2} \\ \tau_v &= k\rho_w v \sqrt{u^2 + v^2} \end{aligned} \quad (V-4)$$

where k is the bed friction coefficient.

The stress on the sea surface caused by the wind has to be added to these equations. It is written as:

$$\tau_w = \rho_a C_d W^2 \quad (V-5)$$

where ρ_a is air density, C_d is a friction coefficient and W is wind speed measured 10 m above the sea surface. The friction coefficient between the air and water is obtained from empirical equations:

$$\begin{aligned} C_d &= (1.29 - 0.024W) \times 10^{-3} \quad W < 8 \text{ m/s} \\ C_d &= (0.581 - 0.063W) \times 10^{-3} \quad 8 < W < 35 \text{ m/s} \end{aligned} \quad (V-6)$$

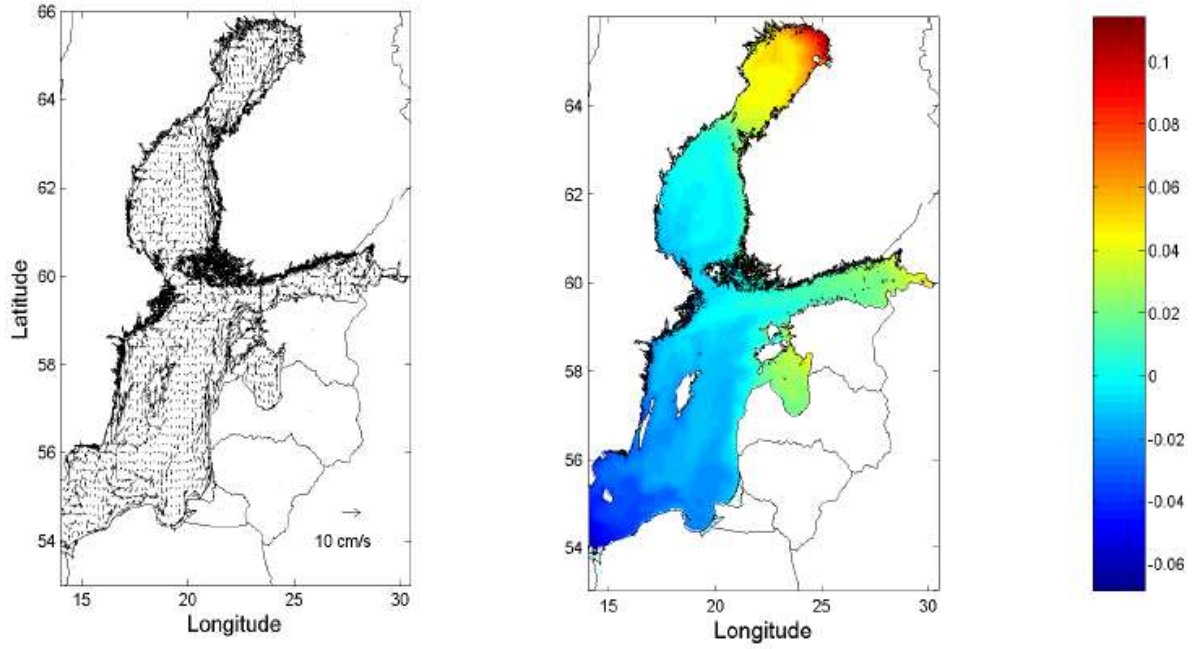


FIG. V-1. 2-D mean annual circulation calculated by USEV model and sea surface set-up forced by a mean wind from the southwest (6 m/s). The scale colour is in meters (m).

As an example, the calculated annual mean circulation and the wind set-up are presented in Figure V-1. Wind set-up is the sea surface displacement from the mean sea level caused by the wind. Since the wind blows from the southwest, the water is piled at the northeast borders of the sea, where the sea level is higher than in the southwest.

V-2. SEDIMENT TRANSPORT

Sediment dynamics is described in a very simple way, but still retains its main aspects. This has proven to be enough to satisfactorily simulate reactive pollutant dispersion. The transport of sediments is described by a 2-D advection–diffusion equation to which some terms are added. These are external sources of particles, terms describing particle deposition on the seabed and erosion from the bed to the water column. The formulation of these processes is based upon standard formulae. Thus, the erodability constant is used for the erosion term. Particle deposition is described using the settling velocity, which is obtained from Stokes' law. Critical erosion and deposition stresses are applied as usual [V-3–5].

The equation for suspended sediment transport is:

$$\frac{\partial(Hm)}{\partial t} + \frac{\partial(uHm)}{\partial x} + \frac{\partial(vHm)}{\partial y} = \frac{\partial}{\partial x} \left(HK_h \frac{\partial m}{\partial x} \right) + \frac{\partial}{\partial y} \left(HK_h \frac{\partial m}{\partial y} \right) + (ER - DEP) + S \quad (V-7)$$

where m is the suspended matter concentration, K_h is an effective horizontal diffusion coefficient, S is the external particle source and ER and DEP are the erosion and deposition terms respectively.

The deposition term is written in the following form:

$$DEP = w_s m \left(1 - \frac{|\bar{\tau}|}{\tau_{cd}} \right) \quad (V-8)$$

where $\bar{\tau}$ is the bottom friction stress (whose components are given by Eq. V-4) and τ_{cd} is a critical deposition stress above which no deposition occurs since particles are kept in suspension by turbulence. The settling velocity of particles is obtained from Stokes' law as mentioned above:

$$w_s = \frac{\rho - \rho_w}{\rho_w} \frac{g D^2}{18 \nu} \quad (V-9)$$

where ρ and D are suspended particle density and diameter respectively and ν is the kinematic viscosity of water.

The erosion rate is written in term of the erodability constant E :

$$ER = E f_p \left(\frac{|\bar{\tau}|}{\tau_{ce}} - 1 \right) \quad (V-10)$$

where f_p gives the fraction of fine particles in the bed sediment and τ_{ce} is a critical erosion stress below which no erosion occurs. The model can also calculate sedimentation rates (SR) as the balance between the deposition and erosion terms.

V-3. RADIONUCLIDE TRANSPORT

The dispersion model includes three phases, i.e. water, suspended matter in the water column and bed sediments. An advection–diffusion equation is solved in order to simulate the transport of radionuclides in the water column. Interactions between the dissolved phase and solid phases (suspended matter and bed sediments) are described through a dynamic approach, in terms of kinetic transfer coefficients. Thus, assuming that adsorption–release reactions are described by a single reversible reaction, a coefficient k_1 characterizes the transfer from the liquid to the solid phase and a coefficient k_2 characterizes the inverse process. Dimensions of these coefficients are $[T]^{-1}$.

The adsorption process is a surface phenomenon that depends on the surface of particles per water volume unit. This quantity has been denoted as the exchange surface [V-6–9]. Thus in general:

$$k_1 = \chi (S_m + S_s) = k_1^{spm} + k_1^{sed} \quad (V-11)$$

where S_m and S_s are the exchange surfaces for suspended matter and bottom sediments respectively (dimensions $[L]^{-1}$). χ is a parameter with the dimensions of a velocity. It is denoted as the exchange velocity [V-6–9].

Assuming spherical particles, the exchange surfaces are written as [V-6–9]:

$$S_m = \frac{3m}{\rho R} \quad (V-12)$$

and:

$$S_s = \frac{3L f_p (1-p) \phi}{RH} \quad (V-13)$$

where R is particle radius, p is sediment porosity, L is the sediment mixing depth (the distance to which the dissolved phase penetrates the sediment) and ϕ is a correction factor that takes into account that part of the sediment particle surface may be hidden by other sediment particles. This formulation has been successfully used in all modelling works cited above. Real particles are not spheres, but with this approach it is possible to obtain an analytical expression for the exchange surface [V-10].

The equation that gives the temporal evolution of pollutant concentration in the dissolved phase, C_d , is:

$$\begin{aligned} \frac{\partial(HC_d)}{\partial t} + \frac{\partial(uHC_d)}{\partial x} + \frac{\partial(vHC_d)}{\partial y} = \frac{\partial}{\partial x} \left(HK_h \frac{\partial C_d}{\partial x} \right) + \frac{\partial}{\partial y} \left(HK_h \frac{\partial C_d}{\partial y} \right) \\ - H(k_1^{spm} + k_1^{sed})C_d + k_2 H m C_s + k_2 \rho_s \phi f_p A_s \end{aligned} \quad (V-14)$$

where A_s and C_s are concentrations in the active fraction of bed sediments and suspended matter respectively.

The temporal evolution of pollutant concentration in suspended particles is given by:

$$\begin{aligned} \frac{\partial(HC_s m)}{\partial t} + \frac{\partial(uHC_s m)}{\partial x} + \frac{\partial(vH_s m)}{\partial y} = \frac{\partial}{\partial x} \left(HK_h \frac{\partial(C_s m)}{\partial x} \right) + \frac{\partial}{\partial y} \left(HK_h \frac{\partial(C_s m)}{\partial y} \right) + \\ k_1^{spm} C_d H - k_2 m C_s H + SED \end{aligned} \quad (V-15)$$

where SED expresses the pollutant exchange between suspended particles and the bed sediment resulting from erosion/deposition:

$$SED = \begin{cases} -SR \cdot C_s & SR > 0 \\ -SR \cdot A_s & SR < 0 \end{cases} \quad (V-16)$$

where SR is the sedimentation rate calculated by the sediment transport model.

The equation for the temporal evolution of concentration in the bed sediment is:

$$\frac{\partial A_s}{\partial t} = k_1^{sed} \frac{C_d H}{L \rho_s f_p} - k_2 A_s \phi + SED \quad (V-17)$$

where now the exchange due to erosion/deposition of suspended particles is written as:

$$SED = \begin{cases} \frac{SR \cdot C_s}{L \rho_s f_p} & SR > 0 \\ \frac{SR \cdot A_s}{L \rho_s f_p} & SR < 0 \end{cases} \quad (V-18)$$

The total concentration of pollutants in the sediment, A_{tot} , is computed from:

$$A_{tot} = f_p A_s \quad (V-19)$$

All equations are solved using explicit finite difference schemes [V-2]. Second order accuracy schemes are used for advective and diffusive terms.

V-4. APPLICATION TO THE BALTIC SEA

In this particular application to the Baltic Sea, a constant and uniform suspended matter concentration over the domain, 4.5 mg/l, has been considered. The model was calibrated using the ^{137}Cs inventories over the whole Baltic Sea in water and sediments estimated from measurements. A standard value, determined for Cs from experiments [V-11] was used for k_2 and the forward rate, k_1 , can be determined from k_2 and the equilibrium distribution coefficient, k_d , as explained in Refs. [V-6–9]:

$$k_d = \frac{\chi}{k_2} \frac{3}{\rho R} \quad (\text{V-20})$$

Good results are obtained with $k_d = 3 \text{ m}^3/\text{kg}$, which is close to the recommended value by the International Atomic Energy Agency [V-12]: $4 \text{ m}^3/\text{kg}$. In addition, the sediment mixing depth (distance until which the dissolved phase interacts with the sediment) was set to 2 cm. Finally, a correction factor which takes into account that part of the sediment particle surface may be hidden by other sediment particles is introduced ($\phi = 0.001$). A detailed formulation of the model may be seen [V-6–9]. In summary, three parameters are optimized, i.e. the equilibrium distribution coefficient, sediment mixing depth and sediment correction factor.

Once the temporal evolution of ^{137}Cs inventories in the Baltic Sea in the water column and sediments are adequately reproduced by the model, mean ^{137}Cs concentrations in several sub-basins were extracted from the model, without any extra tuning, and compared with field data.

REFERENCES TO ANNEX V

- [V-1] <https://www.ngdc.noaa.gov/mgg/geodas/>
- [V-2] KOWALIK, Z., MURTY, T.S., Numerical Modelling of Ocean Dynamics, World Scientific, Singapore (1993).
- [V-3] PERIÁÑEZ, R., Modelling the transport of suspended particulate matter by the Rhone River plume (France), Implications for pollutant dispersion, Environmental Pollution **133** (2005) 351–364.
- [V-4] LIU, W.C., HSU, M.H., KUO, A.Y., Modelling of hydrodynamics and cohesive sediment transport in Tanshui River estuarine system, Taiwan, Marine Pollution Bulletin **44** (2002) 1076–1088.
- [V-5] LUMBORG, U., WINDELIN, A., Hydrography and cohesive sediment modelling: Application to the Romo Dyb tidal area, Journal of Marine Systems **38** (2003) 287–303.
- [V-6] PERIÁÑEZ, R., A modelling study on ^{137}Cs and $^{239/240}\text{Pu}$ behaviour in the Al-borán Sea, western Mediterranean, Journal of Environmental Radioactivity **99** (2008) 694–715.
- [V-7] PERIÁÑEZ, R., Environmental modelling in the Gulf of Cádiz: Heavy metal distributions in water and sediments, Science of the Total Environment **407** (2009) 3392–3406.
- [V-8] PERIÁÑEZ, R., Modelling the environmental behavior of pollutants in Algeciras Bay (south Spain), Marine Pollution Bulletin **64** (2012) 221–232.
- [V-9] PERIÁÑEZ, R., CASAS-RUIZ, M., BOLÍVAR, J.P., Tidal circulation, sediment and pollutant transport in Cádiz Bay (SW Spain): A modelling study, Ocean Engineering **69** (2013) 60–69.
- [V-10] PERIÁÑEZ, R., Modelling the dispersion of radionuclides in the marine environment: an introduction, Springer, Berlin (2005).
- [V-11] NYFFLER, U.P., LI, Y.H., SANTSCHI, P.H., A kinetic approach to describe trace element distribution between particles and solution in natural aquatic systems, Geochimica Cosmochimica Acta **48** (1984) 1513–1522.
- [V-12] INTERNATIONAL ATOMIC ENERGY AGENCY, Sediment distribution coefficients and concentration factors for biota in the marine environment, Technical Reports Series No. 422, IAEA, Vienna (2004).

ANNEX VI. DESCRIPTION OF THE KAERI: LORAS MODEL

After the Fukushima Daiichi NPP accident, a large amount of radioactive material was released into the ocean as well as the atmosphere. Therefore, it is necessary to evaluate marine dispersion for radiological emergency preparedness against a nuclear accident. From this perspective, an oceanic dispersion model named LORAS was developed by KAERI in order to evaluate the transport characteristics of the radionuclides released into the sea for a nuclear accident [VI-1].

The model was designed to calculate radionuclide concentrations in seawater, suspended matter and bed sediments in time and space using a particle tracking method. The particle tracking technique has some advantages over finite difference methods, in particular, numerical diffusion is not introduced and the exact position of the release point may be specified. Thus, it is not necessary to assume that the discharge is instantaneously mixed into a grid cell of a given size. A passive particle is transported by current components and dispersed by turbulent motion. Currents are supplied by the hydrodynamic circulation model and turbulent dispersion is evaluated using a random walk method [VI-1, VI-2]. The dispersion of reactive and non-reactive radionuclides may also be simulated in the model. 3-D turbulent diffusion and the pollutant interactions between water, suspended matter and bottom sediments are simulated using a stochastic method [VI-3]. The movement of the particle is represented by the sum of the movements due to advection by the current and turbulence. The new position x_j of a given particle after a time step Δt is represented as follows:

$$x_j(t + \Delta t) = x_j(t) + v_j(t)\Delta t + v'_j(t)\Delta t \quad (\text{VI-1})$$

where v_j are the oceanic currents in the three spatial directions ($j = 1, 2, 3$) and v'_j are the turbulent motion ($j = 1, 2, 3$). Three-dimensional turbulent mixing is computed by a random walk method:

$$v'_{1,2} = \sqrt{12K_{1,2}\Delta tR} \quad (\text{VI-2})$$

$$v'_3 = \sqrt{2K_3\Delta tR} \quad (\text{VI-3})$$

where K_j are diffusion coefficients in each corresponding direction of space and R is a random number between 0 and 1.

A stochastic method is used to estimate the dispersion of non-conservative radionuclides and provide concentrations in water, suspended matter and bottom sediments. These processes are formulated using kinetic transfer coefficients, considering that exchanges of radionuclides between the liquid and solid phases are governed by a first-order reversible reaction [VI-3]. The differential equations which describe transfers between the three phases are expressed as follows:

$$\frac{\partial C_w}{\partial t} = -k_{1m}C_w - k_{1s}C_w \quad (\text{VI-4})$$

$$\frac{\partial C_s}{\partial t} = -k_2C_s \quad (\text{VI-5})$$

$$\frac{\partial C_b}{\partial t} = -k_2\phi C_b \quad (\text{VI-6})$$

where C_w , C_s and C_b are radionuclide concentrations in seawater, suspended matter and bottom sediments, respectively. k_{1m} is the kinetic coefficient describing radionuclide transfer from

water to suspended matter, k_{1s} describes the transfer from water to bottom sediments and k_2 is the kinetic transfer coefficient which describes radionuclide release from suspended matter or bottom sediments to water. Finally, ϕ is a correction factor which takes into account that some of the sediment particle surface may be hidden by other particles. Radioactive decay is described by the following equation:

$$C(t + \Delta t)_{\text{decay}} = C(t)[1 - \exp(\lambda\Delta t)] \quad (\text{VI-7})$$

where C is the radionuclide concentration and λ is the radioactive decay rate.

Radionuclide concentrations in seawater (C_w), suspended matter (C_s) and bed sediments (C_b) are calculated in the domain of interest by counting the number of particles as follows:

$$C_w = \frac{I \cdot N_w}{\Delta x \Delta y \Delta z} \quad (\text{VI-8})$$

$$C_s = \frac{I \cdot N_s}{m \Delta x \Delta y \Delta z} \quad (\text{VI-9})$$

$$C_b = \frac{I \cdot N_b}{H \rho_b \Delta x \Delta y} \quad (\text{VI-10})$$

Here $I = Q/NP$, where Q is the source term and NP is the number of particles used in the simulation. $\Delta x \Delta y \Delta z$ is the volume of each cell, m is suspended matter concentration, H is the mixing depth in the bottom sediment and ρ_b is sediment bulk density. Finally, N_w , N_s and N_b are the number of particles in each phase.

Parallel techniques on Linux OS are used to reduce the simulation time for emergency response against a nuclear accident. Fastest processing times are achieved when the problem is divided into equally-sized chunks onto the available computer cores. However, splitting the mesh implies some efforts which have to be considered. Each subdivision would have to pass particle information (ghosts) to each other because each particle exerts forces on all other particles. Also, particles that move out of a node boundary will have to be sent to the corresponding node. In LORAS, the interaction between particles can be ignored (between radionuclides) and Figure VI-1 shows a scheme on the particle distribution method through the masking.

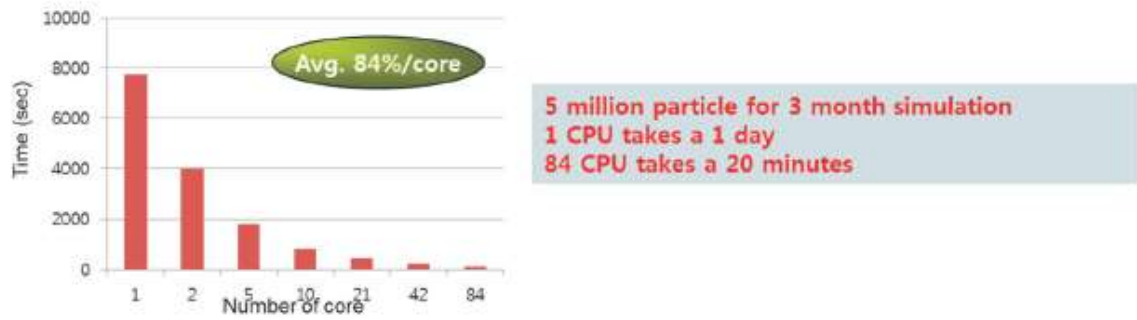
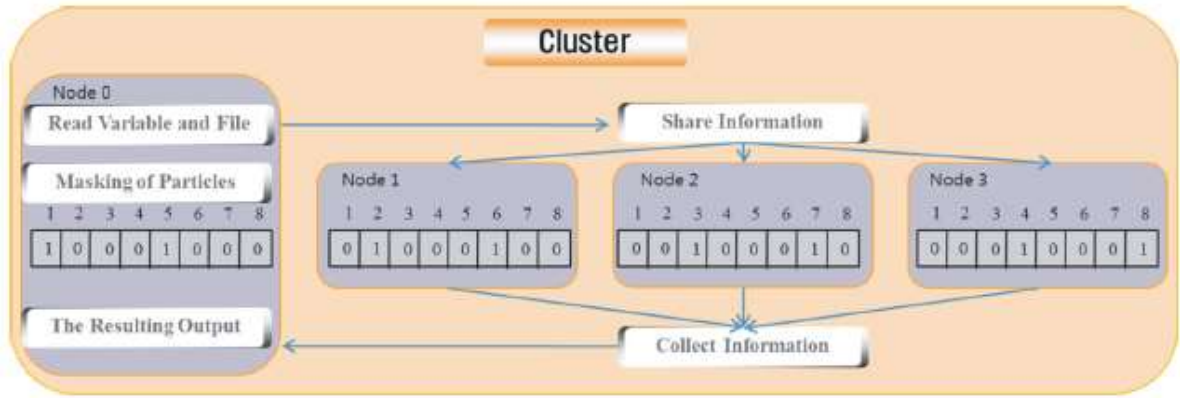


FIG. VI-1. Parallel process scheme in LORAS.

REFERENCES TO ANNEX VI

- [VI-1] MIN, B.I., PERIÁÑEZ, R., KIM, I.G., SUH, K.S., Marine Dispersion Assessment of ¹³⁷Cs Released from the Fukushima Nuclear Accident, *Marine Pollution Bulletin* **72** (2013) 22–33.
- [VI-2] MIN, B.I., PERIÁÑEZ, R., PARK, K., KIM, I.G., SUH, K.S, Assessment in marine environment for a hypothetical nuclear accident based on the database of tidal harmonic constants, *Marine Pollution Bulletin* **87** (2014) 269–275.
- [VI-3] PERIÁÑEZ, R., ELLIOTT, A.J., A particle-tracking method for simulating the dispersion of non-conservative radionuclides in coastal waters, *Journal of Environmental Radioactivity* **58**(1) (2002) 13–33.

ANNEX VII. DESCRIPTION OF THE NATIONAL TECHNICAL UNIVERSITY OF ATHENS (NTUA), DISPERSION MODEL

The NTUA model is an Eulerian dispersion model based on the solution of the equation:

$$\frac{\partial}{\partial t}(\rho C) + \nabla \cdot (\rho \vec{v} C) = \nabla \cdot (\Gamma_s \nabla C) \quad (\text{VII-1})$$

where C is the radionuclide concentration, ρ is water density, v is water velocity and Γ_s is the kinematic viscosity of seawater.

The ^{137}Cs sediment concentration was calculated using the relevant distribution coefficient k_d . The finite-volume method was implemented for the numerical solution of the differential equations.

ANNEX VIII. DESCRIPTION OF THE SISBAHIA HYDRODYNAMIC AND TRANSPORT MODELLING APPROACH

VIII-1. INTRODUCTION

The modelling approach follows the strategy of SisBAHIA, accordingly with a hierarchical database system, in the following way:

- (1) Selected Database: selection is made from the SisBAHIA interface from the many that might have been created. New databases can easily be created as required from the SisBAHIA interface.
- (2) Selected Modelling Project: selection is made from the SisBAHIA interface from those that might have been created within the Selected Database. New Modelling Projects can be created as necessary from the SisBAHIA interface.
- (3) Selected Domain/Mesh: selection is made from the SisBAHIA interface from the many that might have been created within the Selected Modelling Project. New Domain/Meshes can be implemented as required from the SisBAHIA interface and associated meshing tools.
- (4) Selected Hydrodynamic Model: selection is made from the SisBAHIA interface from those that may have been set up and associated with the Selected Domain/Mesh. Each Hydrodynamic Model which has been set up represents a given scenario of interest. The same mesh can be used for vertically averaged 2-DH and for 3-D models of the domain. New models can easily be created and set up as required from the SisBAHIA interface.
- (5) Selected Transport Model: selected from many that may have been set up and associated with the selected Hydrodynamic Model. New models can be created and set up as needed from the SisBAHIA interface. Transport models can be of three different types, i.e general purpose Eulerian models; Eulerian models for water quality (salt, temperature, dissolved oxygen-biochemical oxygen demand (DO-BOD), nitrogen, phosphorous and biomass); general purpose Lagrangian models.

In all cases pertinent to modelling the transport of water constituents and determining their fate during a time period, the focus will be in the far field, i.e. in regions sufficiently far from the water outlets, away from the active turbulent mixing zones typical of the jets that form in the near field of the outlets. In these far regions, the plumes of constituents, including those of heated water, are passively transported by the prevailing currents. Thus, in a far field sense, the considered water constituents, including heat and particulate substances, can be treated as passive scalars. The passive scalar approach allows decoupling of the transport modelling from the hydrodynamic circulation modelling. In this respect, the implicit hypothesis is that the hydrodynamic circulation in the far field is independent of the concentration distribution of a given constituent. The decoupling of the transport model from the hydrodynamic model allows the negligence of baroclinic forcing in the latter.

VIII-2. GENERAL DESCRIPTION

A comprehensive description of SisBAHIA can be found in various publications [VIII-1–5]. In summary, the current version of SisBAHIA has the following main features:

- **Hydrodynamic model:** It is a constant density 3-D/2-DH hydrodynamic circulation model optimized for natural water bodies. Results can be either 3-D or vertically averaged (2-DH) depending on input data. ‘Optimized’ is used in the sense of a model planned for optimal representation of flows in natural water bodies. The calibration process is

minimized due to: spatial discretization via quadratic finite elements and σ transformation, allowing for optimal representation of water bodies with complex geometries and bottom topography; wind field and bottom roughness that can vary dynamically in time and space, and self-adjusting multi-scale turbulence modelling based on Large Eddy Simulation.

- **Eulerian transport model:** It is a general purpose advective–diffusive transport model with kinetic reactions for 2-DH or selected layers of 3-D flows with a given thickness. This model can be used to compute space distribution and fate of dissolved contaminants.
- **Water quality models:** A set of Eulerian transport models for the coupled simulation of water quality parameters like salt, temperature, DO-BOD, nitrogen compounds, phosphorous compounds and biomass. Models can be applied for 2-DH flows or for selected layers of 3-D flows with a given thickness. The temperature module of this set of models can be used to compute the time variation and space distribution of temperature of thermal plumes occupying a surface layer.
- **Lagrangian transport model - deterministic mode:** It is a general purpose advective–diffusive transport model with kinetic reactions for selected layers of 3-D and for 2-DH flows. This model is especially suitable for the simulation of plumes or clouds that are initially small to be well resolved by the discretizing mesh of the associated hydrodynamic model. Any curve representing a kinetic reaction dependent on the lifetime of a given particle can be adopted. This model can be used for computing the space distribution and decay of particulate contaminants. The user can choose to run the model in free transport mode or conditioned transport mode. The latter being particularly suitable for simulations of sedimentological processes. The transport can be conditioned by a minimum velocity, minimum bottom stress due to currents or due to currents and wind waves. The user can also specify a tolerance band for the limiting condition, in which the transport of a particle follows a fuzzy decision process.
- **Lagrangian transport model - probabilistic mode:** In this mode, the user can produce maps of isolines of probabilities based on N events or for a period of time T . Examples of outputs are: isolines of probability of visitation of a plume or cloud with concentrations above a given limit or determination of critical events, as the first event or first time in which a plume or cloud touches the coastline, etc.
- **Wind-wave generation model:** For a given wind field, variable in time, the model computes the wind wave field generated within the model domain, for a persistence of wind, and time intervals defined by the user. For all nodes in a given domain, the model computes parameters like significant and root mean square wave heights and periods, oscillatory bottom stresses, limiting fetches etc.

VIII-3. HYDRODYNAMIC MODELLING DETAILS

The 3-D spatial discretization is achieved via a vertical stack of sub-parametric finite element meshes using σ -coordinate transformation along the vertical dimension. That is, if one looks from the top, one sees the horizontal plane of the domain discretized by a single mesh of finite elements. However, in actual fact, there will be a stack of meshes, one for every σ level. In this way, vertical discretization is performed automatically once the user defines the number of desired σ levels (usually between 10 and 50). The 3-D model is automatically activated if at least 5 σ levels are requested. Elements in a mesh are sub-parametric. The variables in each element are defined by quadratic Lagrangian polynomials whereas the element geometry is defined by linear Lagrangian polynomials. Elements in a mesh can be quadrilaterals and/or triangles. Quadrilaterals are preferred because variables become bi-quadratic, and thus have a higher accuracy. This discretizing scheme is potentially of fourth order on the σ planes and of

second order on the σ dimension. Temporal discretization is achieved through a second order implicit factored scheme for nonlinear terms and a Crank–Nicholson scheme for linear terms. Phase errors are minimized because all terms in the numerical scheme are centered at the same instant, $t = (n + 1/2)\Delta t$. Phase errors are prone to occur in numerical schemes in which all terms are not centered in the same instant.

The 3-D + 2-DH computations are entirely coupled and thence performed at every time step. The 3-D model uses the free surface elevation computed in the 2-DH model, and has a matching condition: the vertically averaged 3-D velocity profiles need to match the 2-DH velocities. When coupled with the 3-D model, the bottom stress in the 2-DH model depends on the 3-D velocity profiles. In simulations in which only the 2-DH model is required, the bottom stress is computed by the usual quadratic law.

The 2-DH solving engine is based on the generalized minimal residual method iterative solver. The 3-D solution is implicit along the vertical σ direction and explicit along σ planes, thence it becomes numerically a 1-D problem for every water column represented by a mesh node. The 1-D problems are solved in a finite difference scheme, using double sweep techniques. An optional numeric-analytic solution for the vertical profiles is also available. This numeric-analytic option renders very good results in regions where 3-D advection is of less importance.

Due to the iterative method of the solver, in general when modelling bays or coastal waters the best gain, i.e. the ratio between real time and simulation time, is obtained with an average Courant number around 5. It is quite common though to have a max Courant > 20 in a given mesh. Depending on the size of the mesh and scales of the problem, it is customary in SisBAHIA to have gains over 120 for coastal area models running on a PC powered by processors above 3 GHz. That is, 2 months of real time 3-D circulation in a coastal area domain would be simulated in 12 hours.

Along open boundaries, elevations can be prescribed in many different ways, including synthetic tides generated by given harmonic constants, and data measured or provided at discrete times. A different value, and/or phase shift, can be given for each node along any open boundary segment. Imposition of radiation condition, in a way similar to the one adopted in the Princeton Ocean Model (POM), can also be used. The angle of inflow along open boundaries can be automatically computed, as a function of the geometry of the domain, or can be enforced. The angle of outflow can be free or enforced. Moreover, prescription of 2-DH current velocities along open boundaries assimilated from ocean circulation models can also be applied.

In the case of land boundaries, one can prescribe either normal or imposed directional fluxes or velocities, both of which can be constant or variable in time (e.g. a river discharge curve). Leaky boundaries are allowed, as are slip and no-slip boundaries, and the equivalent roughness along each boundary node can be prescribed. For the 3-D model, zero velocity is the bottom boundary condition, and the wind stress is prescribed as the free surface condition. Dynamic drying and flooding areas can be modelled with proper discretization, or can be simulated in a virtual way through leaky lateral boundaries.

In computing bottom stresses, the amplitude of the equivalent bottom roughness can be specified for each bottom node, reflecting the type of material (i.e. rock, sand, mud, vegetation, etc.). The computed friction coefficients of the bottom vary dynamically in time and space.

When performing turbulence modelling, a multi-scale model is employed. Horizontal subgrid scale turbulent stresses are based on filtering techniques, also known as Large Eddy Simulation

(LES). Small scale horizontal and vertical turbulent stresses employ an eddy viscosity approach. Eddy viscosity tensor is anisotropic and dynamically variable in space and time for each node.

All models are integrated into a user-friendly interface, through with a number of mesh editing tools and pre-processing facilities are available. Many graphical output options are available, including maps, time series; tidal ellipses, vertical profiles, and animations can be generated, visualized or printed even while models are running.

REFERENCES TO ANNEX VIII

- [VIII-1] ROSMAN, P.C.C., Modeling Shallow Water Bodies via Filtering Techniques, *Numerical Methods in Water Resources* **5** (2001) 1–162.
- VIII-2] CUNHA, C.L.N., ROSMAN, P.C.C., A semi-implicit finite element model for natural water bodies, *Water Research* **39** (2005) 2034–2047.
- [VIII-3] LAMEGO, F.F., Advanced Nuclear Reactors and Tritium Impacts: Modeling the aquatic pathway, *Progress in Nuclear Energy* **68** (2013) 9–22.
- [VIII-4] LAMEGO, F.F., Eulerian modeling of radionuclides in surficial water: The case of Ilha Grande Bay (RJ, Brazil), In: *Integral Methods in Science and Engineering*, Springer, New York (2013) 259–277.
- [VIII-5] SAAD, Y., ILUT: A dual threshold incomplete LU factorization, *Numerical Linear Algebra Applications* **1** (1994) 387–402.

ANNEX IX. DESCRIPTION OF THE JAEA: SEA-GEARN MODEL

The SEA-GEARN model [IX-1] is a particle random-walk model which has been used to simulate radionuclide transport in the Pacific Ocean. SEA-GEARN uses 3-D velocity data calculated by an ocean general circulation model as the input variables. If non-conservative radionuclides are concerned, the interactions with particulate matter need to be considered. In order to take these situations into account, a new model that solves three-phase interaction [IX-2], was adopted in SEA-GEARN. Radionuclides are assumed to exist in three phases, such as dissolved, large particulate matter (LPM) and active bottom sediment, respectively. This model has the following assumptions: (i) the LPM is an aggregate which has a single radius and density; and (ii) the movement of each particle is governed by velocity, diffusivity and settling velocity of the particle itself.

Moreover, the following assumptions are also made: (i) the dissolved phase consists of radionuclides that are dissolved and adsorbed onto fine (diameter < 0.8 μm) particles without settling velocity; (ii) the LPM phase consists of radionuclides that are adsorbed on settling suspended particles; (iii) the active bottom sediment phase consists of radionuclides which are adsorbed on the LPM phase and deposited on the seabed. These particles may resuspend according to the bottom water velocity. Kinetic transfer coefficients are used for the calculation of adsorption/desorption between dissolved phase and LPM phase or between dissolved phase and bed sediment phase [IX-3].

The radionuclides migration model for the dissolved phase is written as:

$$\frac{\partial(C_d)}{\partial t} + \frac{\partial(uC_d)}{\partial x} + \frac{\partial(vC_d)}{\partial y} + \frac{\partial(wC_d)}{\partial z} = \frac{\partial}{\partial x} \left(K_h \frac{\partial C_d}{\partial x} \right) + \frac{\partial}{\partial y} \left(K_h \frac{\partial C_d}{\partial y} \right) + \frac{\partial}{\partial z} \left(K_z \frac{\partial C_d}{\partial z} \right) - k_{1m}C_d + k_{-1}mC_s - \lambda C_d + P_d \quad (\text{IX-1})$$

where C_d is the dissolved phase radionuclide concentration, u , v and w are the 3-D current velocity components and K_h and K_z are the horizontal and vertical diffusion coefficients, respectively. The fourth term of the right hand side is the adsorption from dissolved phase to the LPM phase, the fifth term the desorption from the LPM phase to dissolved phase, k_{1m} and k_{-1} are the kinetic transfer coefficient for the LPM, C_s is the LPM phase radionuclide concentration, m is the LPM concentration, λ is the decay constant and P_d is the input of dissolved radionuclides from the source point. The surface boundary condition is:

$$wC_d - K_z \frac{\partial C_d}{\partial z} = 0 \quad (\text{IX-2})$$

The sea bottom boundary condition is:

$$K_z \frac{\partial C_d}{\partial z} = k_{1s}C_d - k_{-1} \frac{A_s L \rho_s f (1-p)}{\gamma} \quad (\text{IX-3})$$

where k_{1s} is the kinetic transfer coefficient for the active bottom sediment phase, A_s is the active bottom sediment phase radionuclide concentration, L is the mean mixing depth of the active bottom sediment, ρ_s is the bulk density of the active bottom sediment, f is the fraction of active bottom sediments, p is the porosity and γ the thickness of the water layer which interacts with the active bottom sediment phase.

Various methods for defining the kinetic transfer coefficient have been examined by other researchers [IX-3–5]. In this model, the distribution coefficient k_d is used as one of the parameters for determining the kinetic transfer coefficient [IX-4–5] as follows:

$$k_{1m} = k_{-1}k_d m \quad (\text{IX-4})$$

$$k_{1s} = k_{-1}k_d \frac{L\rho_s f(1-p)}{\gamma} \quad (\text{IX-5})$$

The radionuclide migration model for the LPM phase is written as:

$$\frac{\partial(mC_s)}{\partial t} + \frac{\partial(mC_s)}{\partial x} + v \frac{\partial(mC_s)}{\partial y} + (w - w_s) \frac{\partial(mC_s)}{\partial z} = \frac{\partial}{\partial x} \left(K_h \frac{\partial(mC_s)}{\partial x} \right) + \frac{\partial}{\partial y} \left(K_h \frac{\partial(mC_s)}{\partial y} \right) + \frac{\partial}{\partial z} \left(K_z \frac{\partial(mC_s)}{\partial z} \right) + k_{1m}C_d - k_{-1}mC_s - \lambda mC_s + P_s \quad (\text{IX-6})$$

where w_s is the settling velocity of suspended particles, the fourth term of the right hand side represents the adsorption from dissolved phase to the LPM phase and the fifth term the desorption from the LPM phase to dissolved phase. The surface boundary condition is:

$$(w - w_s)mC_s - K_z \frac{\partial(mC_s)}{\partial z} = 0 \quad (\text{IX-7})$$

The sea bottom boundary condition is:

$$w_s mC_s + K_z \frac{\partial(mC_s)}{\partial z} = dep - res \quad (\text{IX-8})$$

where P_s is the input of the radionuclides adsorbed to the LPM from the source point. dep and res are the deposition and resuspension terms, respectively. The deposition term is written as:

$$dep = \frac{w_s(b)C_s(b)m(b)}{\gamma} \left(1 - \frac{\tau_b}{\tau_{cd}} \right) \text{ when } \tau_b < \tau_{cd} \quad (\text{IX-9})$$

$$dep = 0 \text{ when } \tau_b > \tau_{cd} \quad (\text{IX-10})$$

where τ_{cd} and τ_b are the critical deposition shear stress and the seabed stress, respectively, and (b) means the variables at the deepest water layer. The seabed stress is written as:

$$\tau_b = \rho_w C_D u_b^2 \quad (\text{IX-11})$$

where ρ_w is the seawater density, C_D the drag coefficient and u_b the bottom water velocity. The resuspension term is written as:

$$res = \frac{MfA_s}{\gamma} \left(\frac{\tau_b}{\tau_{cr}} - 1 \right) \text{ when } \tau_b > \tau_{cr} \quad (\text{IX-12})$$

$$res = 0 \text{ when } \tau_b < \tau_{cr} \quad (\text{IX-13})$$

where M is the resuspension constant and τ_{cr} the critical resuspension shear stress.

These deposition and resuspension models are used for fine particles such as clay and silt. Fine particles are strongly affected by wind-waves. In this study, however, the effect of wind-waves was not considered and deposition and resuspension processes are solved only by the tidal current.

The radionuclides migration model for the active bottom sediment phase is written as:

$$\frac{\partial A_s}{\partial t} = k_{1s} \frac{C_d(b)\gamma}{L\rho_s f} - k_{-1}A_s(1-p) + (dep - res) - \lambda A_s \quad (\text{IX-14})$$

The deposition and resuspension term are written as:

$$dep = \frac{w_s(b)C_s(b)m(b)}{L\rho_s f} \left(1 - \frac{\tau_b}{\tau_{cd}}\right) \text{ when } \tau_b < \tau_{cd} \quad (\text{IX-15})$$

$$res = \frac{MfA_s}{L\rho_s} \left(\frac{\tau_b}{\tau_{cr}} - 1\right) \text{ when } \tau_b > \tau_{cr} \quad (\text{IX-16})$$

and:

$$dep = 0 \text{ when } \tau_b > \tau_{cd} \quad (\text{IX-17})$$

$$res = 0 \text{ when } \tau_b < \tau_{cr} \quad (\text{IX-18})$$

The diffusion terms of the radionuclide migration model for the dissolved phase and the LPM phase are solved by a particle tracking random-walk model. The location of a particle for sequential time steps with a time interval Δt is determined from:

$$x(t + \Delta t) = x(t) + u\Delta t + \delta x \quad (\text{IX-19})$$

$$y(t + \Delta t) = y(t) + v\Delta t + \delta y \quad (\text{IX-20})$$

$$z(t + \Delta t) = z(t) + w\Delta t + \delta z \quad (\text{IX-21})$$

where $(x, y, z)[t]$ and $(x, y, z)[t + \Delta t]$ are the positions of a particle at the start and the end of a time step, respectively. The second and third terms on the right hand side of Eqs. IX-19–21 represent the movement of a particle due to advection and turbulent diffusion, respectively, in the ocean current. By using a uniform random number $R(0)$ between 0 and 1, the diffusion terms can be expressed as [IX-6]:

$$\delta x = \delta y = \sqrt{24K_h\Delta t}(0.5 - R(0)) \quad (\text{IX-22})$$

$$\delta z = \sqrt{24K_z\Delta t}(0.5 - R(0)) \quad (\text{IX-23})$$

The concentration at each unit Eulerian cell, C_{ijk} (Bq/m³), is calculated by summing up the contribution of each particle to the cell as follows:

$$C_{ijk} = \frac{1}{V_{ijk}} \sum b_{n,ijk} q_n \quad (\text{IX-24})$$

Suffixes i, j and k represent the cell number in the x -, y - and z - directions, respectively. The q_n is the radioactivity (Bq) of the n -th particle and $b_{n,ijk}$ is the contribution ratio of the n -th particle to the corresponding Eulerian cell (ijk). This ratio is defined as the overlapping ratio of a Lagrangian cell whose center is the particle position to the Eulerian model cell. $V_{ijk} = H\Delta x\Delta y\Delta z$ is the volume of the Eulerian model cell. Radioactive decay is considered for each Eulerian cell. The interactions between each phase are also calculated by using a stochastic method. The calculation techniques of this method are given in Ref. [IX-2].

REFERENCES TO ANNEX IX

- [IX-1] KOBAYASHI, T., OTOSAKA, S., TOGAWA, O., HAYASHI, K., Development of a non-conservative radionuclides dispersion model in the ocean and its application to surface cesium-137 dispersion in the Irish Sea, *Journal of Nuclear Science and Technology* **44**(2) (2007) 238–247.
- [IX-2] PERIÁÑEZ, R., ELLIOTT, A.J., A particle-tracking method for simulating the dispersion of non-conservative radionuclides in coastal waters, *Journal of Environmental Radioactivity* **58**(1) (2002) 13–33.
- [IX-3] PERIÁÑEZ, R., Redissolution and long-term transport of radionuclides released from a contaminated sediment: A numerical modelling study, *Estuarine, Coastal and Shelf Science* **56**(1) (2003) 5–14.
- [IX-4] NYFFLER, U.P., LI, Y.H., SANTSCHI, P.H., A kinetic approach to describe trace element distribution between particles and solution in natural aquatic systems, *Geochimica Cosmochimica Acta* **48** (1984) 1513–1522.
- [IX-5] ONISHI, Y., TRENT, D.S., *Mathematical Simulation of Sediment and Radionuclide Transport in Estuaries*, NUREG/CR-2423, U.S. Nuclear Regulatory Commission (1982).
- [IX-6] AHLSTROM, S.W., FOOTE, H.P., ARNETT, R.C., et al., *Multicomponent mass transport model: Theory and numerical implementation (discrete-parcel-random-walk version)*, BNWL-2127, Battelle Pacific Northwest Laboratories (1977).

ANNEX X. DESCRIPTION OF THE UNIVERSITY OF SEVILLE (USEV) 3-D MODEL (PACIFIC OCEAN APPLICATION)

X-1. GENERAL DESCRIPTION

This model is based on the same dispersion equations described in Annex V: USEV 2-D model applied to the Baltic Sea), but written in a 3-D form. Thus, only a brief summary is given. Water circulation has been obtained from the JCOPE2 hydrodynamic model.

There has been evidence to suggest that uptake takes place in two stages: fast surface adsorption followed by slow migration of ions to pores and interlattice spacings [X-1–3]. Consequently, two USEV kinetic models have been tested in the Pacific Ocean application. The one-step model considers that exchanges of radionuclides between water and sediments are governed by a first-order reversible reaction, being k_1 and k_2 the forward and backward rates respectively, as described in the 2-D case. The two-step model considers that exchanges are governed by two consecutive reversible reactions, i.e. surface adsorption is followed by another process that may be a slow diffusion of ions into pores and interlattice spacings, inner complex formation or a transformation such as an oxidation. k_3 and k_4 are forward and backward rates for this second reaction (see Figure X-1). Thus, sediments are divided in two phases, i.e. a reversible and a slowly reversible fraction. It has been shown that the two-step model reproduces both the adsorption and release kinetics of ^{137}Cs in the Irish Sea, where it is released from Sellafield nuclear fuel reprocessing plant [X-4].

Equations are presented below, for the sake of simplicity, in the case of a one-step kinetic model. The extension to the two-step kinetic model may be seen, for instance, in Ref. [X-4].

In a similar way to the depth averaged model shown in Annex V above, the kinetic coefficient k_1 is written as:

$$k_1 = \chi(S_m + S_s\delta_b) = k_1^m + k_1^s \quad (\text{X-1})$$

where S_m and S_s are the exchange surfaces for suspended matter and bottom sediments, respectively (dimensions $[L]^{-1}$) and χ is a parameter with the dimensions of a velocity denoted as the exchange velocity (see Annex V above). The delta function is introduced to take into account that only the deepest water layer interacts with the bed sediment. Thus, $\delta_b = 1$ for the deepest layer and $\delta_b = 0$ elsewhere.

The equation that gives the time evolution of the radionuclide concentration in the dissolved phase, C_d , is:

$$\frac{\partial C_d}{\partial t} + \frac{\partial(uC_d)}{\partial x} + \frac{\partial(vC_d)}{\partial y} + \frac{\partial(wC_d)}{\partial z} = A \left(\frac{\partial^2 C_d}{\partial x^2} + \frac{\partial^2 C_d}{\partial y^2} \right) + \frac{\partial}{\partial z} \left(K \frac{\partial C_d}{\partial z} \right) - k_1 C_d + k_2 m C_s + \delta_b k_2 \frac{L \rho_s \phi f A_s}{\psi} \quad (\text{X-2})$$

where C_s and A_s are, respectively, the concentrations of radionuclides in suspended matter and bottom sediments. u , v and w are water velocities along the x , y and z axis and A and K are, respectively, the horizontal and vertical diffusion coefficients. m is the suspended matter concentration, ρ_s the sediment bulk density, f the fraction of fine sediments and ψ is the thickness of the deepest water layer in contact with the seabed. Finally, ϕ is a correction factor that takes into account that part of the sediment particle surface may be hidden by other sediment particles.

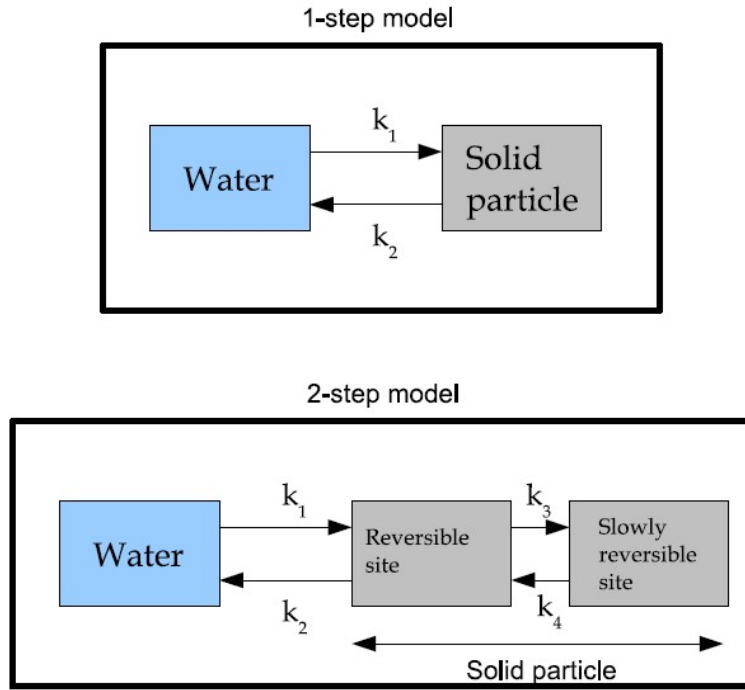


FIG.X-1. Scheme representing 1-step and 2-step kinetic models.

The equation which gives the time evolution of radionuclide concentrations in suspended matter is:

$$\frac{\partial(mC_s)}{\partial t} + \frac{\partial(umC_s)}{\partial x} + \frac{\partial(vmC_s)}{\partial y} + \frac{\partial((w - w_s)mC_s)}{\partial z} = A \left(\frac{\partial^2(mC_s)}{\partial x^2} + \frac{\partial^2(mC_s)}{\partial y^2} \right) + \frac{\partial}{\partial z} \left(K \frac{\partial(mC_s)}{\partial z} \right) - k_1^m C_d - k_2 m C_s - \delta_b SED \quad (X-3)$$

where w_s is the particle settling velocity and SED is the deposition of radionuclides from the deepest water layer to the sediment evaluated according to:

$$SED = w_s(b)m \frac{C_s(b)}{\psi} \quad (X-4)$$

It should be noted that (b) means that the corresponding magnitude is evaluated at the deepest water layer.

The equation for the temporal evolution of radionuclide concentration in the bottom sediment mixed layer is:

$$\frac{\partial A_s}{\partial t} = k_1^s \frac{C_d(b)\psi}{L\rho_s f} - k_2 A_s \phi + SED \quad (X-5)$$

where the deposition is now calculated as:

$$SED = w_s(b)m \frac{C_s(b)}{\rho_s L f} \quad (X-6)$$

X-2. PACIFIC OCEAN APPLICATION

Water circulation has been obtained from the JCOPE2 hydrodynamic model. Daily 3-D currents are imported to solve the advective transport of radionuclides. The model was also adapted to run with HYCOM water circulation. Nevertheless, it was concluded that, in general, model results were in better agreement with measured ^{137}Cs concentrations in water and sediments with JCOPE2 circulation than if HYCOM is used [X-5]. Consequently, USEV model results with HYCOM circulation are not presented in this report.

Concerning the dispersion of ^{137}Cs released from the Fukushima Daiichi NPP accident, the two-step model reproduced measured ^{137}Cs concentrations in bed sediments better than the one-step model [X-5]. Consequently, the two-step model has been used in all Fukushima exercises involving this radionuclide, except when common parameters for all models are defined for Exercise 3 and Exercise 4a as summarized in Table X-1.

Some parameters are required in order to simulate ^{137}Cs dispersion. Rates k_2 , k_3 and k_4 are taken from previous work dealing with dispersion of this radionuclide [X-6–7]. Although it is true that kinetic rates are site specific, there is no information available about them in Japanese Pacific Ocean coastal waters. Thus, representative values already used in the English Channel and Western Mediterranean Sea have been used as a first order approximation. As discussed previously [X-4; X-6–8], the exchange velocity χ can be deduced from the rates mentioned above and the radionuclide distribution coefficient k_d (see Eq. V-20). The mean value of the measured Cs distribution coefficient is 2.1×10^3 [X-9], comparable to the IAEA's recommended value [X-10]. Fixed $k_d = 2 \times 10^3$ was used to deduce χ following the procedure described in such references.

The distribution of fine sediments in the seabed, described by parameter f , was reconstructed from information given in Ref. [X-11]. Fixed $L = 0.05$ m has been used. This parameter typically ranges from 0.035 m [X-6] to 0.10 m [X-7–8; X-12]. Also, $\phi = 0.1$ was used for the sediment correction factor [X-7–8; X-12]. A representative value $R = 10$ μm was used for the mean particle size.

TABLE X-1. KINETIC MODELS APPLIED BY USEV 3-D MODEL IN THE PACIFIC OCEAN RADIOLOGICAL SCENARIO

Exercise	Features	Kinetic model
1	Own circulation and parameters	none (only tracer)
2	Same circulation, own parameters	2-step
3	Same circulation and parameters	1-step
4a	Same circulation and parameters	1-step
4b	Own circulation and parameters	2-step

REFERENCES TO ANNEX X

- [X-1] NYFFLER, U.P., LI, Y.H., SANTSCHI, P.H., A kinetic approach to describe trace element distribution between particles and solution in natural aquatic systems, *Geochimica Cosmochimica Acta* **48** (1984) 1513–1522.
- [X-2] CIFFROY, P., GARNIER, J.M., PHAM, M.K., Kinetics of the adsorption and desorption of radionuclides of Co, Mn, Cs, Fe, Ag and Cd in freshwater systems: Experimental and modelling approaches, *Journal of Environmental Radioactivity* **55** (2001) 71–91.
- [X-3] EL MRABET, R., ABRIL, J.M., MANJÓN, G., GARCÍA-TENORIO, R., Experimental and modelling study of plutonium uptake by suspended matter in aquatic environments from southern Spain, *Water Research* **35** (2001) 4184–4190.
- [X-4] PERIÁÑEZ, R., Kinetic modelling of the dispersion of plutonium in the eastern Irish Sea: two approaches, *Journal of Marine Systems* **38** (2003) 259–275.
- [X-5] PERIÁÑEZ, R., SUH, K.S., MIN, B.I., Local scale marine modelling of Fukushima releases, Assessment of water and sediment contamination and sensitivity to water circulation description, *Marine Pollution Bulletin* **64** (2012) 2333–2339.
- [X-6] PERIÁÑEZ, R., A modelling study on ^{137}Cs and $^{239/240}\text{Pu}$ behaviour in the Al-borán Sea, western Mediterranean, *Journal of Environmental Radioactivity* **99** (2008) 694–715.
- [X-7] PERIÁÑEZ, R., Testing the behavior of different kinetic models for uptake-release of radionuclides between water and sediments when implemented on a marine dispersion model, *Journal of Environmental Radioactivity* **71** (2004) 243–259.
- [X-8] PERIÁÑEZ, R., Environmental modelling in the Gulf of Cádiz: Heavy metal distributions in water and sediments, *Science of the Total Environment* **407** (2009) 3392–3406.
- [X-9] HONDA M., AONO T., AOYAMA M., HAMAJIMA Y., KAWAKAMI H., KITAMURA M., MASUMOTO Y., MIYAZAWA Y., TAKIGAWA M., SAINO T., Dispersion of artificial caesium-134 and -137 in the western North Pacific one month after the Fukushima accident, *Geochemical Journal* **46** (2012) 1–9.
- [X-10] INTERNATIONAL ATOMIC ENERGY AGENCY, Sediment distribution coefficients and concentration factors for biota in the marine environment, Technical Reports Series No. 422, IAEA, Vienna (2004).
- [X-11] SAITO, Y., Late pleistocene coastal sediments, drainage patterns and sand ridge systems on the shelf off Sendai, northeast Japan, *Marine Geology* **89** (1989) 229–244.
- [X-12] PERIÁÑEZ, R., Redissolution and long-term transport of radionuclides released from a contaminated sediment: A numerical modelling study, *Estuarine, Coastal and Shelf Science* **56**(1) (2003) 5–14.

ANNEX XI. HYDRODYNAMIC MODELS APPLIED TO THE PACIFIC OCEAN RADIOLOGICAL SCENARIO

Some brief comments on the hydrodynamic models which were used to calculate ocean circulation to be used in Pacific Ocean radiological scenario are given below (references where full details are provided are included).

XI-1. DESCRIPTION OF THE JCOPE2, JAPAN COASTAL OCEAN PREDICTABILITY EXPERIMENT

JCOPE2 was developed by the Japan Agency of Marine-Earth Science and Technology [XI-1]. It is based on one of the world community models, Princeton Ocean Model. Open boundary conditions are obtained from a global scale circulation model with lower resolution, using a one-way nesting procedure.

JCOPE2 consists of 23 vertical levels and spatial resolution is about 9 km. The model is driven by wind stresses, plus heat and salt fluxes. The wind stress and heat flux field are calculated from the 6 hourly National Centers for Environmental Prediction (NCEP) Global Forecast system data using bulk formulae. The salinity at the surface is restored to the monthly mean climatology with a timescale of 30 days.

The output of JCOPE2 is used for ship routing of oil tankers, fishery and drilling ships. Some examples of applications are described in Refs. [XI-2–4]. It has also been applied to simulate the dispersion of Fukushima Daiichi NPP accidental releases in the Pacific [XI-5–8].

XI-2. NTUA, NATIONAL TECHNICAL UNIVERSITY OF ATHENS

The NTUA model is a general deterministic model which solves the full Navier–Stokes equations for transient, 3-D turbulent flow and utilizes an Eulerian approach. The turbulence model adopted for the present study is the renormalization group $k \sim \rho$. Additional processes and equations which are relevant are also included in the model: density variation with salinity (salinity is computed by solving an additional transport equation), expressions for describing wind-induced currents, etc.

The finite-volume method was implemented for the numerical solution of the system of equations. The above model is implemented in the Computational Fluid Dynamics code PHOENICS (Parabolic, Hyperbolic, or Elliptic Numerical Integration Code Series). At solid walls, such as the coast, the sea bottom or any other solid, wall functions are used. Grid-independency runs were also performed to obtain grid-independent results. To ensure convergence, relaxation of the false time step type was used for all other variables; and linear for pressure. The false time step used was equal to the fluid average residence time in the smallest cell in the domain [XI-9–11].

XI-3. NCOM, NAVY COASTAL OCEAN MODEL

NCOM is a numerical model used to produce surface currents and temperature, mixed layer depth, current and thermohaline profiles in global scale [XI-12]. NCOM is a free surface, primitive-equation model with a curvilinear horizontal grid. Horizontal resolution varies from 19.5 km near the Equator to 8 km in the Arctic, with mid-latitude resolution of about $1/8^\circ$ latitude (~ 14 km). The hybrid sigma/ z vertical schemes are adopted with 19 terrain following sigma levels in the upper 137 meters, and 21 fixed thickness z -levels extending to a maximum depth of 5500 m. NCOM extends from the Arctic Ocean to the coast of Antarctica and from the open ocean over the shelf break to near-shore regions. The present daily model run consists of

a 72 hour hindcast to assimilate fields which include recent observations, and a 72 hour forecast. Global NCOM produced sea surface height, salinity, temperature, u-velocity and v-velocity. Global NCOM can include atmospheric forcing, but it does not include tidal heights and currents.

Global NCOM was retired on 5 April 2013 and replaced by operational 1/12° HYCOM. After the Fukushima Daiichi NPP accident took place, 3 hour averaged 3-D currents near the Fukushima region were produced from NCOM, operated by the US Navy operational global Nowcast/Forecast system between 12 March and 30 June 2011. There were 40 vertical levels and the spatial resolution was 1 km.

XI-4. HYCOM, HYBRID COORDINATE OCEAN MODEL

The HYCOM consortium is a multi-institutional effort sponsored by the National Ocean Partnership (NOPP) as a part of the United States of America Global Ocean Data Assimilation Experiment (GODAE) [XI-13]. HYCOM is a primitive equation, general circulation model with vertical coordinates that remain isopycnic in the open stratified ocean.

Computations in global HYCOM are carried out on a Mercator grid between 78° S and 47° N (1/12° horizontal resolution at the equator). A bipolar patch is used for regions north of 47° N. The horizontal dimensions of the global grid are 4500 × 3298 grid points resulting in ~ 7 km spacing on average. There are 33 vertical layers. Surface forcing includes wind stress, wind speed, heat flux and precipitation. HYCOM uses the United States of America Navy Coupled Ocean Data Assimilation System (NCODA) for data assimilation. The outputs are surface heat flux, sea surface height, surface salinity trend, surface temperature trend, salinity, potential temperature, u-velocity and v-velocity. Global HYCOM can include atmospheric forcing, but it does not include tidal heights and currents.

XI-5. KYOTO UNIVERSITY

The coastal model was developed by Kyoto University, Japan Agency of Marine-Earth Science and Technology and the Japan Marine Science Foundation [XI-14]. A nesting method enables downscale calculation from the largest area that covers the northwestern part of North Pacific, with horizontal resolutions of 1/8° in latitude and 1/6° in longitude, to the two-step-nested finer domain around the Fukushima area, with horizontal resolutions of 1/72° in latitude and 1/54° in longitude (approximately 1.5 km). The model domain for the coastal model extends from 140.5°E to 144°E longitude and from 35.5°N to 38.5°N latitude. There are 78 layers set in the vertical. The four dimensional variation (4-D-VAR) method was applied for the outermost model to obtain the reanalysis data.

XI-6. MARS3D, IFREMER (FRANCE)

Circulation modelling was performed using the operational MARS3D code (3-D hydrodynamical Model for Applications at Regional Scale) developed by IFREMER (French Research Institute for Exploitation of the Sea). This is a 3-D model with reduced sigma vertical coordinates based on the resolution of the Navier–Stokes equations [XI-15]. This model with free surface resolves primitive equations using a time-splitting scheme under assumptions of Boussinesq approximation, hydrostatic equilibrium and incompressibility.

Application to the Fukushima area is described in Ref. [XI-16]. The model domain covers the oceanic area off Fukushima, i.e. 31°N–43.2°N, 137°E–150°E (1000 km × 1200 km). The horizontal resolution is 1/60° (one nautical mile), in both E-W and N-S directions, with 742 grid cells in the E-W direction and 622 in the N-S direction. The vertical resolution of the sigma coordinate is 40 layers refined near the surface. Bathymetric data are derived from the Japan Oceanographic Data Center.

Wind forcing, water and heat flux are downscaled from the atmospheric forecast and hindcast of the NCEP meteorological global model [XI-17] with a resolution of 1/2°. At the scale of thermohaline and geostrophic effects, the initial and boundary conditions are derived from the daily oceanic forecast and hindcast of the global model proposed by Mercator-Ocean with a resolution of 1/12°[XI-18]. For the downscaling procedure, the temperature, salinity, currents and sea level are interpolated in both time and space to provide initial and boundary conditions. The tide at open boundary conditions is prescribed using 16 tidal harmonic components from the FES2004 numerical atlas with a horizontal resolution of 1/8°.

Radionuclide dispersion is calculated using an Eulerian method. The parallelized MARS3D code runs on 256 Message Passing Interface (MPI) ranks for the present Fukushima application. An example of calculated currents is presented in Figure XI-1.

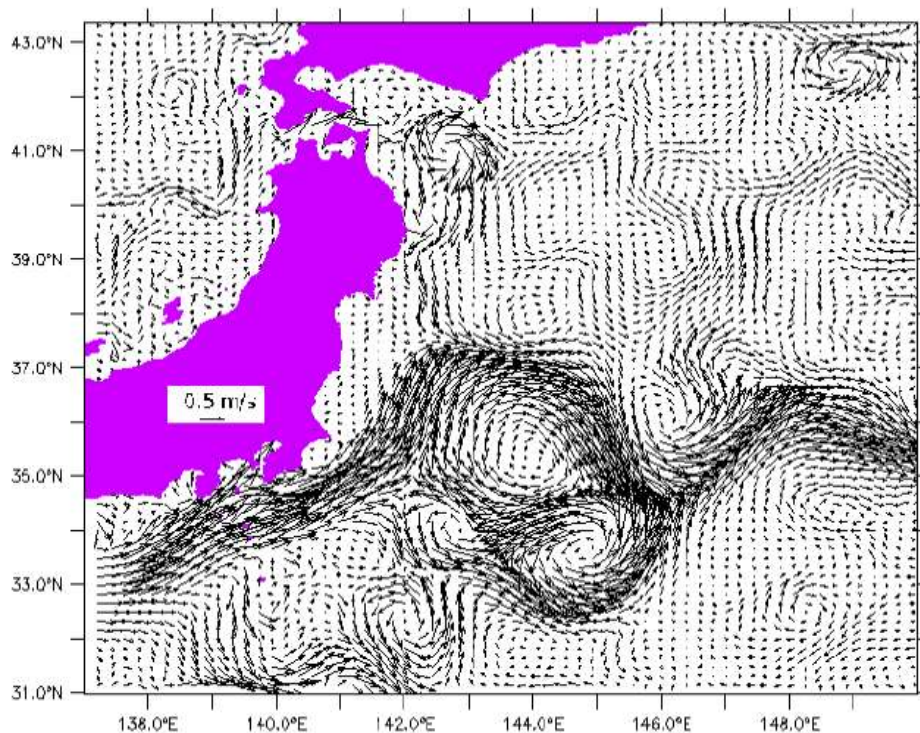


FIG.XI-1. Calculated mean surface currents for April 2011.

XI-7. SYMPHONIE (SIROCCO, UNIVERSITY OF TOULOUSE, FRANCE)

The model used is the non-hydrostatic ocean model following the Boussinesq hydrostatic SYMPHONIE model developed by the Sirocco system team. The model uses an Arakawa type

finite difference method for the C grid and the principal equations of the physical engine are detailed in Ref. [XI-19–20].

The model uses a stretched horizontal grid with a variable horizontal resolution, from $600\text{ m} \times 600\text{ m}$ at the nearest grid point from Fukushima, to $5\text{ km} \times 5\text{ km}$ offshore. The vertical grid is based on a generalized s-coordinate system. The 30 vertical levels are irregularly distributed, with increased resolution near the sea surface.

The model was initialized and forced at its lateral boundaries with the global NCOM real time operational ocean model of the United States of America Navy [XI-12] operated by the National Oceanic and Atmospheric Administration (NOAA). At the sea surface, the ocean model is forced by the meteorological fluxes delivered every 3 hours by the European Centre for Medium-Range Weather Forecasts (ECMWF). The tidal forcing at the lateral open boundaries is provided by the T-UGO model, implemented for this purpose by the SIROCCO team on coast of the Japanese Pacific Ocean. The main rivers of the region (between 35.5°N and 38.5°N), the Tone to the south, and the Natori and Abukuma to the north, were introduced into the model on the basis of climatological freshwater discharges (190 , 17 and $67\text{ m}^3/\text{s}$ respectively).

The model was initialized on 21 February 2011. Currents and vertical diffusivities computed by the model were averaged over 3 hour periods and stored to compute the advection and diffusion of tracers in off-line mode, using an Eulerian representation (Figure XI-2). An inverse-method calculation was carried out to estimate the source term.

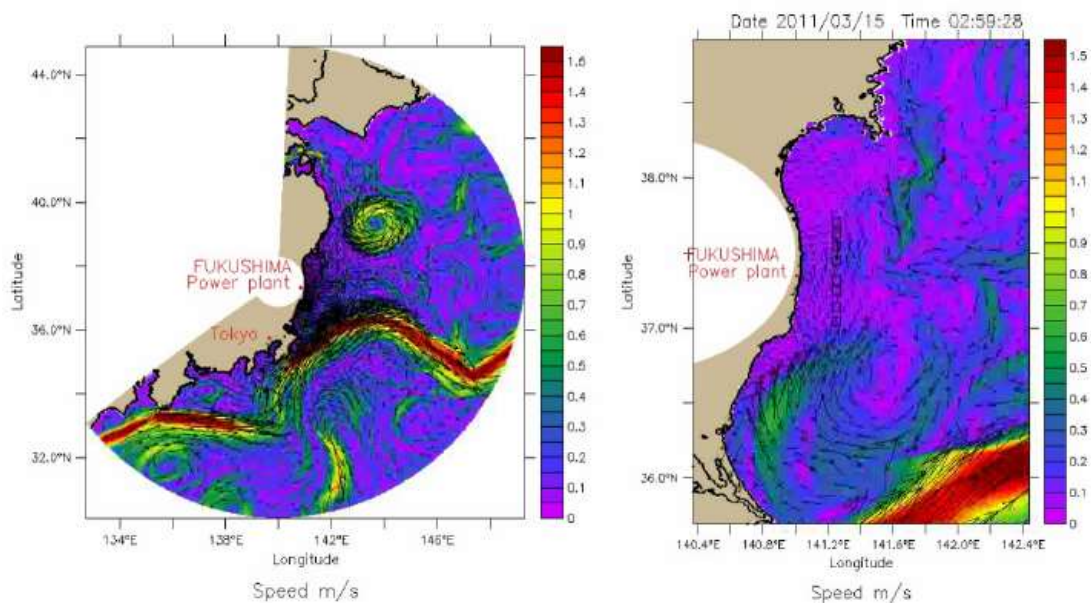


FIG.XI-2. Calculated surface currents on 15 March 2011.

REFERENCES TO ANNEX XI

- [XI-1] <http://www.jamstec.go.jp/jcope/htdocs/e/home.html>
- [XI-2] MIYAZAWA, Y., MASUMOTO, Y., VARLAMOV, S.M., MIYAMA, T., Transport simulation of the radionuclide from the shelf to the open ocean around Fukushima, *Continental Shelf Research* **50–51** (2012) 16–29.
- [XI-3] MIYAZAWA, Y., MASUMOTO, Y., VARLAMOV, S.M., MIYAMA, T., TAKIGAWA, M., HONDA, M., SAINO, T., Inverse estimation of source parameters of oceanic radioactivity dispersion models associated with the Fukushima accident, *Biogeosciences* **10** (2013) 2349–2363.
- [XI-4] MIYAZAWA, Y., ZHANG, R., GUO, X., TAMURA, H., AMBE, D., LEE, J.S., OKUNO, A., YOSHINARI, H., SETOU, T., KOMATSU, K., Water mass variability in the western North Pacific detected in a 15-year eddy resolving ocean reanalysis, *Journal of Oceanography* **65** (2009) 737–756.
- [XI-5] PERIÁÑEZ, R., SUH, K.S., MIN, B.I., Local scale marine modelling of Fukushima releases, Assessment of water and sediment contamination and sensitivity to water circulation description, *Marine Pollution Bulletin* **64** (2012) 2333–2339.
- [XI-6] MIN, B.I., PERIÁÑEZ, R., KIM, I.G., SUH, K.S., Marine Dispersion Assessment of ¹³⁷Cs Released from the Fukushima Nuclear Accident, *Marine Pollution Bulletin* **72** (2013) 22–33.
- [XI-7] PERIÁÑEZ, R., SUH, K.S., MIN, B.I., CASACUBERTA, N., MASQUÉ, P., Numerical modelling of the releases of ⁹⁰Sr from Fukushima to the ocean: An evaluation of the source term, *Environmental Science and Technology* **47** (2013) 12305–12313.
- [XI-8] PERIÁÑEZ, R., SUH, K.S., MIN, B.I., Should we measure plutonium concentrations in marine sediments near Fukushima? *Journal of Radioanalytical Nuclear Chemistry* **298** (2013) 635–638.
- [XI-9] MARKATOS, N.C., Mathematical modelling of single-and two-phase flow problems in the process industries, *Revue de l’Institut Francais du Petrole* **48**(6) (1993) 631–661.
- [XI-10] PSALTAKI, M., MARKATOS, N.C., Implementing the Finite-Volume method in simulating the behaviour of pollutants in marine environment, Proc. of the 4th IASME/World Scientific and Engineering Academy and Society International Conference on Continuum Mechanics (CM ’09), 24–26 February 2009, Cambridge, UK (2009) 187–199.
- [XI-11] PSALTAKI, M., FLOROU, H., TRABIDOU, G., MARKATOS, N.C., Modelling and assessment of pollutant impact on marine environments, 2nd WSEAS International Conference on Computer Engineering and Applications (CEA ’10), 27–29 January 2010, Harvard University, Cambridge USA (2010) 176–180.
- [XI-12] BARRON, C.N., KARA, A.B., MARTIN, P.J., RHODES, R.C., SMEDSTAD, L.F., Formulation, implementation and examination of vertical coordinate choices in the global Navy Coastal Ocean Model (NCOM), *Ocean Modelling* **11**(3–4) (2006) 347–375.
- [XI-13] BLECK, R., An oceanic general circulation model framed in hybrid isopycnic-Cartesian coordinates, *Ocean Modeling* **4**(1) (2002) 55–88.
- [XI-14] KAWAMURA, H., KOBAYASHI, T., FURUNO, A., IN, T., ISHIKAWA, Y., NAKAYAMA, T., SHIMA, S., AWAJI, T., Preliminary numerical experiments on oceanic dispersion of ¹³¹I and ¹³⁷Cs discharged into the ocean because of the Fukushima Daiichi NPP disaster, *Journal of Nuclear Science and Technology* **48** (2011) 1349–1356.

- [XI-15] LAZURE, P., DUMAS, F., An external-internal mode coupling for a 3D hydrodynamical model for applications at regional scale (MARS), *Advances in Water Resources* **31**(2) (2008) 233–250.
- [XI-16] BAILLY DU BOIS, P., GARREAU, P., LAGUIONIE, P., KORSAKISSOK, I., Comparison between modelling and measurement of marine dispersion, environmental half-time and ^{137}Cs inventories after the Fukushima Daiichi accident, *Ocean Dynamics* **64** (2014) 361–383.
- [XI-17] <http://www.ncep.noaa.gov/>
- [XI-18] <http://www.mercator-ocean.fr/>
- [XI-19] MARSALEIX, P., AUCLAIR, F., ESTOURNEL, C., Considerations on open boundary conditions for regional and coastal ocean models, *Journal of Atmospheric and Oceanic Technology* **23** (2006) 1604–1613.
- [XI-20] MARSALEIX, P., AUCLAIR, F., ESTOURNEL, C., Low-order pressure gradient schemes in sigma coordinate models: The seamount test revisited, *Ocean Modelling* **30** (2009) 169–177.

CONTRIBUTORS TO DRAFTING AND REVIEW

Bezhenar, R.	Institute of Mathematical Machines and System Problems, Ukraine
Brovchenko, I.	Institute of Mathematical Machines and System Problems, Ukraine
Duffa, C.	Institut de Radioprotection et de Sûreté Nucléaire, France
Iosjpe, M.	Norwegian Radiation Protection Authority, Norway
Jung, K.T.	Korean Institute of Ocean Science and Technology, Republic of Korea
Kennedy, A.	International Atomic Energy Agency
Kobayashi, T.	Japan Atomic Energy Agency, Japan
Lamego Simões Filho, F.	Instituto de Engenharia Nuclear, Brazil
Maderich, V.	Institute of Mathematical Machines and System Problems, Ukraine
McGinnity, P.	International Atomic Energy Agency
Min, B.I.	Korea Atomic Energy Research Institute, Republic of Korea
Nies, H.	Consultant, Germany
Osvath, I.	International Atomic Energy Agency
Outola, I.	Radiation and Nuclear Safety Authority, Finland
Psaltaki, M.	National Technical University of Athens, Greece
Periáñez, R.	University of Seville, Spain
Suh, K-S.	Korea Atomic Energy Research Institute, Republic of Korea
Telleria, D.	International Atomic Energy Agency
de With, G.	Nuclear Research and Consultancy Group, Netherlands
Zheleznyak, M.	Institute of Mathematical Machines and System Problems, Ukraine

LIST OF PARTICIPANTS

Abdel-Aal, N.	Egyptian Nuclear & Radiological Regulatory Authority, Egypt
Addad, Y.	Khalifa University of Science, Technology and Research, United Arab Emirates
Ahn, S.	Korea Institute of Nuclear Safety, Republic of Korea
Al Neaimi, A.	Emirates Nuclear Energy Corporation, United Arab Emirates
Alotaibi, K.	Environment Protection and Meteorology General Authority, Saudi Arabia
Armand, P.	Commissariat à l'Energie Atomique et aux énergies alternatives, France
Attarilar, A.	Iran Nuclear Regulatory Authority, Iran
Baumgärtner, F.	Consultant, Germany
Behradfar, M.	Iran Nuclear Regulatory Authority, Iran
Bezhenar, R.	Institute of Mathematical Machines & System Problems, Ukraine
Blixt Buhr, A.	Vattenfall Atkiebolag, Sweden
Bosc, E.	Federal Authority for Nuclear Regulation, United Arab Emirates
Bradshaw, C.	Stockholm University, Sweden
Brovchenko, I.	Institute of Mathematical Machines & System Problems, Ukraine
Burgos Gallego, J.	Consultant, Spain
Chouhan, S.	Canadian Nuclear Laboratories, Canada
Daniel, P.	Meteo-France, France
de With, G.	Nuclear Research and Consultancy Group, Netherlands
Duffa, C.	Institut de Radioprotection et de Sûreté Nucléaire, France
Florou, H.	National Center for Scientific Research "Demokritos", Greece
Grzechnik, M.	Australian Radiation Protection and Nuclear Safety Agency, Australia
Güngör, E.	Cekmece Nuclear Research and Training Center, Turkey
Hägg, A.	Swedish Radiation Safety Authority, Sweden
Higley, K.	Oregon State University, United States of America
Iosjpe, M.	Norwegian Radiation Protection Authority, Norway
Johansen, M.	Australian Nuclear Science and Technology Organisation, Australia
Jung, K.T.	Korean Institute of Ocean Science and Technology, Republic of Korea
Kautsky, U.	Swedish Nuclear Fuel and Waste Management Company, Sweden

Kautsky, M.	United States Department of Energy, United States of America
Kennedy, P.	Food Standards Agency, United Kingdom
Kim, K.O.	Korean Institute of Ocean Science and Technology, Republic of Korea
Kobayashi, T.	Japan Atomic Energy Agency, Japan
Krös, C.	South African Nuclear Energy Corporation Limited, South Africa
Lamego Simões Filho, F.	Instituto de Engenharia Nuclear, Brazil
Liptak, L.	ABmerit, Slovakia
Maderych, V.	Institute of Mathematical Machines and System Problems, Ukraine
McDonald, P.	Sellafield Limited, United Kingdom
McGinnity, P.	International Atomic Energy Agency
Melintescu, A.	"Horia Hulubei" National Institute of Physics and Nuclear Engineering, Romania
Min, B.I.	Korea Atomic Energy Research Institute, Republic of Korea
Miyamoto, K.	Marine Ecology Research Institute, Japan
Montero, M.	CIEMAT, Spain
Mothersill, C.	McMaster University, Canada
Muikku, M.	Radiation and Nuclear Safety Authority, Finland
Nies, H.	Consultant, Germany
Nohpal Jiménez, X.	Comisión Nacional de Seguridad Nuclear y Salvaguardias, Mexico
Osvath, I.	International Atomic Energy Agency
Outola, I.	Radiation and Nuclear Safety Authority, Finland
Park, K.	Korea Atomic Energy Research Institute, Republic of Korea
Parviainen, L.	Posiva Oy, Finland
Periáñez, R.	University of Seville, Spain
Pham, C.	Electricité de France, France
Picel, M.	Argonne National Laboratory, United States of America
Pryakhin, E.	Urals Research Center for Radiation Medicine, Russian Federation
Psaltaki, M.	National Technical University of Athens, Greece
Ramadan Ahmed, A.	Egyptian Nuclear and Radiological Regulatory Authority, Egypt
Ravi, P.	Bhabha Atomic Research Centre, India
Real, A.	CIEMAT, Spain
Rougé, D.	Electricité de France, France

Ruedig, E.	Los Alamos National Laboratory, United States of America
Sam, A.	International Atomic Energy Agency
Sazykina, T.	Research and Production Association "Typhoon", Russian Federation
Siclet, F.	Electricité de France, France
Sika-Boafo, D.	Ghana Atomic Energy Commission, Ghana
Simonsen, M.	Norwegian University of Life Sciences, Norway
Sotiropoulou, M.	National Center for Scientific Research "Demokritos", Greece
Suh, K-S.	Korea Atomic Energy Research Institute, Republic of Korea
Tagami, K.	National Institute of Radiological Sciences, Japan
Tanaka, T.	Electricité de France, France
Torpo, L.	Fennovoima Oy, Finland
Udomsomporn, S.	Ministry of Sciences and Technology, Thailand
Vetrov, V.	Institute of Global Climate and Ecology, Russian Federation
Vives i Batlle, J.	Studiezentrum für Kernenergie, Belgium
Voitsekhovych, O.	Ukrainian Hydrometeorological Institute, Ukraine
Willemsen, S.	Nuclear Research and Consultancy Group, Netherlands
Woodruffe, A.	Federal Authority for Nuclear Regulation, United Arab Emirates
Wu, Q.	Tsinghua University, People's Republic of China
Xu, S.	Swedish Radiation Safety Authority, Sweden
Yu, C.	Argonne National Laboratory, United States of America
Zheleznyak, M.	Institute of Mathematical Machines and System Problems, Ukraine

MODARIA Technical Meetings, IAEA Headquarters, Vienna

19–22 November 2012, 11–15 November 2013, 10–14 November 2014,
9–13 November 2015

Interim Working Group Meetings, MODARIA Working Group 10

Vienna, Austria, 28–30 May 2013, Monaco, 3–5 June 2014, Sevilla, Spain, 17–19 June 2015



IAEA

International Atomic Energy Agency

No. 26

ORDERING LOCALLY

IAEA priced publications may be purchased from the sources listed below or from major local booksellers.

Orders for unpriced publications should be made directly to the IAEA. The contact details are given at the end of this list.

NORTH AMERICA

Bernan / Rowman & Littlefield

15250 NBN Way, Blue Ridge Summit, PA 17214, USA

Telephone: +1 800 462 6420 • Fax: +1 800 338 4550

Email: orders@rowman.com • Web site: www.rowman.com/bernan

Renouf Publishing Co. Ltd

22-1010 Polytek Street, Ottawa, ON K1J 9J1, CANADA

Telephone: +1 613 745 2665 • Fax: +1 613 745 7660

Email: orders@renoufbooks.com • Web site: www.renoufbooks.com

REST OF WORLD

Please contact your preferred local supplier, or our lead distributor:

Eurospan Group

Gray's Inn House

127 Clerkenwell Road

London EC1R 5DB

United Kingdom

Trade orders and enquiries:

Telephone: +44 (0)176 760 4972 • Fax: +44 (0)176 760 1640

Email: eurospan@turpin-distribution.com

Individual orders:

www.eurospanbookstore.com/iaea

For further information:

Telephone: +44 (0)207 240 0856 • Fax: +44 (0)207 379 0609

Email: info@eurospangroup.com • Web site: www.eurospangroup.com

Orders for both priced and unpriced publications may be addressed directly to:

Marketing and Sales Unit

International Atomic Energy Agency

Vienna International Centre, PO Box 100, 1400 Vienna, Austria

Telephone: +43 1 2600 22529 or 22530 • Fax: +43 1 26007 22529

Email: sales.publications@iaea.org • Web site: www.iaea.org/books

International Atomic Energy Agency
Vienna
ISBN 978-92-0-103619-3
ISSN 1011-4289